A Feasibility Study of High Lift Devices on Blended Wing Body Large Transport Aircraft

A Project

Presented to

The Faculty of the Department of

Mechanical and Aerospace Engineering

San Jose State University

In Partial Fulfillment

of the Requirements for Degree

Master of Science

In

Aerospace Engineering

By

Mark DeMann

May 2007

San Jose State University

The Undersigned Faculty Committee Approves

A Feasibility Study of High Lift Devices on Blended Wing Body Large Transport Aircraft

of

Mark DeMann

APPROVED FOR THE DEPARTMENT OF MECHANICAL AND AEROSPACE ENGINEERING

____

Dr. Nikos Mourtos, Committee Chair Date

____

Dr. Periklis Papadopoulos Date

____

Dr. Sean Swei Date

ABSTRACT

A Feasibility Study of High Lift Devices on Blended Wing Body Large Transport Aircraft

By Mark DeMann

In recent years there has emerged a significant increase of interest in the design of a blended wing body (BWB) aircraft, specifically applied to a large commercial transport vehicle. The BWB design has been proven to have significant improvements in aerodynamic efficiency as compared to the conventional wing-fuselage design. However, due to the inability to counteract significant pitching moments there is difficulty in the design of high lift devices for the BWB, specifically trailing edge devices. This project develops an in depth study of this problem to provide specific results as to the necessity of the high lift devices, the moments created, and the ability for the aircraft to remain stable. The BWB-450 configuration, recently being developed by NASA, was roughly used as the baseline design configuration, though much additional design needed to be assumed/added due to a lack of information. Due to the large wing area and increased lift to drag ratio, it was found that, in terms of longitudinal stability, high lift devices could be successfully applied to the aircraft which would meet the takeoff and landing requirements for a field length comparable to those of current conventional large transport aircraft.

Table Of Contents

List of Figures

List of Tables

Nomenclature

a	Acceleration/Deceleration
AC	Aerodynamic center
a_n	Normal acceleration during landing flare
AR	Aspect ratio
AR_{Trap}	Trapezoidal aspect ratio
b	Wingspan
$b_i/2$	Inboard half span
$b_o/2$	Outboard half span
c	Chord length
C_{Di}	Induced drag coefficient
$(C_{Di})_{IGE}$	Induced drag coefficient corrected to include ground effect
C_{Do}	Parasite drag coefficient
c_e/c_w	Elevon to wing chord ratio
C_f	Skin friction coefficient
c_f/c	Flap chord to wing chord ratio
CG	Center of gravity
$C_{L\ max}$	Maximum lift coefficient
C_l	Airfoil lift coefficient
C_L	Wing/Aircraft lift coefficient
ΔC_L	Difference between the maximum C_L and required C_L
$\Delta C_{L,f}$	Lift coefficient increment due to flap deflection
$C_{l\alpha}$	Airfoil lift coefficient derivative
$C_{L\alpha}$	Wing lift coefficient derivative
$C_{L\delta e}$	Lift coefficient elevon control derivative
C_{lo}	Airfoil lift coefficient at zero angle of attack
C_{Lo}	Wing lift coefficient at zero angle of attack
C_M	Moment coefficient

$C_{M\delta e}$	Moment coefficient elevon control derivative
$C_{m,ac}$	Local airfoil moment coefficient about the aerodynamic center
$C_{m,c/4_\alpha}$	Moment coefficient about c/4 derivative with respect to α
$\Delta C_{m,f}$	Moment coefficient increment due to flap deflection
C_{Mac}	Moment coefficient about the aerodynamic center of the wing
C_{Mcg}	Moment coefficient of airplane about the CG
$C_{Mcg\alpha}$	Moment coefficient of airplane about the CG, derivative with respect to α
C_{Mcgo}	Moment coefficient of airplane about the CG for zero angle of attack
c_o	Root chord
CP	Center of pressure
c_t	Tip chord
D	Drag
FAR	Federal Aviation Regulations
FF	Form factor
g	Acceleration due to gravity
h	Height (above ground level)
i	Current segment/iteration or total number of segments/iterations
ILS	Instrument landing system
L	Lift
L_α	Lift derivative with respect to α
L'	Lift per unit length
Lt	Tail lift
$\dot{m}$	Engine air mass flow rate
M	Mach number or moment
M_A	Moment about point A
$M_{A\alpha}$	Moment about point A derivative with respect to α
MAC	Mean aerodynamic chord
M_{AC}	Moment about the aerodynamic center
MAC_i	Inboard mean aerodynamic chord

MAC_o	Outboard mean aerodynamic chord
M_{CG}	Moment about the aircraft center of gravity
MLW	Maximum landing weight
MTOW	Maximum takeoff weight
q	Dynamic pressure $\left(=\frac{1}{2}\rho V^2\right)$
R	Landing flare radius
R/C	Rate of climb
Re	Reynolds number
s	Horizontal distance
S	Wing area
S_A	Airborne distance
S_G	Ground roll distance
S_i	Inboard wing area
SM	Static margin
s_o	Initial horizontal distance
S_o	Outboard wing area
S_T	Landing transition distance
S_{total}	Total landing distance
S_{Trap}	Trapezoidal reference area
S_{wet}	Aircraft wetted area
Δt	Time interval
T	Thrust
t/c	Thickness to chord ratio
TOGW	Takeoff gross weight
TSFC	Thrust specific fuel consumption
V	Velocity
V_2	Velocity as the aircraft clears a 35 ft obstacle on takeoff
V_A	Approach velocity

V_e	Engine exit velocity
V_{LOF}	Lift off velocity
V_o	Initial velocity or engine inlet velocity
V_s	Stall velocity
W	Weight
Δx	Distance interval
x/c	Location along chord with respect to the chord length
$(x/c)_m$	Chord location of maximum thickness
X_A	Chordwise distance between point A and aircraft aerodynamic center
x_{ac}	Chordwise location of local airfoil aerodynamic center
$x_{ac,y=o}$	Chordwise location of local airfoil aerodynamic center at wing root
y	Spanwise distance
α	Angle of attack
α_{abs}	Absolute angle of attack
α_e	Effective angle of attack
α_I	Induced angle of attack
α_{stall}	Stall angle of attack
Γ	Circulation
Γ_o	Circulation at root (y=0)
δ_e	Elevon deflection angle
δ_f	Flap deflection angle
η_{ie}	Inboard edge of elevon spanwise location
η_{oe}	Outboard edge of elevon spanwise location
η_{of}	Outboard edge of flap spanwise location
θ	Aircraft angle during takeoff
θ_D	Glide slope angle
θ_o	Initial aircraft angle at takeoff

λ	Taper ratio
Λ	Wing sweep angle
Λ_m	Wing sweep angle at maximum thickness
μ	Friction coefficient
ρ	Air density

1. Introduction

1.1 Motivation

To best understand the motivation for this project it will be broken down into three categories which define the specific application of the project: the very large transport aircraft, the blended wing body aircraft, and the application of high lift devices. The motivation to study each of these categories is connected to the others and will define the overall motivation for this project.

1.1.1 Very Large Transport Aircraft

The recent unveiling of the new Airbus A380 has officially ushered in the new era of very large transport aircraft. Though there is some disagreement and uncertainty about how successful the new very large transport aircraft will be, as well as whether or not it will eventually replace current smaller aircraft, there is definitely a use and desire for the very large transport. "Boeing had forecast in 1991 that 54 percent of the value of the commercial market up to 2005, or roughly $334 billion, was for 350-seaters and upward" [1]. As the aviation industry continues to grow, airport congestion becomes more and more of an issue. Because physically there is a limited number of aircraft an airport can handle it makes sense to increase the size of the individual aircraft rather than increase the number of aircraft in operation. Also, an increase in size of the aircraft allows for a reduction in seat-mile or ton-mile costs, especially for long-range flights.

1.1.2 Blended Wing Body Aircraft

The blended wing body aircraft is an unconventional aircraft design that has continued to attract a great deal of interest due to the promise of great aerodynamic advantages. The conventional wing-fuselage configuration has been a proven design for many years but, from an aerodynamic point of view, is lacking in efficiency. The fuselage provides for a great amount of drag while contributing nothing to the lift of the aircraft. This deficiency has always been balanced by the need for an adequate section to hold the passengers and cargo. The idea for the blended wing body, or flying wing, is to provide a single lifting surface stretching the entire wingspan of the aircraft. There is no tail and no conventional fuselage. Also, the shape of the blended wing body allows for a much smaller wetted area, which in turn increases the lift to drag ratio. Figure 1.1 shows an example of how the surface area is decreased just by approximating the body as a circular disc.

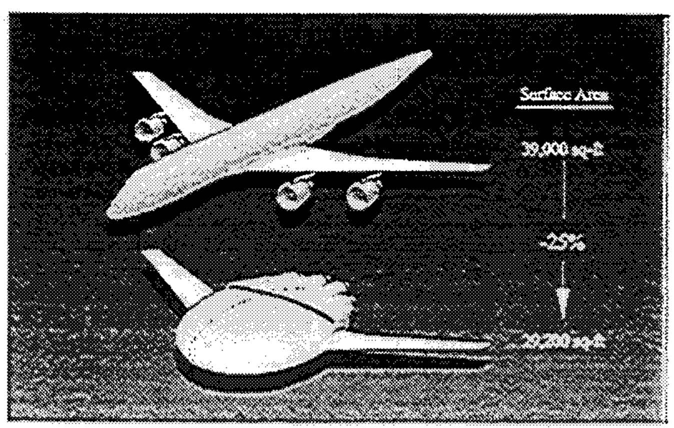

Figure 1.1. *Surface Area Reduction for the Blended Wing Body Aircraft [2]*

The idea of the blended wing body fits well with the very large transport because of the restriction that the passengers and cargo must fit inside the wing of the blended wing body. To get the necessary vertical space requires a 15-17% thickness-to-chord ratio for the center of the body. As the wing tapers smoothly down along the span a great deal of spanwise volume is created. In other words, in order to meet the minimum height requirement to fit the passengers and create a lifting surface, a great deal of volume is created inside the aircraft. Therefore, it makes sense to apply this type of configuration to a very large transport aircraft. Other designs in the past with small payloads have had to implement a bubble type of a cockpit to minimize the spanwise volume. Figures 1.2 and 1.3 provide two examples of this, the Northrop XB-35 and B-2.

Figure 1.2. *Northrop XB-35 [3]*

Figure 1.3. *Northrop B-2 [3]*

1.1.3 High Lift Devices

The motivation behind studying high lift devices is based on the difficulties involved in applying them to a tailless aircraft as well as their advantage and necessity for large aircraft in takeoff and landing configurations.

Typically, for a conventional aircraft with a tail, high lift devices can be applied and the moments created by the additional lift are countered by the deflection of the tail as illustrated in Figure 1.4.

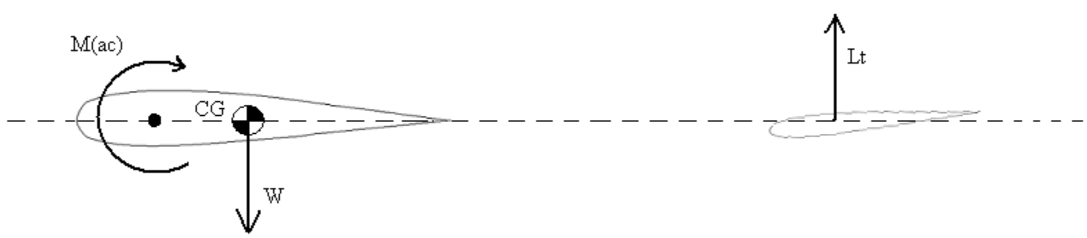

Figure 1.4. *Conventional Aircraft Moments*

However, with tailless aircraft there is no way of counteracting the pitching moment created by the high lift devices. Because of this, most blended wing body designs do not include high lift devices or only employ simple leading edge slats. Not having high lift devices results in high angles and velocities for landing and takeoff in order to achieve the required lift. This also creates a higher wing area in order to decrease the wing loading (W/S) and increase the lift. For large commercial transports these effects can be very difficult to handle. Large approach and takeoff velocities and angles not only make the flight uncomfortable but also include a significant increase in risk and safety. Also, because of the large size of the aircraft to begin with, increasing the wing area makes airport operations even more difficult.

1.2 Objective

The objective for this project, simply stated, is to determine the feasibility of applying:

1. Only leading edge slats
2. Only trailing edge flaps
3. A combination of leading edge and trailing edge devices

to a large transport blended wing body aircraft. As stated earlier, and will be discussed in further detail in the following section, tailless aircraft have previously been designed without high lift devices or only incorporating simple leading edge slats due to the difficulty of countering the resulting pitching moments. However, there is not a whole lot of information regarding solutions to the landing and takeoff problems associated with a lack of high lift devices, as well as a specific study regarding the feasibility to still apply traditional or non-traditional high lift devices to a blended wing body aircraft. This project aims to provide a detailed study into high lift devices for this type of aircraft and may at the very least show the impossibility of applying current high lift designs, but hopes to determine a method for the opposite – that high lift designs are possible.

1.3 Literature Review

Serious interest in the modern Blended Wing Body (BWB), as applied to very large transport aircraft, formally began in 1988. Dennis Bushnell, then Senior Scientist of NASA Langley Research Center, was concerned with the idea that over the past 50 years there had been a lack of revolutionary advances in terms of commercial airlines. This concern, illustrated by the major similarities in configuration of the original B-47 of the 1940s and current aircraft, caused him to propose the question: "Is there a renaissance for the long-haul transport?" [4]. This sparked the first preliminary design by Robert Liebeck of the McDonnel Douglas Corporation (Figure 1.5). This first design showed that the BWB had significant advantages over the conventional configuration, including an estimated 40% increase in L/D and a 25% reduction in fuel burn [5].

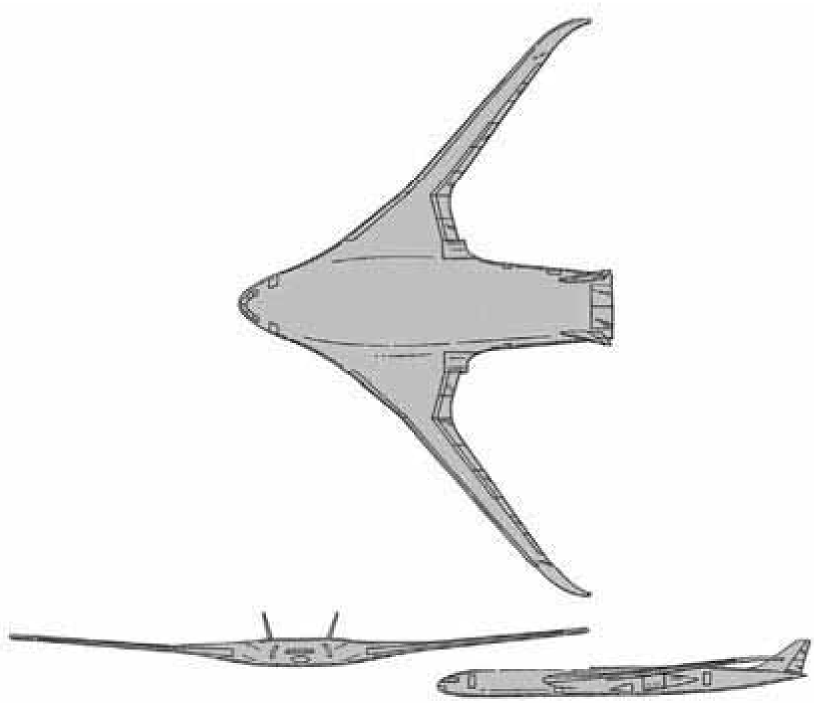

Figure 1.5. *First Generation Blended Wing Body [4]*

The initial success of this first design led to a number of studies throughout the next decade focused on improving this design and addressing some of the issues associated with the BWB. Some of these issues included the structural difficulties associated with the design of a pressurized fuselage which does not have a tubular geometry and stability and control issues associated with tailless aircraft.

In the mid 1990s the focus (taken on by both NASA and McDonnell Douglas) was on designing an 800 passenger BWB transport with a 7,000 nautical mile range. NASA's Advanced Concepts for Aeronautics Program (created in 1994) began a three-year program using this BWB configuration in their analysis. Figure 1.6 provides a three view drawing of the 800 passenger design. Their study recognized the traditional

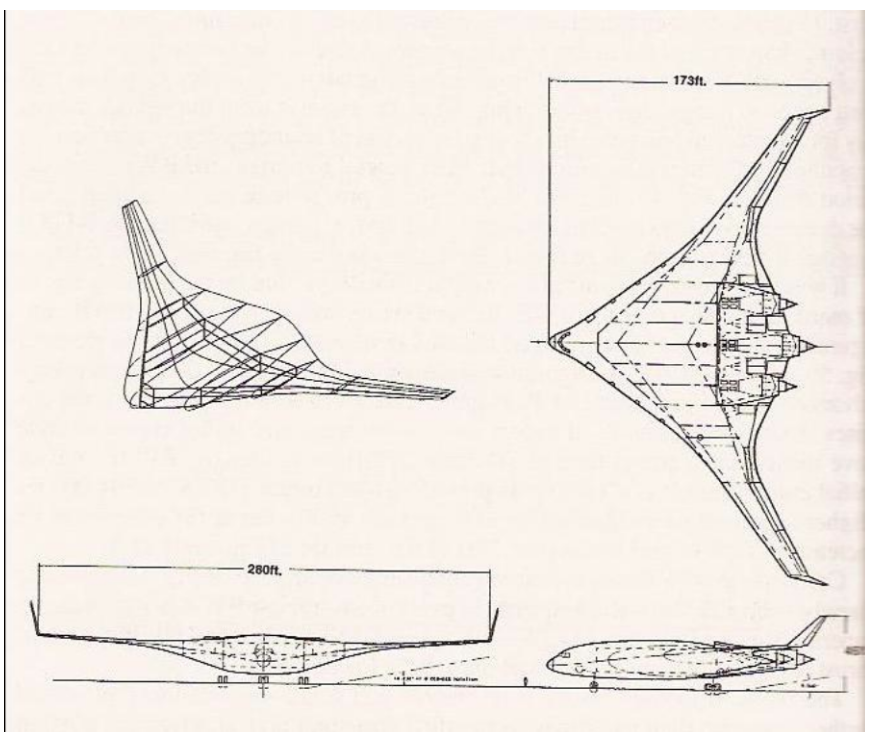

Figure 1.6. *Three View Drawing of 800 Passenger BWB Design [5]*

challenge of low-speed, high lift associated with trailing edge flaps. Their design had no trailing edge flaps, which resulted in a maximum lift less than that of a conventional design. To solve this problem the wing area was increased to lower the wing loading. Also, leading edge slats were used to provide additional lift at high angles of attack [4]. Robert Liebeck, from McDonnell Douglas, explained the balance and control of this configuration as such:

> "To trim the BWB with only centerbody reflex requires a statically unstable airplane, and this instability creates a trimmed lift curve that is higher than untrimmed. Thus, the trim deflections of the elevons add positive flap effect. Combined with the low effective wing loading of the BWB, the beneficial trim effect means that the airplane does not require an exotic high-lift system." [5]

During this study a remote controlled model, shown in Figure 1.7, was created and successfully flown by a team from Stanford led by Professor Ilan Kroo. This model, dubbed the "BWB-17", was a 6% scale model with a 17 ft wingspan. In 1997 the model was flown and successfully demonstrated satisfactory flight characteristics [4].

Figure 1.7. *Remote Controlled 6% Model, BWB-17 [4]*

Also, in the mid 1990s another group from NASA's Advanced Concepts Program, John McMasters from Boeing and Ilan Kroo from Stanford, began to look into another advanced concept related to the BWB: the C-Wing. Shown in Figure 1.8, their C-Wing design was aimed at reducing the wing area necessary for a BWB without high lift devices. Their results however, did not show much of a significant improvement over

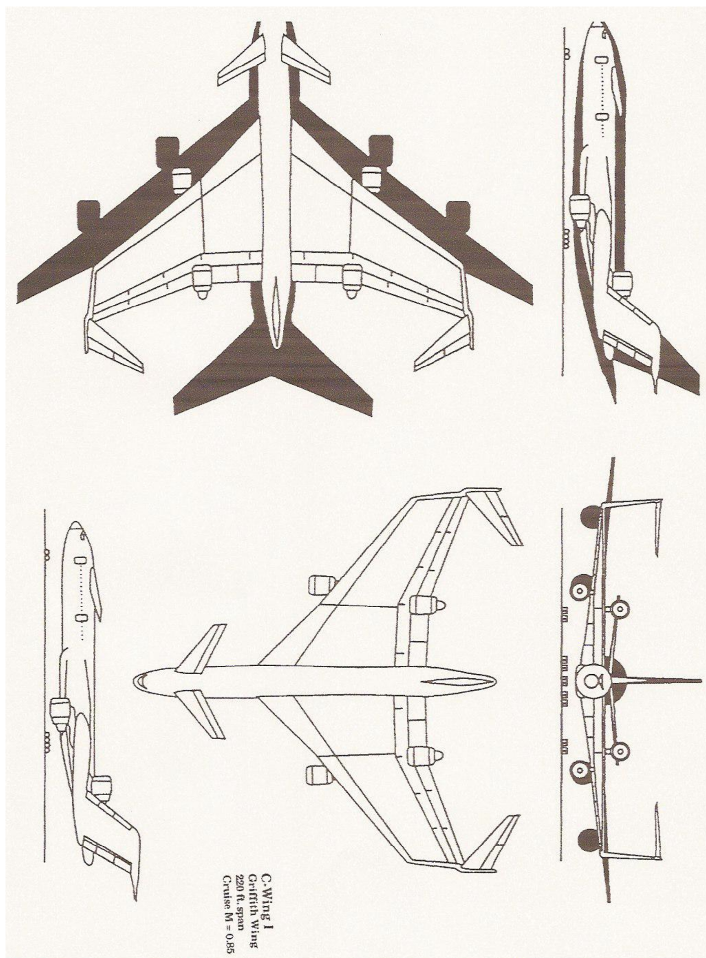

Figure 1.8. *C-Wing BWB Design [6]*

a conventional aircraft though the results claimed to be conservative. The C-Wing also has negative effects such as increased structural weight, stability and control issues, as well as possible trailing wake issues [6].

In 1997, after McDonnell Douglas merged with Boeing, Boeing began a complete reevaluation of the BWB program. The previous designs had shown the benefits and feasibility of a BWB compared to a conventional transport. Now Boeing shifted the BWB from the 800 passenger configuration to a smaller 450 passenger configuration, the BWB-450 (Figure 1.9).

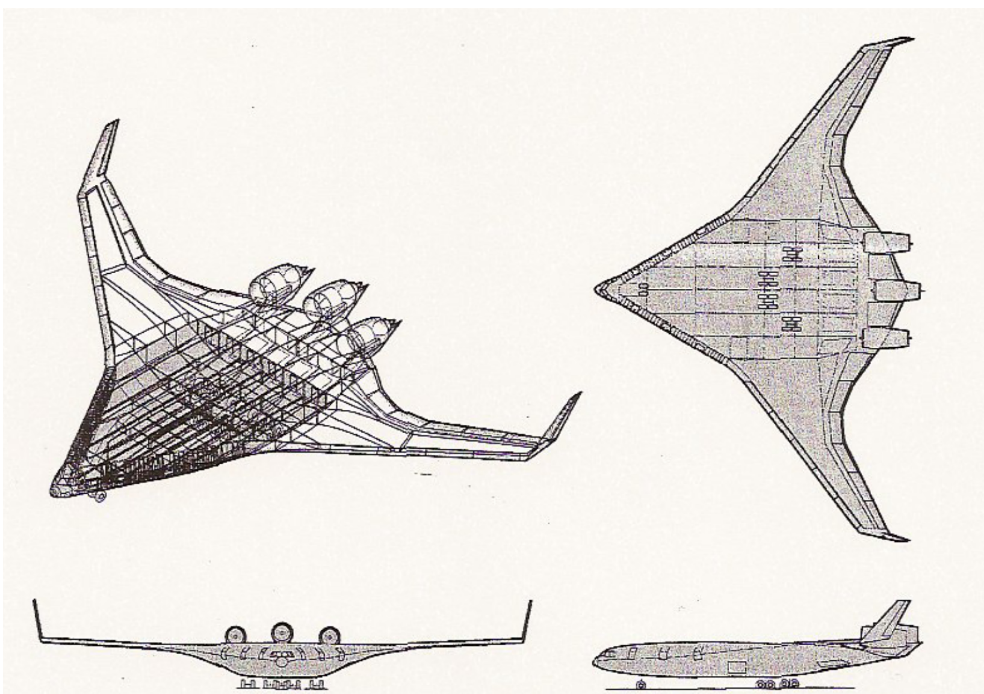

Figure 1.9. *BWB-450 [7]*

In Reference 7, Liebeck provides a summary of the results of the BWB-450 design which was optimized using multidisciplinary design optimization. In his brief description of the stability and control of the aircraft, Liebeck explains how the MDO optimization has caused a significant improvement in stability:

> "Historically, flying wings have been trimmed by sweeping the wing and downloading the wingtips. Whereas this approach allows the wingtips to functionally serve as a horizontal tail, it imposes a significant induced drag penalty. The effective aerodynamic wingspan is less than the physical span, and this penalty is a primary reason that flying-wing airplanes have failed to live up to their performance potential. As described earlier, the first and second generation BWB were allowed to have significantly negative static margins to preserve a near-elliptic spanload. The BWB-450 has been trimmed by a careful distribution of spanload coupled with a judicious application of wing washout. The result is a flying wing airplane that is trimmed at a stable center of gravity (+5% static margin) with all control surfaces faired, and with no induced drag penalty." [7]

The BWB-450 has no trailing edge flaps, only leading edge slats, as Liebeck states in his BWB design requirements.

In 2003, another current BWB design analysis was conducted by Martin Hepperle of the German Aerospace Center, and Wolfgang Heinze of the Technical University of Brunswick [8]. In their analysis they compared a BWB long range transport to a more conventional design. Their BWB configuration, shown in Figure 1.10, did not include any high lift devices and therefore the aircraft could only achieve a $C_{L\ max}$ of about 0.85 when an estimated $C_{L\ max}$ of about 1.8 was needed. This caused unacceptable landing speeds of about 90 m/s [8]. Thus, they concluded that an innovative high lift design was required for the blended wing body aircraft.

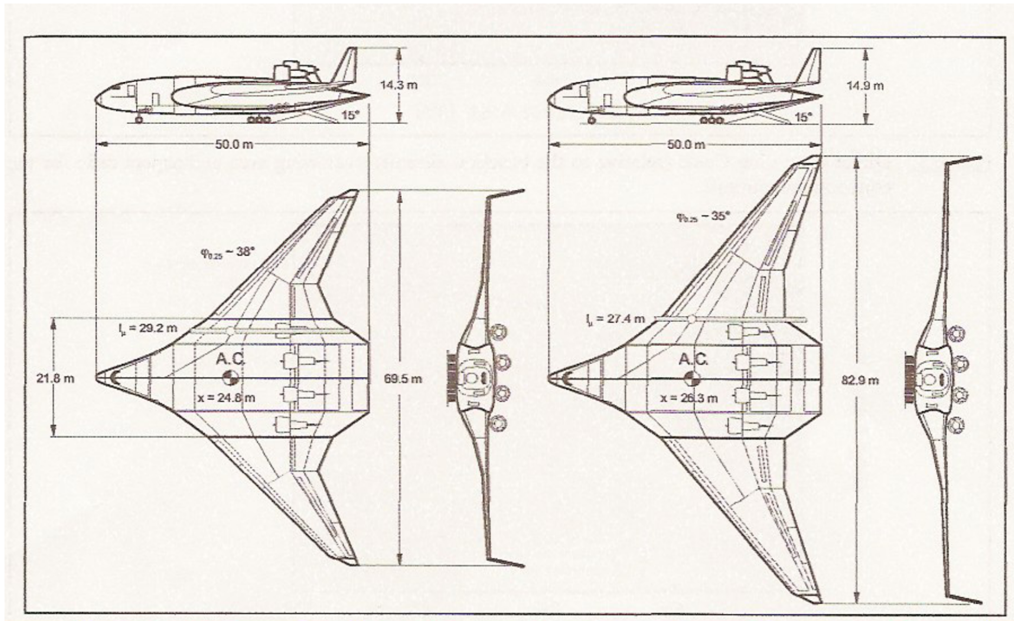

Figure 1.10. *BWB Long Range Transport [8]*

2. Configuration

The configuration used in this analysis is based on the most recent configuration from the ongoing Boeing/NASA design, the BWB-450, summarized in References 2 & 7. This design is the result of a multidisciplinary design optimization and is currently undergoing wind tunnel testing on a scaled down model (X-48B; see Figure 2.1). Therefore, this configuration seems to be the best reference for this project.

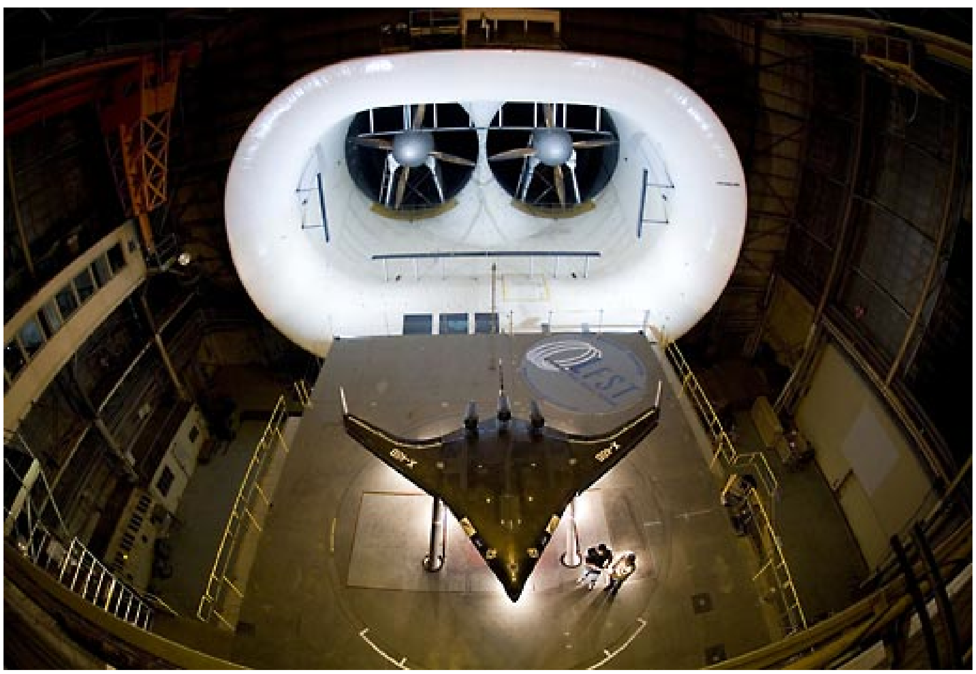

Figure 2.1. *X-48B Blended Wing Body [9]*

2.1 Blended Wing Body Geometry

For obvious reasons, the amount of specific information provided by Boeing and NASA in References 2 & 7 is limited. Therefore, much of the geometry and configuration must be determined using the little information available, as well as estimations and comparisons with other, similar sources/aircraft.

The geometry was determined based on a wingspan of 249 feet, a trapezoidal aspect ratio of 7.55 (both provided in Reference 7), and a scaled drawing of the wing planform shown in Figure 2.2 (from Reference 2). From the trapezoidal aspect ratio and wingspan the trapezoidal reference area can be calculated as 8213 ft^2.

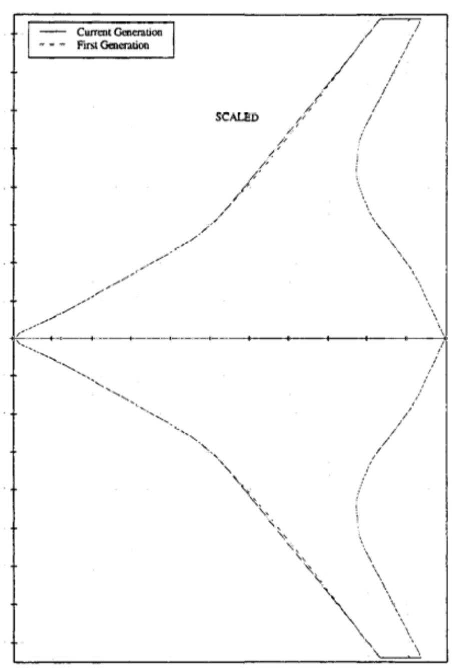

Figure 2.2. *Wing Planform [2]*

To approximate the geometry of the wing, which will be needed to adequately calculate the drag, the wing was divided into two sections, the inner wing and the outer wing. The two sections are divided at the point where the leading edge sweep changes significantly, as seen in Figure 2.2. These two sections also use two different airfoil geometries. Figure 2.3 provides the approximate wing geometry based on Figure 2.2.

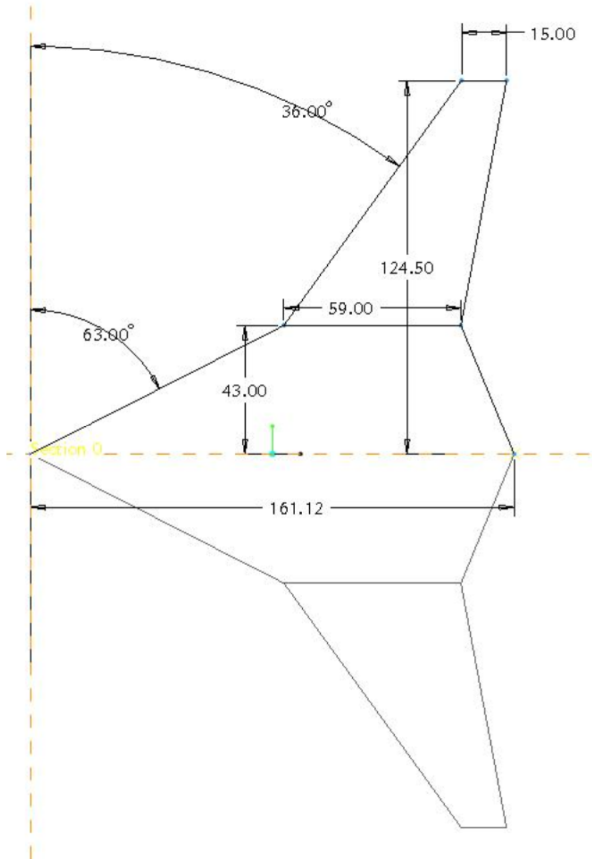

Figure 2.3. *Approximate Wing Geometry*

Though the geometry of Figure 2.3 is not an exact representation of Figure 2.2 it is adequate for this analysis, and should provide accurate drag results.

Other important geometric parameters that will be used to calculate the parasite drag are the maximum thickness ratio, t/c, and the point of maximum thickness of the airfoil, x/c. Figure 2.4 was taken from Reference 2 and was used to approximate the x/c location of the maximum thickness, which is located at the point of minimum pressure. The maximum thickness of the inner portion of the wing is constrained by the necessary cabin height and adequate transonic airfoil performance and is assumed to be limited to 15-17% [10]. The outer portion of the wing is characterized as a supercritical airfoil and has an 8% thickness-to-chord ratio [2] [11].

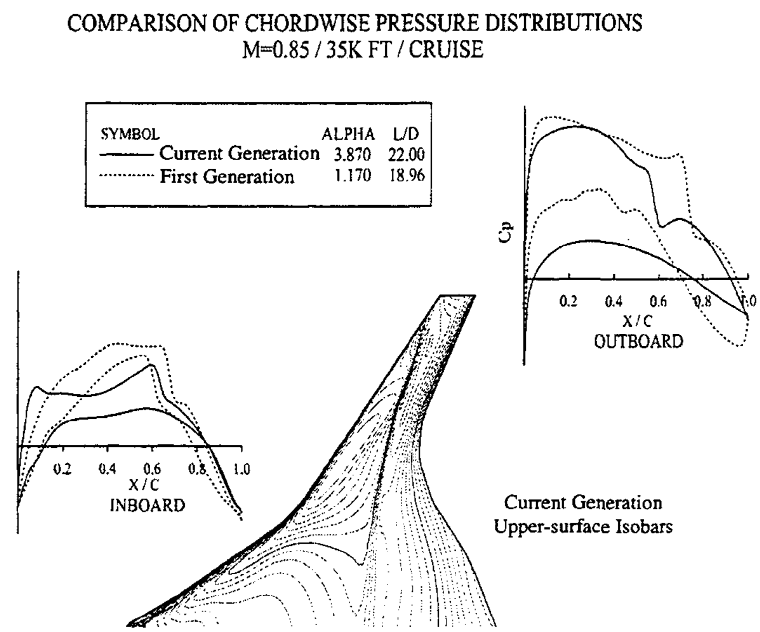

Figure 2.4. *Pressure Distributions For Inboard and Outboard Airfoils [2]*

A summary of the important geometric parameters that will be necessary for this project, along with the equation or reference used to determine each parameter is provided in Table 2.1.

Table 2.1. BWB Geometry

Parameter	Symbol	Value	Units	Eqn or Reference
Wingspan	b	249	ft	Ref. 7
Wing Area	S	15,496	ft^2	$S = S_o + S_i$
Aspect Ratio	AR	4.00	-	$AR = \frac{b^2}{S}$
Trapezoidal Aspect Ratio	AR_{Trap}	7.55	-	Ref. 7
Trapezoidal Reference Area	S_{Trap}	8212	ft^2	$S_{Trap} = \frac{b^2}{AR_{Trap}}$
Inboard Wing Section				
Root Chord	c_o	161	ft	Figure 2.3
Tip Chord	c_t	59	ft	Figure 2.3
Taper Ratio	λ	0.37	-	$\lambda = \frac{c_t}{c_o}$
Half Span	$b_i/2$	43	ft	Figure 2.3
Inboard Wing Area	S_i	9,465	ft^2	$S_i = \frac{c_o(1+\lambda)b_i}{2}$
Mean Aero Chord	MAC	118	ft	$MAC = \frac{2c_o}{3}\frac{1+\lambda+\lambda^2}{1+\lambda}$
Thickness to Chord Ratio	t/c	0.17	-	Ref. 7 & 10
% Chord of Max Thickness	$(x/c)_m$	0.6	-	Ref. 2
Sweep at Max Thickness	Λ_m	30	degrees	Figure 2.3
Outboard Wing Section				
Root Chord	c_o	59	ft	Figure 2.3
Tip Chord	c_t	15	ft	Figure 2.3
Taper Ratio	λ	0.25	-	$\lambda = \frac{c_t}{c_o}$
Half Span	$b_o/2$	81.5	ft	Figure 2.3
Outboard Wing Area	S_o	6,031	ft^2	$S_o = \frac{c_o(1+\lambda)b_o}{2}$
Mean Aero Chord	MAC	41	ft	$MAC = \frac{2c_o}{3}\frac{1+\lambda+\lambda^2}{1+\lambda}$
Thickness to Chord Ratio	t/c	0.08	-	Ref. 10
% Chord of Max Thickness	$(x/c)_m$	0.3	-	Ref. 2
Sweep at Max Thickness	Λ_m	30	degrees	Figure 2.3

2.2 Weight, Propulsion, and Passengers

Other important configuration details include the different weights of the aircraft, the propulsion, and the number of passengers. These will be necessary when studying the aircraft performance at takeoff and landing.

Because this project is ultimately concerned with the takeoff and landing configurations, the two most important weights of the aircraft are its takeoff gross weight (TOGW) and its maximum landing weight (MLW). Both of these can be determined from Reference 7. Though Liebeck does not explicitly state the different weights of the aircraft, he includes an aircraft comparison which claims a specific weight reduction over the Airbus A380-700. This weight reduction is 18% for the maximum takeoff weight. Using the A380 takeoff weight from Reference 1 the takeoff gross weight is calculated as 1,012,700 lbs. In the same way, the maximum landing weight is calculated as 697,820 lbs assuming a similar weight reduction from the A380. The calculations are summarized as follows:

TOGW: (1,235,000 lbs) – 18% = 1,012,700 lbs

MLW: (851,000 lbs) – 18% = 697,820 lbs

The propulsion configuration can easily be viewed from Figure 1.9, repeated below.

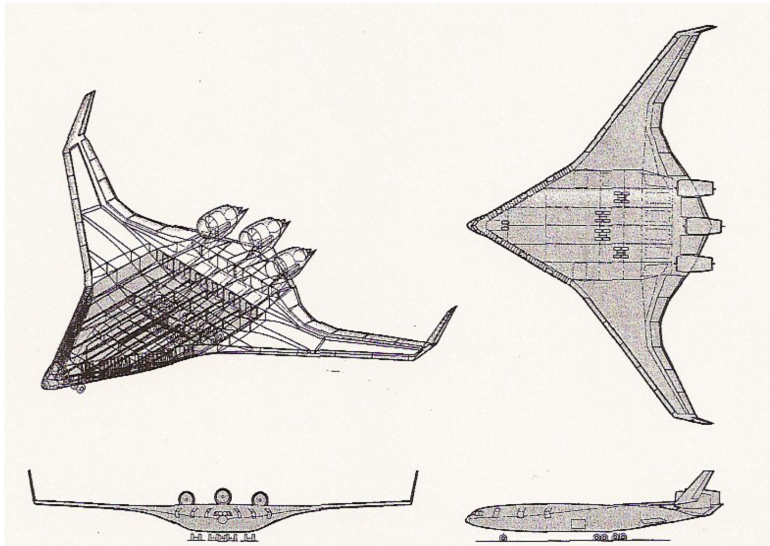

Figure 1.9. *BWB-450 [7]*

This includes 3 pod-mounted engines placed on the top surface, towards the rear of the aircraft, spaced along the centerbody – the middle being on the centerline. Though there is no information provided on the actual engine performance, a variety of turbofan engines will be applied in the analysis based on similar aircraft and engines that are currently available.

As for the number of passengers of the BWB-450, Liebeck in Reference 7 specifically gives a passenger count of 478, based on three-class international rules. All of the configuration data in this section is summarized in Table 2.2, for ease of reference.

Table 2.2. Weight, Propulsion, and Passengers

Weight		**Reference**
Takeoff Gross Weight (TOGW)	1,012,700 lbs	18% Reduction From A380
Maximum Landing Weight (MLW)	697,820 lbs	18% Reduction From A380
Propulsion		
3 Pod-Mounted Engines		Ref. 7
Passenger Count		
478 Passengers		Ref. 7

3. Lift Coefficient

To study the requirements for high lift devices on an aircraft, an analysis of the required lift coefficient for a safe, FAR approved takeoff and landing is important. The required lift coefficient can then be compared to the lift coefficient of the aircraft without high lift devices to determine the necessity for and type of high lift devices.

3.1 Airplane Comparison

The first step in calculating the required lift coefficient is to create a comparison between the configuration used (BWB-450) and aircraft of similar size and passenger count. This comparison presents a starting point for determining the takeoff and landing distances that will be desired for this type of aircraft. This comparison also provides a starting point for the amount of thrust required and type of engine that will be used. Table 3.1 provides a summary of this information as well as data for the BWB-450 configuration, applying two of the different engines that will be used in this analysis.

Table 3.1. Airplane Comparison [12] - [15]

Airplane	Passengers	Max Thrust (lbs)	MTOW (lbs)	MLW (lbs)	Takeoff Distance (ft)	Landing Distance (ft)
747-400 (PW4056)	416 - 524	57100	875000	630000	10500	7400
747-400 (RB211-524G2)	416 - 524	60000	875000	630000	10000	7400
747-400 (CF6-80C2B1)	416 - 524	56500	875000	630000	10500	7400
747-400ER (CF6-80C2B5F)	416 - 524	62100	910000	652000	10500	7800
747-400ER (PW4062)	416 - 524	63300	910000	652000	10200	7800
747-400ER (RB211-524H8-T)	416 - 524	59500	910000	652000	11000	7800
747-400F (CF6-80C2B1)	N/A	62100	875000	666000	10700	7900
747-400ER F (RB211-524H8-T)	N/A	59500	910000	666000	11000	8100
747-400ER F (PW4062)	N/A	63300	910000	666000	10100	8100
747-400ER F (CF6-80C2B5F)	N/A	62100	910000	666000	10400	8100
747-8 (GEnx-2B67)	467	66500	970000	675000	11000	
An-124 (ZMKB D-18T)	N/A	51590	892875	727500	9840	2955
An-225 (ZMKB D-18T)	N/A	51590	1322750		11485	
A380 (Trent 900)	555	76500	1235000	851000	9800	6200
A380F (Trent 900)	N/A	76500	1300727	941374		6800
BWB-450 (Trent 1000)	**478**	**75000**	**1012700**	**697820**		
BWB-450 (Trent 500)	**478**	**56000**	**1012700**	**697820**		

3.2 Takeoff Method

The takeoff analysis begins by first understanding the FAR requirements and definitions for the takeoff field length as well as the required velocities throughout. The field length is defined as the ground distance from rest until the aircraft has cleared a height of 35 feet. Figure 3.1 shows the takeoff field length as well as the velocities along the way.

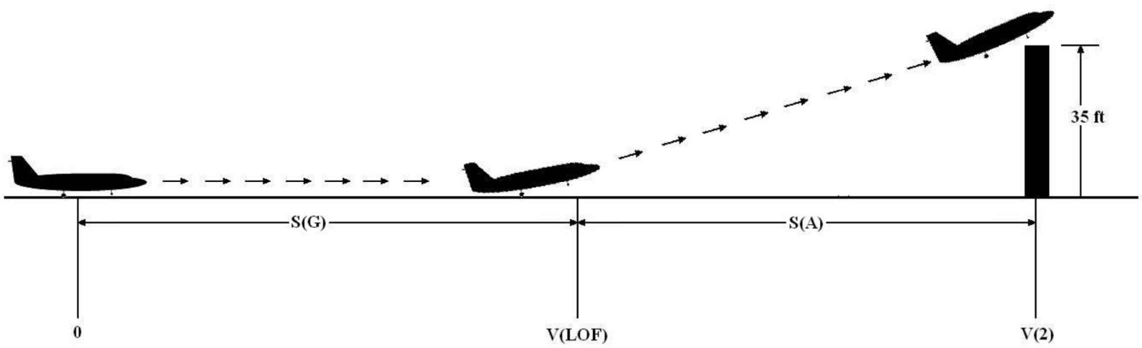

Figure 3.1. *FAR Takeoff Field Length*

For this analysis there are two velocities of importance, V_{LOF} and V_2. V_{LOF} is the lift off velocity, when the aircraft actually leaves the ground. V_2 is the velocity of the aircraft as it reaches the obstacle height of 35 feet. In order to satisfy the FAR takeoff requirements the minimum V_{LOF} must be 10% greater than V_S and V_2 must be 20% greater than V_S. The stall speed, V_S , can be calculated for various values of C_L (using $L=W$ at stall) as:

$$V_s = \sqrt{\frac{2W}{\rho C_L S}} \qquad \text{(Eqn 3.1)}$$

Also, for the airborne distance (V_{LOF} to V_2), FAR requirements limit the C_L to approximately $C_{Lmax}/1.21$ at V_{LOF} and $C_{Lmax}/1.44$ at V_2. Between these two points the C_L is assumed to vary linearly. Therefore the FAR takeoff requirements are summarized as follows:

$$
\begin{gathered}
V_{LOF} = 1.1 V_S \\
V_2 = 1.2 V_S \\
h = 35\,ft \\
@V_{LOF} \rightarrow C_L = \frac{C_{L,\max}}{1.21} \\
@V_2 \rightarrow C_L = \frac{C_{L,\max}}{1.44}
\end{gathered}
$$

The takeoff distance can be calculated within the FAR constraints by separating the takeoff segment into a ground roll (V=0 to V_{LOF}) and airborne distance (V_{LOF} to V_2) and applying a simple force balance for each.

3.2.1 Ground Roll

By applying a force balance in the horizontal direction, an equation for the acceleration of the aircraft can be obtained:

$$a = \frac{g}{TOGW}\left[T - D - \mu(TOGW - L)\right] \qquad \text{(Eqn 3.2)}$$

where:

T = Thrust
D = Total Drag
μ = Friction Coefficient
$TOGW$ = Takeoff Gross Weight
L = Lift

Each of the terms in this equation are either constants or can be represented as a function of velocity for a given C_L. The method and equations for thrust, drag, and lift are provided in Section 3.4. The friction coefficient, μ, is dependent on the type of runway surface. For this analysis a value of 0.03 is used, corresponding to a hard, dry, paved surface [11] [16].

Since the acceleration is now represented as a function of velocity, the ground roll can be broken up into a number of segments where for each segment the acceleration is considered to be constant. For ease in calculations the segments have been broken up into segments of time with length Δt. From the initial conditions that $V_o = 0$ and $s_o = 0$ (s_o is the horizontal distance) the acceleration, a_o can be obtained from Equation 3.2. The velocity and distance at the next point can be obtained using simple equations of motion for a constant acceleration over a given time:

$$V_{i+1} = V_i + a_i \Delta t \qquad \text{(Eqn 3.3)}$$

$$s_{i+1} = s_i + V_i \Delta t + a_i \frac{(\Delta t)^2}{2} \qquad \text{(Eqn 3.4)}$$

This process is then repeated until the velocity has reached the FAR constraint velocity of V_{LOF} so that the process ends with:

$$\begin{gathered} V_{i+1} = V_{LOF} \\ s_{i+1} = S_G \end{gathered}$$

Where S_G is the ground roll distance.

3.2.2 Airborne Distance

The airborne distance is calculated in a similar way, only with a few added conditions. There are now two FAR constraints to determine the airborne distance, V_2 and h. Also, it is known that the aircraft lifts off the ground at V_{LOF} and S_G, but what is not known is the initial angle of the aircraft at liftoff. Beginning in the same way as the ground roll, a summation of forces along the flight path and normal to it gives an equation for the acceleration and dθ/dt (where θ is the aircraft angle):

$$a = \frac{g}{TOGW}\left(T - D - TOGW\,\sin\theta\right) \qquad \text{(Eqn 3.5)}$$

$$\frac{d\theta}{dt} = \left(L - TOGW\,\cos\theta\right)\left(\frac{g}{V \cdot TOGW}\right) \qquad \text{(Eqn 3.6)}$$

Beginning with the initial conditions of V_{LOF}, $s_o = 0$, and $\theta_o = 0$ and by approximating Equation 3.6 as Δθ/Δt, the velocity at the next point can be calculated in a similar fashion as the ground roll distance – using the equations of motion (Eqn 3.3 and 3.4). However Equation 3.4 needs to be modified to calculate the ground distance as opposed to the flight path distance and therefore becomes:

$$s_{i+1} = s_i + \left(V_i \Delta t + a_i \frac{(\Delta t)^2}{2}\right)\cos\theta \qquad \text{(Eqn 3.4')}$$

The height of the aircraft can be calculated using the rate of climb of the aircraft, dh/dt, which is given by:

$$\frac{dh}{dt} = V\sin\theta \qquad \text{(Eqn 3.7)}$$

Where this is approximated as Δh/Δt.

As stated earlier the FAR constraints of both the height and V_2 must be achieved. Also, though the initial condition of $\theta_o = 0$ is used, this is not necessarily valid. The aircraft angle at liftoff does not need to be zero. To solve this issue, and assure both FAR constraints are achieved the iteration procedure is first run with $\theta_o = 0$ until the final velocity is equivalent to V_2. The final height is then checked to see if the aircraft has reached the necessary altitude of 35 feet. If this constraint has not been met the process is repeated with a slight increase in θ_o and continued until both FAR constraints have been met. This method must be very precise, however, because as θ_o is increased the final height will increase but the aircraft acceleration will decrease and it will take longer for the aircraft to reach V_2. Also, there will be a point where θ_o is so high that the aircraft will never reach V_2. Figure 3.2 shows the variation of height (for a specific $C_{L,max}$ and propulsion system) as the aircraft accelerates to V_2 and how θ_o is increased to meet the 35 ft requirement at V_2.

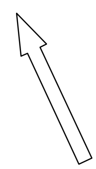

Figure 3.2. *Takeoff Climb to 35 ft Obstacle (Height vs. Velocity)*

Figure 3.3 provides the takeoff trajectory for a specific case (of $C_{L,max}$ and propulsion system), as θ_o is increased to meet the 35 ft requirement. This figure also shows how the airborne distance increases as θ_o increases.

Figure 3.3. *Takeoff Trajectory For Increasing Values of θ_o*

One important consideration is that the change in θ_o and Δt must be small enough so that the solution does not have such a "jump" from one segment to the next that the closest values become much greater than the necessary constraints – meaning that at one segment the constraints have not yet been met while at the next segment the values are significantly larger than the constraints and therefore the solution is found there – these would be inaccurate results.

In the same way as the ground roll distance, the airborne distance and final velocity are determined, once all the constraints have been satisfied, as:

$$V_{i+1} = V_2$$
$$s_{i+1} = S_A$$

Where S_A is the airborne distance.

From this method, given a C_L value, the minimum takeoff distance can be calculated that satisfies the FAR requirements. Therefore, the C_L required can be determined from a desired field length.

3.2.3 Sensitivity Study

When using a segment method where parameters are estimated/assumed constant across the segment, obviously the size of the segment, in this case Δt, is important. The smaller Δt is, the more accurate the solution, but the greater the runtime. Therefore it is important to do a study into the sensitivity of the results with varying values of Δt in order to determine the maximum Δt allowable to obtain accurate results. Figure 3.4 provides the results of the sensitivity study. From this figure it can be seen that below a

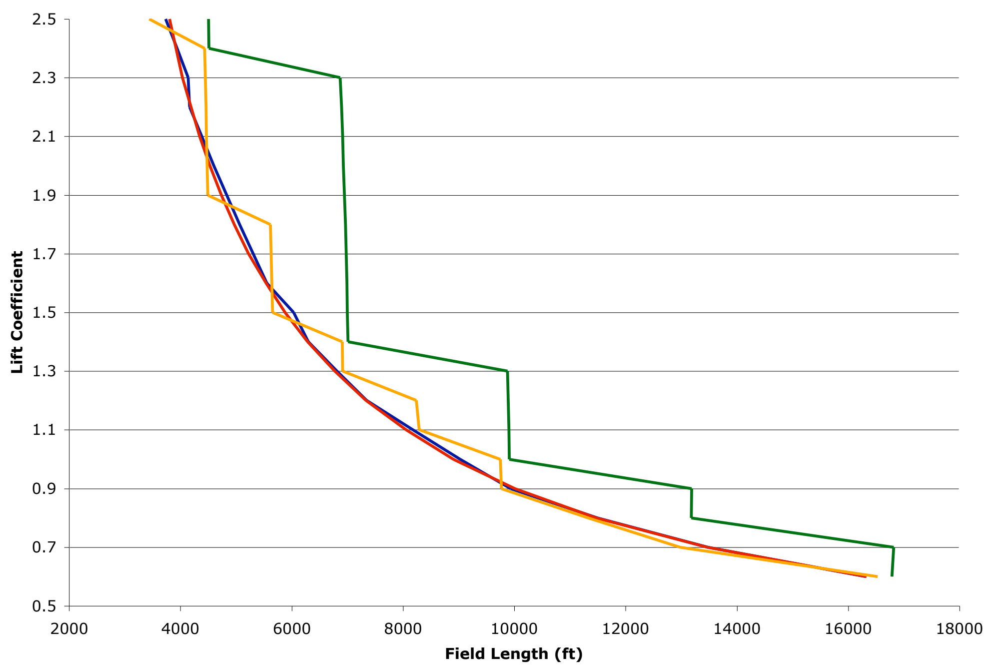

Figure 3.4. *Takeoff Sensitivity Study*

Δt value of approximately 1 second the data seems to converge – meaning there is little variation in the results as Δt is decreased further. From this study a value of 0.1 sec for Δt will be used for all takeoff calculations.

3.3 Landing Method

The landing analyses is similar to the takeoff analyses in that they both use a segment method with the governing equations based on a simple force balance and the equations of motion. The entire landing distance is also based on the FAR constraints which include the clearance over a 50 foot obstacle with an approach velocity 30% greater than V_S , until the aircraft comes to a complete stop. There is also a correction factor of 1.667 to accommodate for an engine inoperative situation. The FAR requirements are summarized as:

$$V_A = 1.3V_s$$
$$h = 50\,ft$$
$$S_{total} = 1.667\left(S_A + S_T + S_G\right)$$

Where V_A is the approach velocity and S_A , S_T , and S_G are the approach, transition, and ground distances, respectively.

The landing distance is calculated by dividing the field length into three areas: approach, transition, and ground roll. By using an incremental distance segment method (using Δx instead of Δt, as in the takeoff case) the calculations work backward from the end of the runway where the velocity is zero to the point where the aircraft has cleared a 50 ft obstacle. Figure 3.5 shows the entire landing distance, from the approach over a 50 foot obstacle to the point where the aircraft comes to a complete stop.

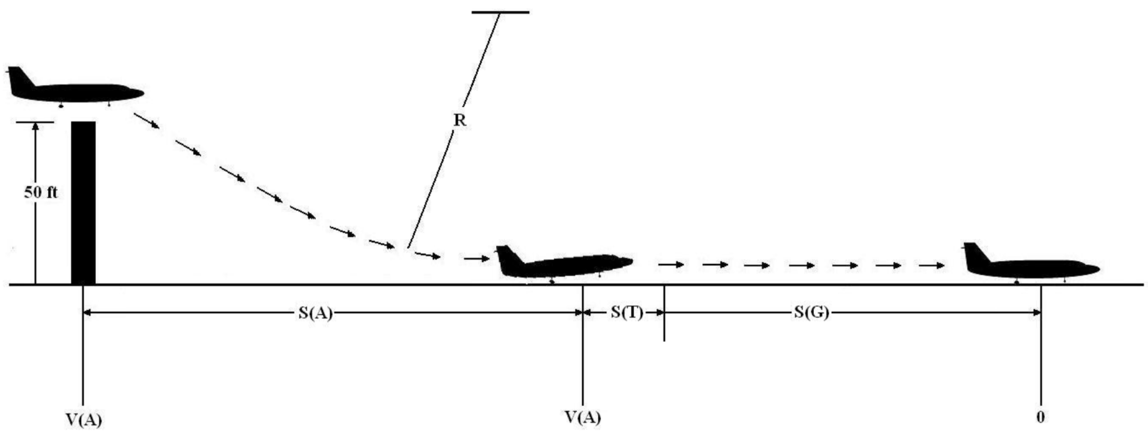

Figure 3.5. *FAR Landing Field Length*

3.3.1 Ground Roll & Transition

The landing ground roll analysis is very similar to the takeoff ground roll analysis. The deceleration is calculated using the force balance equation:

$$a = \frac{g}{W}\left[D + \mu \cdot W\right] \qquad \text{(With spoilers)} \qquad \text{(Eqn 3.8)}$$

$$a = \frac{g}{W}\left[D + \mu(W - L)\right] \qquad \text{(Without spoilers)} \qquad \text{(Eqn 3.9)}$$

Where μ is the breaking friction coefficient (0.5 is used in this analysis [11] [16]). Using the initial conditions of $V_o = 0$ and $s_o = 0$, and the input segment length Δx, the velocity can be calculated using an equation of motion:

$$V_{i+1} = \sqrt{2a_i \Delta x + V_i^2} \qquad \text{(Eqn 3.10)}$$

and the distance can simply be calculated by:

$$S_G = \Delta x \cdot (i+1) \qquad \text{(Eqn 3.11)}$$

The transition portion of the ground roll provides for a 2 second delay for the pilot to transition from landing to braking configurations. Therefore this value is simply calculated as:

$$S_T = 2(V_A) \qquad \text{(Eqn 3.12)}$$

3.3.2 Approach

The approach distance is calculated using a constant glide slope and flare with radius R. Figure 3.6 provides a representation of this approach method and the distance is calculated as:

$$S_A = \frac{50}{\theta_D} + \frac{R\theta_D}{2} \qquad \text{(Eqn 3.13)}$$

Where θ_D is the glide slope angle (3° for ILS).

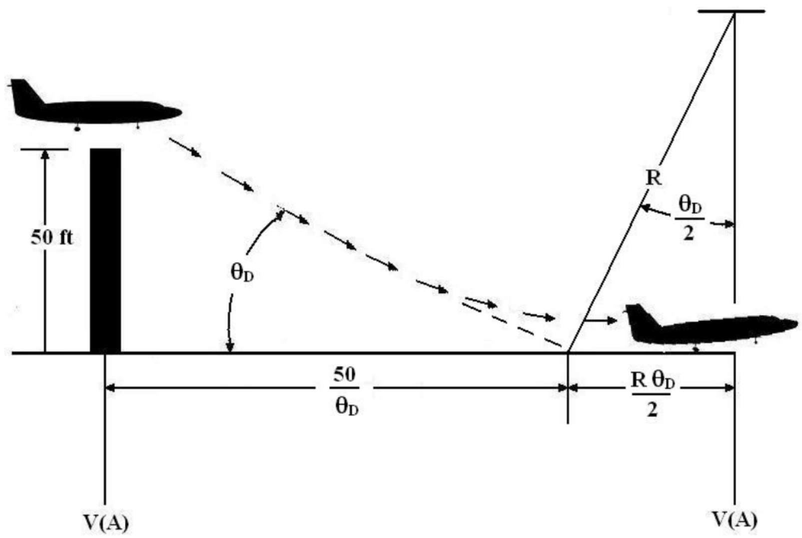

Figure 3.6. *Approach*

The radius of the flare, R, is determined by equating the normal acceleration in terms of the radius ($a_n = V_A^2/R$) with the force balance in the normal direction. This results in:

$$R = \frac{V_A^2}{g(L/W - 1)} \qquad \text{(Eqn 3.14)}$$

Instead of calculating the total landing distance based on the FAR required V_A, which is one way to approach the solution, the method used was based on a fixed input field length. The result from the equations is a final V_A for a given field length and C_L. The segment model does this by calculating first the ground distance for one segment and then the approach and transition distances based on $V_A = V_{i+1}$. The total distance, S_{total} , is then compared to the input field length. If the distance is less, the method begins again and goes one segment further on the ground roll (thus determining the value of *i* in Eqn 3.11) and recalculates the approach and transition distances. This process continues until the total distance is equal to the input field length. Figure 3.7 shows how the number of segments of ground roll is increased until the desired field length is reached, which results in a specific required approach velocity. This approach velocity is the maximum allowable velocity in order for this aircraft to land in the given field length with a specific C_L. It is easy to see from Figure 3.7 that if the approach velocity is less, the landing distance will be less, and vice versa.

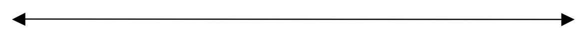

Figure 3.7. *Landing Trajectory For Various Number of Ground Segments*

The results of this method provide a data curve relating the C_L and V_A for a given field length. These results can be compared to the FAR required values for V_A for different C_L's thus providing the minimum allowable C_L for a given landing field length.

3.3.3 Sensitivity Study

In a similar way as the takeoff analysis, a sensitivity study must also be carried out for the landing analysis. This will define the necessary value of Δx in order to get accurate solutions. If Δx is too big, not only will the constant acceleration assumption be invalid, but the solution may "jump" past the solution from one increase in *i* for the ground roll. Figure 3.8 shows the results of the sensitivity study. From this figure a value of approximately 0.25 feet and smaller will provide very accurate results.

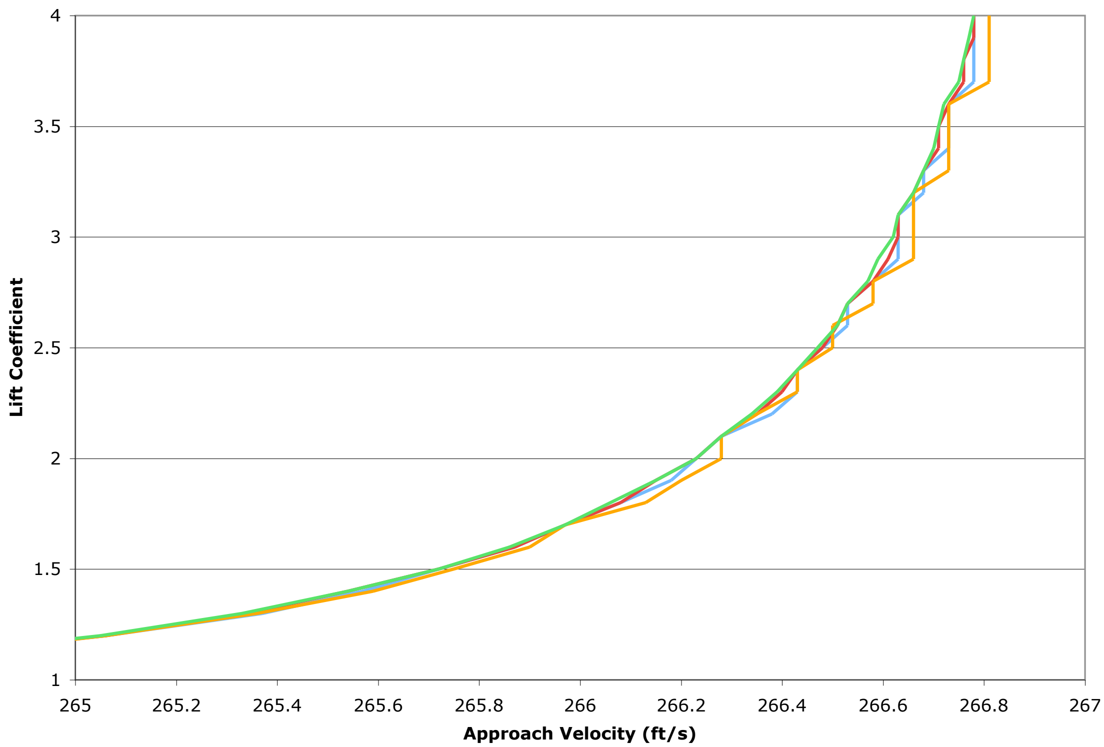

Figure 3.8. *Landing Sensitivity Study*

3.4 Lift, Drag, and Thrust

In order to properly calculate the lift coefficient required for takeoff and landing using the methods discussed, the lift, drag, and thrust forces must be defined as functions of velocity (for a given C_L).

Lift:

$$L = \frac{1}{2}\rho V^2 S C_L \qquad \text{(Eqn 3.15)}$$

Drag:

The drag is divided into two components: the induced drag and the parasite drag. The induced drag is calculated assuming (optimistically) an elliptical lift distribution, which is one of the goals of the blended wing body aircraft. Because this analysis is concerned with takeoff and landing it is important to take into account the ground effect on the induced drag. Reference 11 provides a factor which, when multiplied by the induced drag coefficient, takes into account the ground effect.

Induced Drag Coefficient:

$$C_{Di} = \frac{C_L^2}{\pi AR} \qquad \text{(Eqn 3.16)}$$

Correction for Ground Effect:

$$\left(C_{Di}\right)_{IGE} = C_{Di} \cdot \frac{33(h/b)^{1.5}}{1 + 33(h/b)^{1.5}} \qquad \text{(Eqn 3.17)}$$

***For landing with spoilers, zero lift is assumed for the ground roll, so the induced drag is also neglected.*

Parasite Drag Coefficient:

The parasite drag is calculated using a method provided by Daniel Raymer in Reference 11. The equations are as follows:

$$C_{Do} = C_f \cdot FF \cdot \frac{S_{wet}}{S} \qquad \text{(Eqn 3.18)}$$

Skin friction coefficient (for turbulent flow):

$$C_f = \frac{0.455}{(\log_{10} \mathrm{Re})^{2.58}\left(1+0.144M^2\right)^{0.65}} \qquad \text{(Eqn 3.19)}$$

$$\mathrm{Re} = \frac{\rho V(MAC)}{\mu} \qquad \text{(Eqn 3.20)}$$

Form factor (wing):

$$FF = \left[1+\frac{0.6}{(x/c)_m}\left(\frac{t}{c}\right)+100\left(\frac{t}{c}\right)^4\right]\left[1.34M^{0.18}(\cos\Lambda_m)^{0.28}\right] \qquad \text{(Eqn 3.21)}$$

where:

$\left(\frac{x}{c}\right)_m$ = max thickness Λ_m = sweep of max thickness

$$\frac{S_{wet}}{S} = 1.977 + 0.52(t/c) \qquad \text{(Eqn 3.22)}$$

Thrust:

The thrust calculations are based on the assumptions for an ideal turbojet engine. If the gas is calorically perfect throughout, the exit pressure is equal to the ambient pressure, and the fuel to air ratio is much less than one, the ideal thrust relation is given as [17]:

$$T = \dot{m}\left(V_e - V_o\right) \qquad \text{(Eqn 3.23)}$$

3.5 Results

The results of the takeoff and landing analysis described above are summarized in Tables 3.3 - 3.5. Table 3.2 provides the engine data used for the takeoff analysis. Five different engines were chosen for this study with varying thrust values. These engines were chosen to give a variety of thrust values (within the range for this type of aircraft) as well as a variety of prominent engine manufacturers (Rolls Royce, Pratt & Whitney, and General Electric). References 13, 18, and 19 provide the maximum thrust and flow rate data. The corresponding exit velocities can be calculated using Equation 3.23 (in the previous section) with $V_o = 0$ for maximum thrust.

Table 3.2. Engine Data [13, 18, 19]

Engine	Max Thrust (lbs)	Mass Flow Rate (lb/s)	Exit Velocity (ft/s)
Trent 1000	75000	2670	904
PW4168	68600	1990	1109
CF6-80E1	66870	1926	1117
PW4060	60000	1800	1072
Trent 500	56000	1939	929

From the airplane comparison presented in Table 3.1 the desired takeoff field length for this aircraft was determined to be between 9000 – 11000 feet. Therefore the required lift coefficient was calculated for field lengths of 9000, 10000, and 11000 feet for each of the engines provided in Table 3.2. Figure 3.9 provides the output from the takeoff segment procedure: the lift coefficient vs. field length curve, for each engine. By looking at the C_L corresponding to the desired field length the data in Table 3.3 was determined.

Figure 3.9. *Takeoff Results*

Table 3.3. Required Lift Coefficient Results: Takeoff

Engine	Max Thrust (lbs)	Field Length (ft)	C(L)	V2 (ft/s)
Trent 1000	75000	9000	1.0	281.81
		10000	0.9	297.05
		11000	0.85	305.66
PW4168	68600	9000	1.05	275.02
		10000	0.95	289.13
		11000	0.85	305.66
		9000	1.05	275.02

CF6-80E1	66870	10000	0.95	289.13
		11000	0.875	301.26
PW4060	60000	9000	1.25	252.06
		10000	1.1	268.69
		11000	1	281.81
Trent 500	56000	9000	1.425	236.07
		10000	1.275	249.57
		11000	1.15	262.79
TOGW (lbs) =	1012700			

Also, from the airplane comparison table, values for the desired landing field length were determined to be 6000, 7000, and 8000 feet. Figure 3.10 provides the resulting landing data, C_L vs. V_A , for landing with and without spoilers at the take off gross weight (1,012,700 lbs). The figure also includes the curve (green) which represents the minimum required FAR approach speed, V_A. Therefore, where the two curves coincide represents the minimum required C_L for that specific configuration. Figure 3.11 provides the same data only for the maximum landing weight (698,720 lbs). From these two figures the data of Table 3.4 and 3.5 could be determined.

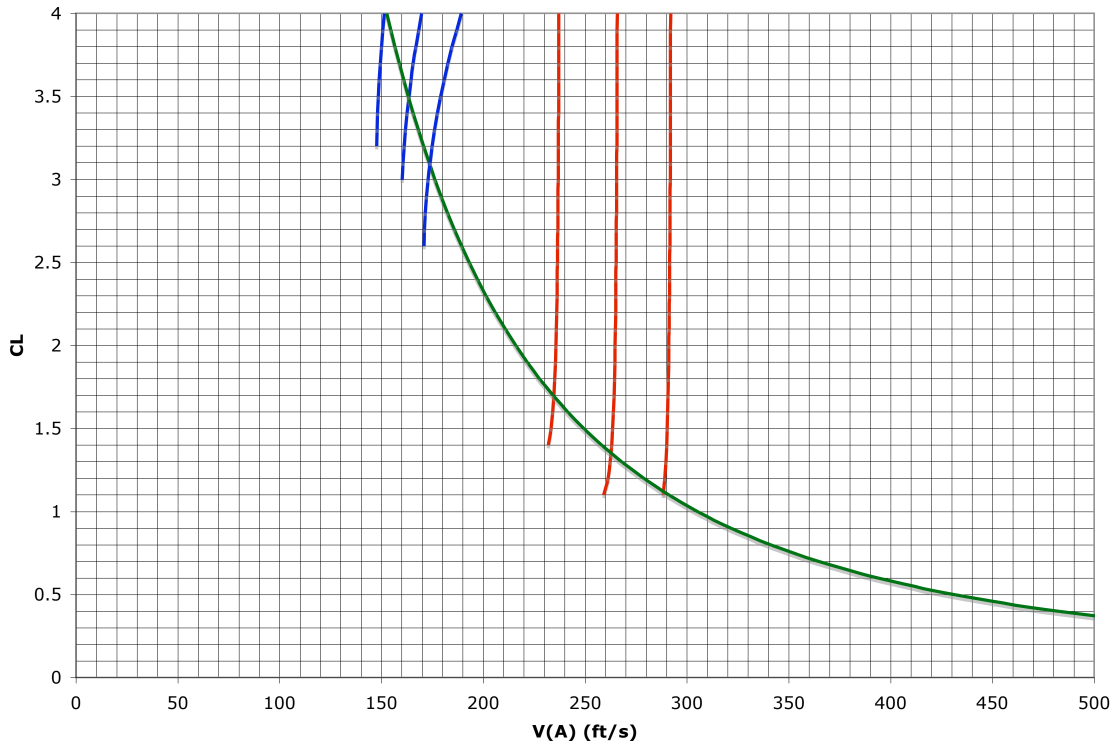

Figure 3.10. *Landing Results At TOGW (1,012,700 lbs)*

The data from Figures 3.10 and 3.11, the results of the method described above, is labeled in the tables as the "Segment" method. The other data in Tables 3.4 & 3.5 is the result of using a constant deceleration, calculated at a velocity of $V_A/\sqrt{2}$. This constant deceleration method was used to validate the data obtained from the segment method and is presented in Reference 16. The data in Table 3.4, representing landing without spoilers, shows a very close agreement between the two methods. Table 3.5, representing landing with spoilers, shows some difference between the two. This seems expected and acceptable because the constant deceleration at $V_A/\sqrt{2}$ is not specifically described as taking into account the effects created without spoilers.

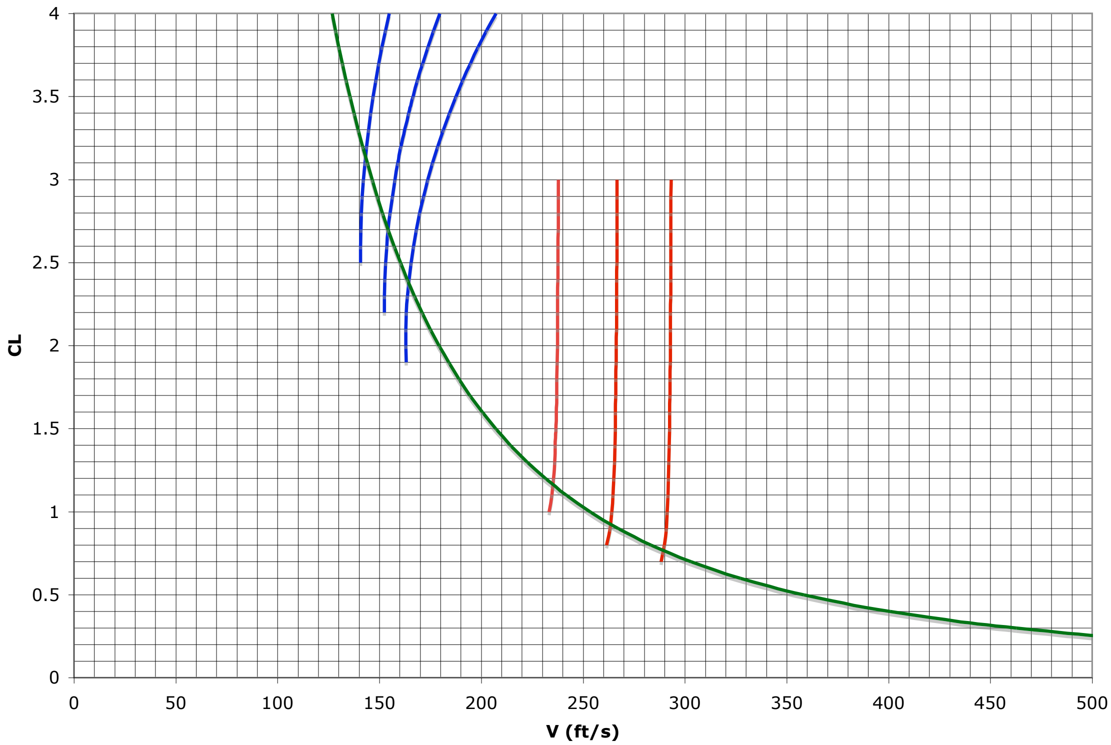

Figure 3.11. *Landing Results At MLW (697,820 lbs)*

Table 3.4. Required Lift Coefficient Results: Landing With Spoilers

Method	Weight (lbs)	Field Length (ft)	CL	V_a (ft/s)
Segment	697820	6000	1.15	235
Constant Ac	697820	6000	1.15	236
Segment	1012700	6000	1.7	235
Constant Ac	1012700	6000	1.7	234
Segment	697820	7000	0.9	263
Constant Ac	697820	7000	0.9	267
Segment	1012700	7000	1.35	262
Constant Ac	1012700	7000	1.35	262
Segment	697820	8000	0.75	289
Constant Ac	697820	8000	0.75	292

Segment Constant Ac	1012700 1012700	8000 8000	1.1 1.1	288 291

Table 3.5. Required Lift Coefficient Results: Landing Without Spoilers

Method	Weight (lbs)	Field Length (ft)	CL	V_a (ft/s)
Segment Constant Ac	697820 697820	6000 6000	3.15 3.6	143 133
Segment Constant Ac	1012700 1012700	6000 6000	4 >4.0	151 <152
Segment Constant Ac	697820 697820	7000 7000	2.7 3.1	154 144
Segment Constant Ac	1012700 1012700	7000 7000	3.5 4	163 152
Segment Constant Ac	697820 697820	8000 8000	2.35 2.75	164 153
Segment Constant Ac	1012700 1012700	8000 8000	3.1 3.6	174 161

4. Longitudinal Stability

4.1 Static Longitudinal Stability – Basic Requirements

The basic idea of stability is based on the principle that if an object or system at equilibrium is perturbed it will either return to its original state, remain in the perturbed state, or continue to change to a different state. The system is said to be stable if, after being perturbed, it returns to the initial state. In terms of the longitudinal stability of an aircraft, the equilibrium state refers to the trim position in which the aircraft is under no acceleration in pitch, i.e. the pitching moment is zero, and the stability requirement means the aircraft will have a tendency to return to this trimmed state if perturbed (an applied nose up or nose down moment due to a gust, for example). Figure 4.1 provides the two basic pitch relations of an aircraft. The aircraft is at trim at some angle of attack, α. If it then undergoes some type of pitch up moment, such as a wind gust, which increases the angle of attack, the aircraft can then react to this increased angle of attack by producing a nose up (unstable) or a nose down (stable) pitching moment. If the aircraft produces a nose down moment, the angle of attack will then decrease and the aircraft will return to the trim location – this is the stable condition. If the aircraft produces a nose up moment, the angle of attack will increase further and the aircraft will move further and further away from the trim location – this is the unstable condition. These two conditions are represented in Figure 4.1.

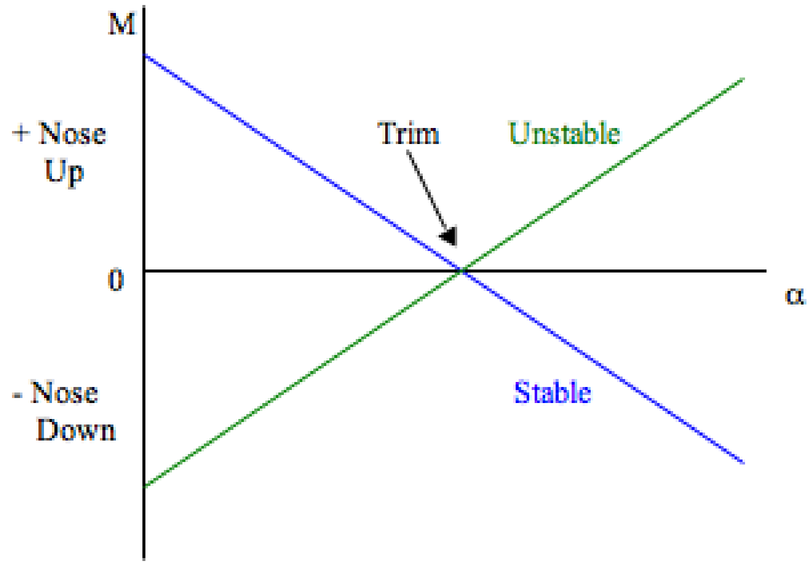

Figure 4.1. *Aircraft Pitching Moment vs Angle of Attack*

From the stable plot of pitching moment versus angle of attack in Figure 4.1, two basic longitudinal stability requirements can be determined in order to produce this relation between pitching moment and angle of attack:

1. The slope of the M-α relation must be negative, or:

$$\frac{dM}{d\alpha} < 0 \qquad \text{(Eqn 4.1)}$$

2. At a zero angle of attack the moment must be positive, or:

$$M > 0 \ @ \ \alpha = 0 \qquad \text{(Eqn 4.2)}$$

Requirement #1:

The first requirement, Equation 4.1, states that as the angle of attack increases, the pitching moment must decrease (nose down). In order for this to be satisfied this requires that the center of gravity be in front of the aerodynamic center of the aircraft in terms of their chordwise location. This is because the lift force is assumed to act at the aerodynamic center (of the aircraft) and increases as the angle of attack increases. Therefore the pitching moment of the aircraft (about the center of gravity) will decrease as the angle of attack increases only if the aerodynamic center is behind the center of gravity (this refers to a positive static margin – the chordwise distance between the center of gravity and aerodynamic center).

Requirement #2:

In order to satisfy the second requirement, Equation 4.2, typical aircraft use a horizontal tail which creates a positive pitching moment on the aircraft. Tailless aircraft such as the blended wing body, typically use a reflexed airfoil or washout combined with a swept wing (greater lift at the root than the tip creates a positive pitching moment). The reflexed airfoil is shaped in such a way that the moment about the airfoil aerodynamic center is positive, as opposed to a typical cambered airfoil which has a negative moment.

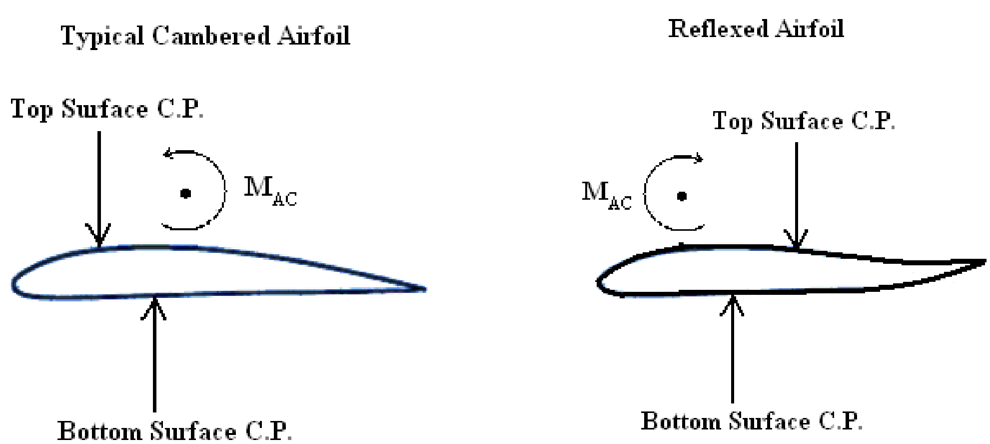

Figure 4.2. *Airfoil Moments: Typical and Reflexed*

4.2 Aerodynamic Center and Moment

The calculation of the location of the aerodynamic center becomes more complex than a typical wing due to the cranked wing shape. Therefore, a general approach is necessary. This approach follows the method of Reference 15. Referring to Figure 4.3, the point A corresponds to the point on the aircraft centerline that runs through the local aerodynamic center line (the red line). The moment about point A is determined by integrating along the span of the wing the local moment (about the local aerodynamic center) as well as the moment due to the local lift force.

$$M_A = q\int_{-b/2}^{b/2} c^2 C_{m,ac}\,dy - q\int_{-b/2}^{b/2} cC_l\,y\tan(\Lambda)\,dy \qquad \text{(Eqn 4.3)}$$

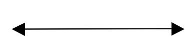

Figure 4.3. *Aerodynamic Center*

It also follows from Figure 4.3 that the moment about the aerodynamic center of the wing can be calculated as:

$$M_{ac} = M_A + LX_A \qquad \text{(Eqn 4.4)}$$

From the definition of the aerodynamic center, the derivative of the moment about the aerodynamic center with respect to α must be zero. Solving for X_A this yields:

$$X_A = -\frac{M_{A\alpha}}{L_\alpha} \qquad \text{(Eqn 4.5)}$$

Where:

$$L_\alpha = q\int_{-b/2}^{b/2} cC_{l\alpha} dy \qquad \text{(Eqn 4.6)}$$

And $M_{A\alpha}$ is found by differentiating Equation 4.3:

$$M_{A\alpha} = q\left[-\int_{-b/2}^{b/2} cC_{l\alpha} y \tan(\Lambda) dy\right] \qquad \text{(Eqn 4.7)}$$

Combining Equations 4.5 – 4.7 gives the equation of the distance of the aerodynamic center behind point A:

$$X_A = \frac{\int_0^{b/2} cC_{l\alpha} y \tan(\Lambda) dy}{\int_0^{b/2} cC_{l\alpha} dy} \qquad \text{(Eqn 4.8)}$$

Therefore the aerodynamic center location (from the nose of the aircraft) is:

$$X_{AC} = X_A + x_{ac,y=0} \qquad \text{(Eqn 4.9)}$$

Since c(y) and the sweep angle, Λ, are defined along the wing the only unknown variable in Equation 4.8 is the local lift curve slope of the airfoil. Therefore, once the airfoil is defined for the span of the wing (airfoil selection and aerodynamic twist) the aerodynamic center can be determined.

The moment about the aerodynamic center of the aircraft can then be calculated from Equation 4.4 once X_A is found. This becomes:

$$C_{Mac} = \frac{2}{S}\left[\int_0^{b/2} c^2 C_{m,ac}\,dy - \int_0^{b/2} cC_l\, y\tan(\Lambda)\,dy + X_A \int_0^{b/2} cC_l\,dy\right] \qquad \text{(Eqn 4.10)}$$

4.3 Total Aircraft Moment About The Center of Gravity

Once the moment about the aerodynamic center of the aircraft is calculated the total aircraft moment about the center of gravity can be determined. Figure 4.4 shows the resulting forces on the aircraft once the contributions from the entire wing are taken into account and placed at the aerodynamic center and the center of gravity.

Figure 4.4. *Total Aircraft Forces and Moments*

The only unknown parameter in Figure 4.4 is the location of the center of gravity. The center of gravity is a function of all the individual component weights of the aircraft. An estimation of the center of gravity would involve assumptions and approximations (unless a full aircraft design project was completed) that would create a great amount of error and uncertainty in the results. Preliminary aircraft designs usually use weight estimates based on other similar aircraft. However, in the case of the blended wing body this is much more difficult due to the lack of other blended wing body aircraft. In Reference 7 the BWB-450 claims a 5% static margin (SM). This would define the location of the center of gravity (with a defined aerodynamic center). Since an in depth study of the location of the center of gravity would either produce inaccurate results or be beyond the scope and objective of this project, it will be assumed that the design could obtain a CG that would give a 5% static margin. Also, in reality the static margin will change as the center of gravity moves. However, this project is focused on specifically the landing and takeoff configurations. So as an approximation the static margin will be assumed to be set at 5% for the landing and takeoff configurations. By assuming a positive static margin, the first stability requirement is satisfied.

Once the center of gravity is set, the total moment about the CG, from Figure 4.4, is:

$$M_{CG} = M_{ac} - (0.05 \cdot c_o)L \qquad \text{(Eqn 4.11)}$$

In order to satisfy the second stability requirement:

$$C_{Mac} \geq \frac{(0.05 \cdot c_o)}{MAC} C_L \rightarrow @\alpha = 0 \qquad \text{(Eqn 4.12)}$$

Where the *MAC* for a cranked wing is determined by [20]:

$$MAC = \frac{MAC_i \cdot S_i + MAC_o \cdot S_o}{S_i + S_o} \qquad \text{(Eqn 4.13)}$$

Equation 4.12 gives a direct relationship between the lift coefficient and moment coefficient about the aerodynamic center. This will be a useful design requirement to be used in the following sections.

4.4 Wing Geometric Specifications

To complete an adequate stability analysis requires a much more detailed definition of the wing – its shape and aerodynamic characteristics – than has been previously presented. Up to this point this project was based around the BWB-450 configuration as presented in References 2 & 7. However, the detailed amount of information required for the stability analysis is not available for the BWB-450. Therefore, at this point this project becomes less focused on the BWB-450 design directly and more a design of a BWB aircraft similar to the BWB-450. The following three sections: airfoil selection, geometric twist, and aerodynamic twist, must be designed for this project based on the limited information available for the BWB-450, but mostly based on the stability and aerodynamic efficiency of the aircraft.

The airfoil selection, geometric twist, and aerodynamic twist are presented in three individual sections. However, it is important to note that these design parameters are dependent on one another. The airfoil selection will change the design of the geometric twist and aerodynamic twist, and so on. Therefore, the process presented in the following three sections (4.4.1 – 4.4.3) is actually an iterative process in which all three categories need to be considered at the same time. The resulting design has taken this into account as well as the individual design criteria presented as follows.

4.4.1 Airfoil Selection

The first geometric specification that must be defined is the airfoil shape. Once the airfoil shape is defined the 2D airfoil aerodynamic characteristics can be determined as well as the 3D wing/aircraft aerodynamic characteristics.

The airfoil selection was based on a number of design requirements/goals. First, References 2 & 7 provide a starting point by stating that the wing is split into an inboard section with a reflexed airfoil and an outboard section with a supercritical airfoil. Also, from Table 2.1 the inboard section is approximately 17% thick (thickness to chord ratio) and the outboard section is approximately 8% thick (thickness to chord ratio). The last design requirement is that the two airfoils need to be chosen so that the geometric twist does not require a significant change or abnormal twist in order to get an approximate elliptic lift distribution. From these requirements, along with the design goals of getting a positive pitching moment about the aircraft aerodynamic center and satisfying the stability requirements with a realistic, controllable design, the two airfoils were chosen. The UIUC Airfoil Database Version 2.0, an extensive airfoil database with a large variety of airfoils [21], was used to find the appropriate airfoils.

4.4.1.1 Inboard Airfoil

The inboard airfoil that was chosen was the Eppler 336 airfoil. This airfoil was modified to have a 17% thickness using the JavaFoil program – a potential flow tool using a higher order panel method - created by Martin Hepperle [22]. Figures 4.5 to 4.7 present the airfoil shape and aerodynamic characteristics determined using the JavaFoil application. Figure 4.7, which provides the moment coefficient versus angle of attack data, shows two plots – the moment about the quarter chord and the moment about the aerodynamic center. JavaFoil determines the moment vs. angle of attack for the quarter

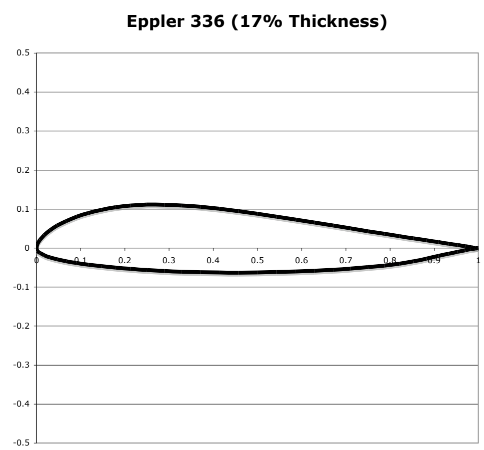

Figure 4.5. *Eppler 336 Airfoil*

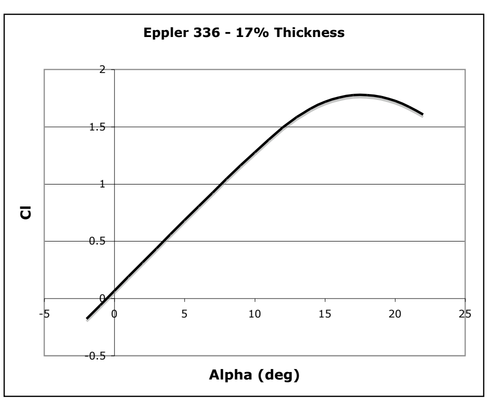

Figure 4.6. *Eppler 336 - Lift Curve(Re=1x10^{8})*

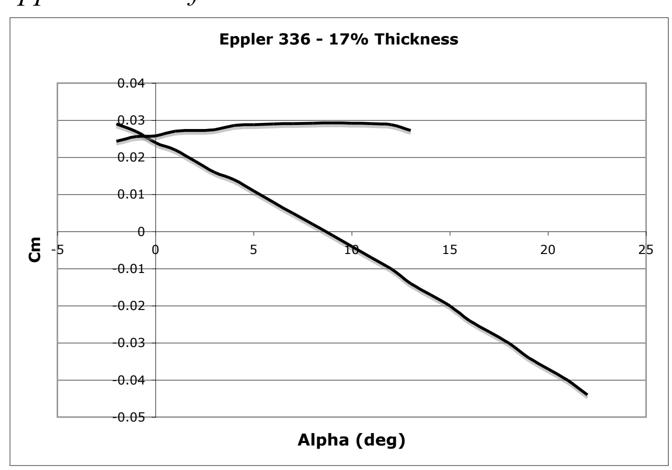

Figure 4.7. *Eppler 336 – Moment Curve (Re=1x10^{8})*

chord point, which, as Figure 4.7 shows, is not the aerodynamic center (the moment is varying with angle of attack). Therefore, the location of and moment about the aerodynamic center of the airfoil was determined using the method of Reference 23 which provides the equations:

$$x_{ac} = -\frac{C_{m,c/4\alpha}}{C_{l\alpha}} + 0.25 \qquad \text{(Eqn 4.14)}$$

$$C_{m,ac} = C_l\left(x_{ac} - 0.25\right) + C_{m,c/4} \qquad \text{(Eqn 4.15)}$$

The resulting airfoil parameters and data can be found in Table 4.1 in the following section.

4.4.1.2 Outboard Airfoil

The outboard airfoil that was chosen was the SC(2)-0406 airfoil. This NASA designed, supercritical airfoil was also modified to 8% thickness using JavaFoil. The supercritical airfoil allows for a higher drag divergence Mach number which is important for the outer section with a lower sweep angle (this will be discussed further in Section 4.4.2). Figures 4.8 & 4.9 present the airfoil shape and aerodynamic characteristics for the SC(2)-0406.

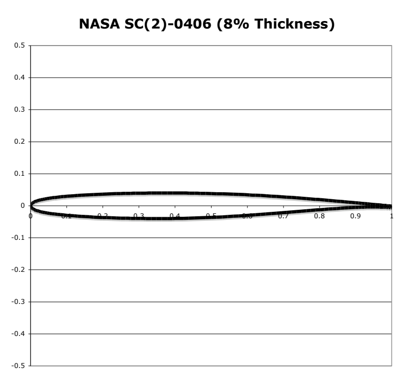

Figure 4.8. *SC(2)-0406 Airfoil*

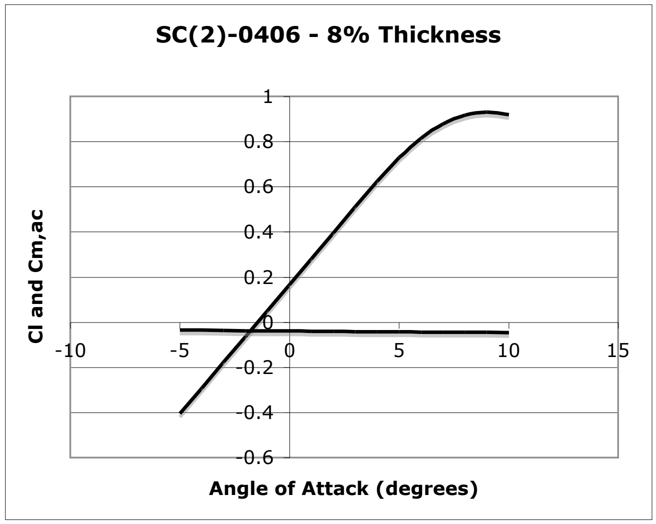

Figure 4.9. *SC(2)-0406 Lift and Moment Curve (Re=1x10^8)*

Table 4.1 gives a summary of the important airfoil data for both the inboard and outboard sections.

Table 4.1. Airfoil Data *(Re=1x10^8)*

		Inboard Wing Section	**Outboard Wing Section**
Parameter	**Symbol**	**Value**	**Value**
Airfoil	**-**	**Eppler 336**	**NASA SC(2)-0406**
Lift Coefficient @ α=0	C_{lo}	0.0781	0.1667
Lift Curve Slope	$C_{l\alpha}$	0.1193	0.1141
Moment Coefficient – AC	$C_{m,ac}$	0.028	-0.04
Location of AC	x_{ac}	0.276c	0.25c
End of Linear Lift Coefficient	-	13°	5°
Stall Angle of Attack	-	18°	9°

4.4.2 Aerodynamic Twist

The aerodynamic twist design essentially is just a matter of defining which portion of the wing has the inboard (reflexed) airfoil shape, the outboard (supercritical) airfoil shape, and the region in between where the shape changes from the inboard to the outboard. For this project the start of the aerodynamic twist refers to the spanwise location where the inboard airfoil begins to change shape and the end of the aerodynamic twist refers to the spanwise location where the shape becomes fixed as the outboard airfoil shape.

It is obvious from Equations 4.8 & 4.10 that the variation of the airfoil placement and thus, properties, will have a significant impact on the location of the aerodynamic center and the moment about the aerodynamic center of the aircraft. Table 4.1 gives the airfoil data for both the inboard and outboard airfoils. For the portion of the wing where the shape is varying (between the start and end of aerodynamic twist) it will be assumed that these values change linearly from the inboard to the outboard value.

Equation 4.12 provides a direct relationship between the aircraft moment coefficient about the aerodynamic center and the aircraft lift coefficient that will satisfy the second stability requirement. This relation provides a starting point for the design of the aerodynamic twist. Also, for more optimum drag characteristics it makes sense that the supercritical airfoil must begin at the location where the sweep of the wing changes. The lower sweep angle will produce a greater normal component of the velocity. Because the supercritical airfoil's drag rise will occur at a much higher Mach number than the reflexed airfoil, it is most efficient for a design cruise of approximately M=0.85

to keep the reflexed airfoil limited to the portion of the wing with the larger sweep angle. A quick approximation using JavaFoil produces a critical Mach number for the reflexed airfoil of 0.667 at a zero angle of attack (and decreases slightly as the angle of attack increases). Using the sweep angles of the inboard and outboard sections, the normal Mach components (for a cruise M=0.85) are 0.39 and 0.69, respectively. Therefore, at cruise, the outboard portion of the wing will be in the drag rise region for the reflexed airfoil. To prevent this, as stated above, the reflexed airfoil is limited to the inboard section of the aircraft. By doing this the location of the end of the aerodynamic twist is fixed at the "kink" in the wing (y=43 ft).

The only other design variable is the start of the aerodynamic twist. It is easy to see that the further outboard this location is, the greater amount of the aircraft will have a positive moment about the aerodynamic center (reflexed airfoil) and thus will produce more stable results in terms of Equation 4.12. However, the tradeoff is that as the start of the aerodynamic twist is pushed closer to the end of aerodynamic twist the shape, as well as the aerodynamic properties, must change more abruptly. This has negative effects in terms of a smooth and realistic geometric and aerodynamic twist. Therefore, the goal here is to satisfy the stability requirements with the start of the aerodynamic twist as close to the wing root as possible. The result being that the start of aerodynamic twist was placed 36 feet from the centerline. The results of the aerodynamic twist design, as well as the complete wing information and properties are summarized in Section 4.4.4.

4.4.3 Geometric Twist

The geometric twist of the aircraft is based on two design criteria/goals: the desired twist is washout and the lift distribution is elliptic. Washout is desired because it allows for better stall characteristics – the root is at a higher angle of attack than the tip, so the root will stall first, allowing the control devices on the outer wing to be effective. Also, washout has an impact on the stability of the aircraft. If the wing is swept the lower lift produced at the tips will create a positive pitching moment on the aircraft. Obviously the airfoil selection and placement (aerodynamic twist) will have a significant impact on these effects as well.

In order to determine the geometric twist of the wing, 3D effects of the wing must be taken into account. This means that the induced angle of attack due to downwash must be considered when looking at the entire wing in three dimensions. Prandtl's Lifting Line Theory was used and applied to an elliptical lift distribution [23]. First, an elliptic lift distribution corresponds to a circulation distribution given as:

$$\Gamma(y) = \Gamma_o \sqrt{1 - \left(\frac{2y}{b}\right)^2} \qquad \text{(Eqn 4.16)}$$

where:

$$\Gamma_o = \frac{2VSC_L}{b\pi} \quad \text{(from the definition of lift)} \qquad \text{(Eqn 4.17)}$$

Also, since:

$$L' = qcC_l = \rho V \Gamma \qquad \text{(Eqn 4.18)}$$

$$C_l(y) = C_{l\alpha}\alpha(y) + C_{lo} \qquad \text{(Eqn 4.19)}$$

Combining Equations 4.16 – 4.19 and solving for α(y) yields:

$$\alpha(y) = \frac{4SC_L}{C_{l\alpha} b\pi} \left\{ \frac{\sqrt{1-\left(\frac{2y}{b}\right)^2}}{c(y)} \right\} - \frac{C_{lo}}{C_{l\alpha}} \qquad \text{(Eqn 4.20)}$$

Equation 4.20 is very useful because once the airfoil characteristics are known throughout the span of the wing, the geometric twist is defined that will give an elliptic lift distribution. The only unknown variable in Equation 4.20 is the lift coefficient of the wing, C_L. This could be thought of as the lift coefficient desired for the wing (at zero angle of attack) and Equation 4.20 will give the required twist to get that lift coefficient. So as a starting point the desired lift coefficient needs to be determined. Since the plain wing is designed to be most efficient during the cruise portion of flight (this is the longest portion of flight) and during cruise a small angle of attack is desired (~ 0), the desired lift coefficient at zero angle of attack will be determined from the required lift coefficient at cruise.

The lift coefficient at cruise is dependent on the weight of the aircraft and is determined simply by:

$$C_L = \frac{L}{\frac{1}{2}\rho V^2 S} = \frac{W}{\frac{1}{2}\rho V^2 S} \qquad \text{(Eqn 4.21)}$$

Since the weight of the aircraft will vary during cruise due to the fuel burned, the lift coefficient will also vary. To determine this range of C_L , the weight at the beginning and end of cruise must be determined. The beginning of cruise weight is calculated as the weight burned in climb subtracted from the takeoff weight. To determine the fuel weight burned in climb the rate of climb and time to climb can be calculated as:

$$R/C = \frac{V(T-D)}{W} \qquad \text{(Eqn 4.22)}$$

$$\Delta t = \frac{\Delta h}{(R/C)_2 - (R/C)_1} \ln\left[\frac{(R/C)_2}{(R/C)_1}\right] \quad [15] \qquad \text{(Eqn 4.23)}$$

Once the time to climb is determined, the fuel burn can be calculated from the TSFC. Using the TOGW and a cruise altitude of 35,000 ft the initial cruise lift coefficient was found to be $C_L = 0.24$. The weight at the end of cruise can be approximated by finding the weight of the aircraft minus the usable fuel. Data for the Airbus A380 from Reference 13 could be reduced by 19% [7] to determine this weight. From this the resulting minimum cruise lift coefficient was found to be $C_L = 0.15$. This provides a lift coefficient range of: $0.15 > C_L > 0.24$ for cruise. The desired lift coefficient for Equation 4.20 was taken as the average cruise lift coefficient, $C_L = 0.20$. By setting the desired C_L the geometric twist is now defined for specific airfoil data and aerodynamic twist.

It is interesting to note that this lift coefficient in Equation 4.20 was chosen as a fixed value because if it differed (at different angles of attack for example) it would mean the twist would have to change in flight. Therefore, a specific design lift coefficient must be chosen to define the geometric twist of the aircraft. Also, this means that the lift distribution will be elliptic for the aircraft at a zero angle of attack. However, as the angle of attack proceeds away from zero the distribution will not be perfectly elliptic, this would require a change in the geometric twist.

4.4.4 Base Wing Configuration and Properties

4.4.4.1 Wing Geometry

In the previous three sections (4.4.1 – 4.4.3) the design method and goals/requirements for the wing design, specifically the local shape and twist, were presented. Figures 4.10, 4.11, and Table 4.2 show the results of this design – the geometric properties of the wing for this project. Figure 4.10 gives the location of the start and end of aerodynamic twist, meaning that between these points on the wing the shape is varying from the inboard airfoil to the outboard airfoil and the sections outside are completely the inboard and outboard airfoil shape. Figure 4.11 shows the geometric twist distribution from the root (y = 0) to the tip (y = 124.5 ft) – where the x-axis represents the root to tip span. This is the geometric twist required to get the lift

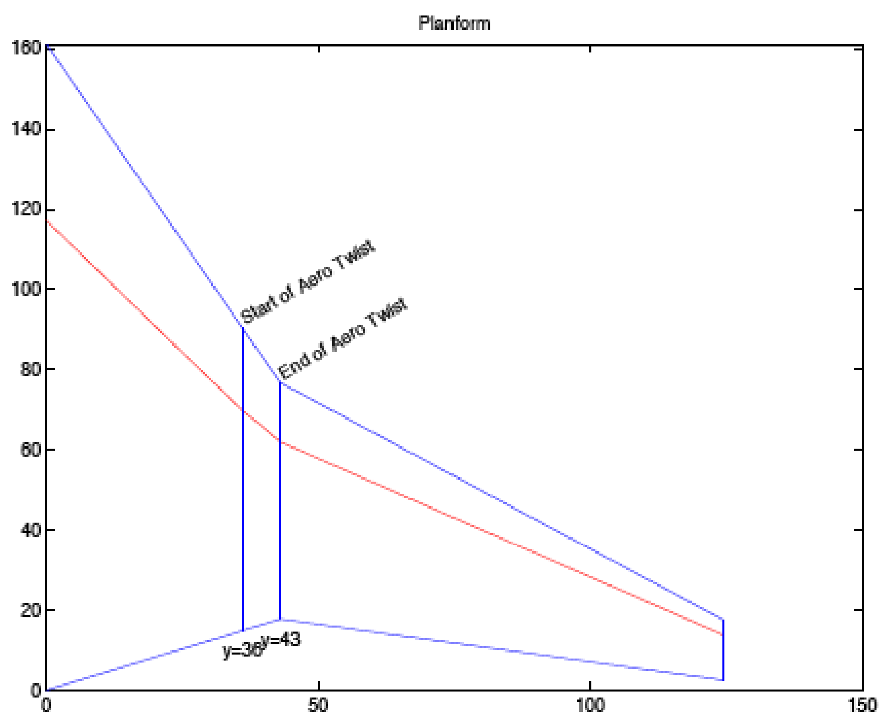

Figure 4.10. *Aerodynamic Twist*

coefficient distribution (from root to tip) which will produce an elliptic lift distribution at a zero angle of attack, also provided in Figure 4.11. From Figure 4.11 it is easy to see that most of the twist (washout) occurs at the tip of the wing, the majority of the wing is under minimal twist. Also, with the aerodynamic twist defined in Figure 4.10, the geometric twist and lift distribution remain smooth throughout the span, including the section of aerodynamic twist. Table 4.2 gives the complete numerical results of Figures 4.10 & 4.11 – the wing geometric design, including the calculated location of the aerodynamic center and center of gravity.

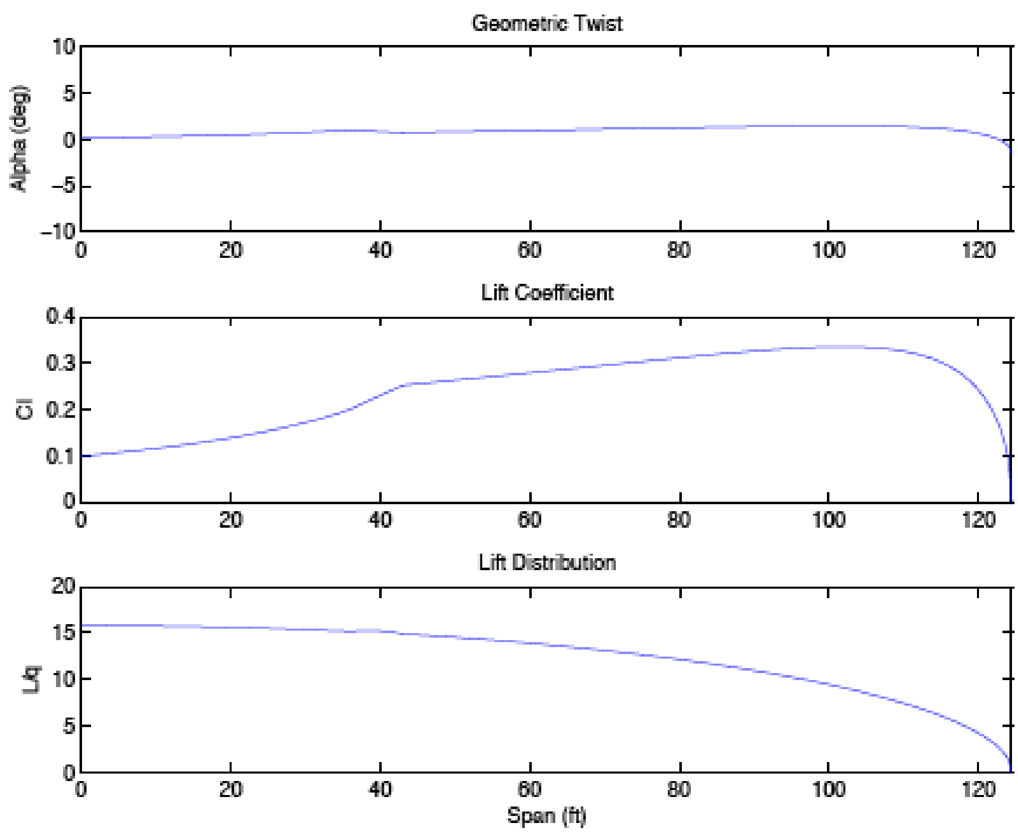

Figure 4.11. *Geometric Twist and Lift Distribution (α = 0)*

Table 4.2. Wing Geometric Parameters

Parameter		Value	Units	Notes
Geometric Twist		2.93	deg	Washout
Aerodynamic Twist:	Start of Twist	36	ft	Spanwise distance from root
	End of Twist	43	ft	Spanwise distance from root
Aerodynamic Center		46.87	%	% root chord (from nose)
		75.52	ft	Distance from nose
Center of Gravity		41.87	%	% root chord (from nose)
		67.46	ft	Distance from nose
Static Margin		5	%	% root chord – Reference 7

4.4.4.2 Wing Aerodynamic Properties

With the wing geometric design set, the aerodynamic aspects of the wing can be determined. Again using Prandtl's Lifting Line Theory, the 3D effects of the wing are taken into account, which include the induced angle of attack due to washout for an elliptical lift distribution, defined as:

$$\alpha_i = \frac{C_L}{\pi AR} \qquad \text{(Eqn 4.24)}$$

Also, using:

$$\alpha_{abs} = \alpha_e + \alpha_i \qquad \text{(Eqn 4.25)}$$

Where α_e is the effective angle of attack, or the 2D angle of attack and α_{abs} is the absolute angle of attack.

Figure 4.12 shows the resulting lift and moment curve (in the linear range) for the wing.

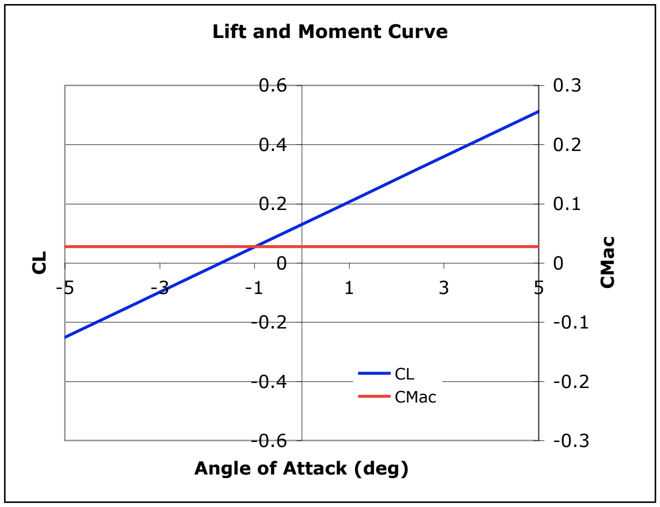

Figure 4.12. *Wing Lift and Moment Curve (Linear Range)*

In order to calculate the maximum lift coefficient for the clean wing the approximate stall angle must first be determined. From Table 4.1 the stall angle of the 2D supercritical airfoil is approximately 9°, significantly lower than the stall angle for the reflexed airfoil. This means that the supercritical portion of the wing will stall first (also taking into account the geometric twist). The overall stall of the wing, at which the maximum lift is determined, will be defined as the angle where any point of the wing begins to stall. Therefore, at a 9° angle of attack the wing will begin to stall. In order to determine the lift coefficient at this angle of attack the nonlinear characteristics of the lift curve slope must be taken into account – though for the inboard portion the airfoil is still within the linear range. Using the lift data for the airfoil as a function of the span, the maximum lift coefficient could be determined as $C_{L,max} = 0.80$. Table 4.3 summarizes the lift and moment properties of the wing.

Once the wing lift and moment about the aerodynamic center are defined, using Equation 4.11 the moment of the aircraft about the center of gravity can be determined as a function of angle of attack, provided in Figure 4.13. This figure is similar to Figure 4.1

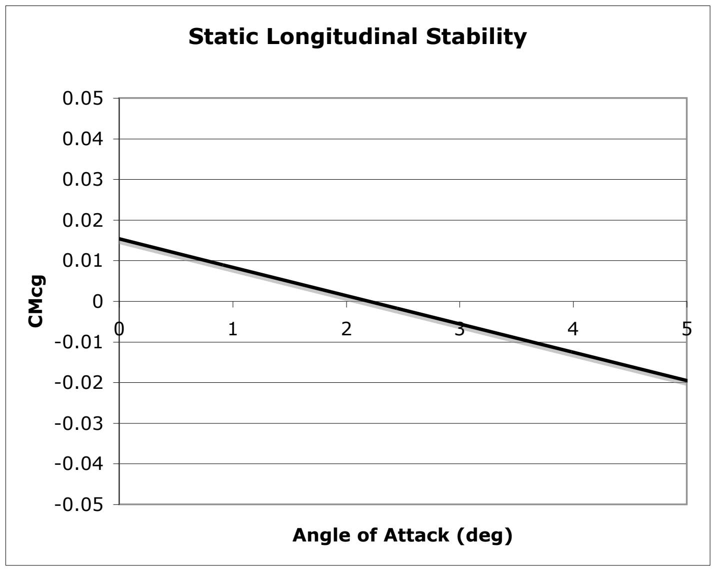

Figure 4.13. *Static Longitudinal Stability* ($C_{M,cg}$ *vs.* α)

of Section 4.1 and illustrates the static longitudinal stability of the aircraft – both the negative slope (Requirement #1) and the positive moment at zero angle of attack (Requirement #2). The angle of attack pitching moment derivative along with other stability results are summarized in Table 4.3.

Table 4.3. Wing Lift and Pitching Moment Properties

Parameter		Symbol	Value	Units
Derivatives:	Lift Coefficient	$C_{L\alpha}$	0.076	(1/deg)
	Moment Coefficient	$C_{M,cg\alpha}$	-0.007	(1/deg)
α=0 Properties:	Lift Coefficient	C_{Lo}	0.1305	N/A
	Moment Coefficient	$C_{M,cgo}$	0.0154	N/A
Maximum Lift Coefficient		$C_{L,max}$	0.80	N/A
Stall Angle of Attack (beg. of stall)		α_{stall}	9	degrees

4.5 Control Devices

Once the plain wing geometry and characteristics have been determined the next step is to size and study the effects of the basic control devices. For tailless aircraft, pitch control is typically achieved using elevons. An elevon is essentially the same as an aileron, the only difference being that they can be deflected in the same direction on both sides of the wing, thus creating a pitching moment about the aircraft. Since the elevons will be most effective (create the largest pitching moment) the further away they are from the center of gravity, a look at the basic planform of the wing puts them as far outward as possible, which corresponds to the furthest aft location of the wing. This is also beneficial because of stall characteristics – the washout will keep the tip from stalling early so the control devices will remain effective as the aircraft begins to stall – as well as creating the largest rolling moment possible.

The other sizing consideration is the need to leave enough room to place the trailing edge flaps. The wing planform again shows that the best location for the flaps, in order to produce the minimal pitching moment possible, would be at the furthest foreword location, where the wing sweep changes, and moving toward the tip. Therefore, both the trailing edge flaps and elevons must fit in the outboard portion of the aircraft. This is also beneficial because the inboard portion has the reflexed airfoil shape which would be more difficult to apply devices to the trailing edge.

One other design consideration is that the control devices need to be large enough to be able to keep the airplane trimmed for the range of α while maintaining a reasonable elevon deflection angle. As a design goal/requirement this deflection angle is limited to the range where the control derivatives remain constant. At a certain deflection angle the control derivatives begin to decrease, thus decreasing the effectiveness of the control device. For this configuration the maximum deflection angle was found to be 12°. Therefore, the sizing of the control device needs to be such that at the maximum angle of attack the deflection angle does not exceed ±12°.

To determine the effects of the control devices on the lift and pitching moment characteristics of the aircraft, first the control derivatives need to be determined. These derivatives were determined using the AAA (Advanced Aircraft Analysis) program [24] based on the Airplane Design Series by Jan Roskam and Part VI of that series [25]. Table 4.4 and Figure 4.14 provide the resulting size and location of the elevons while Figure 4.15 provides the control derivatives as a function of the velocity determined from AAA.

Table 4.4. Elevon Sizing Data

Parameter	Symbol	Value	Notes
Inboard Elevon Edge	η_{ie}	68 %	% half span location ($y_{inner}/(b/2)$)
Outboard Elevon Edge	η_{oe}	99 %	% half span location ($y_{outer}/(b/2)$)
Elevon Chord Ratio	c_e/c	30 %	% wing chord

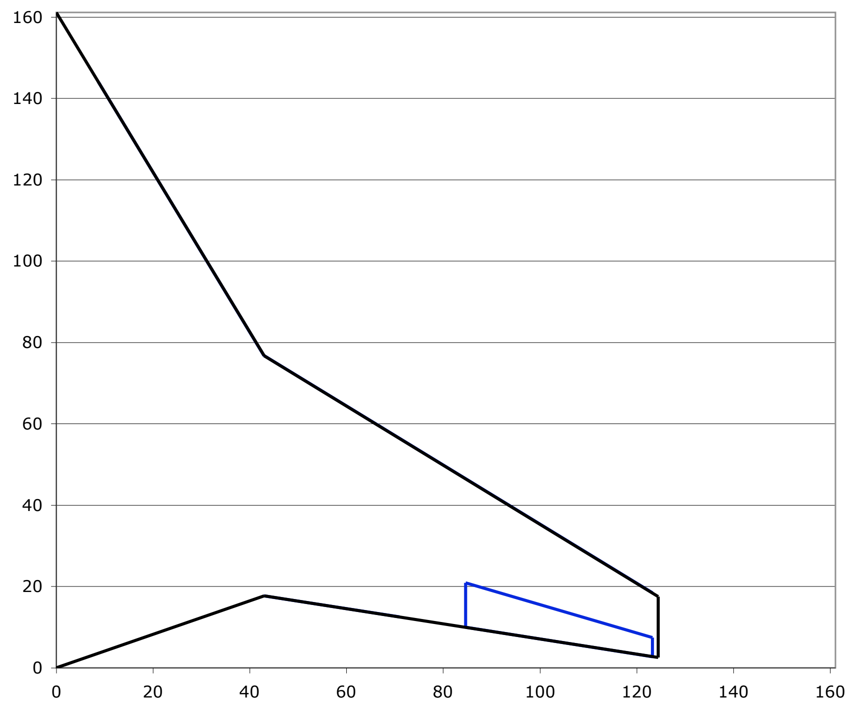

Figure 4.14. *Elevon Location and Sizing*

From the control derivative relations shown in Figure 4.15 the deflections and ability to trim the aircraft could then be determined. As in the previous sections, this is an iterative process: sizing the control devices, determining the deflection and trim, and then resizing as necessary. The results of this process have been presented here. The trim equation (sum of the moments = 0), from Reference 26 is as follows:

$$0 = C_{Mcg,o} + C_{Mcg,\alpha}\alpha + C_{M\delta e}\delta_e \qquad \text{(Eqn 4.26)}$$

Also, since the elevon deflection creates an additional lift component, the lift equation for the aircraft becomes [26]:

$$C_L = C_{Lo} + C_{L\alpha}\alpha + C_{L\delta e}\delta_e + \left(\frac{T}{qS}\right)\sin(\alpha) \qquad \text{(Eqn 4.27)}$$

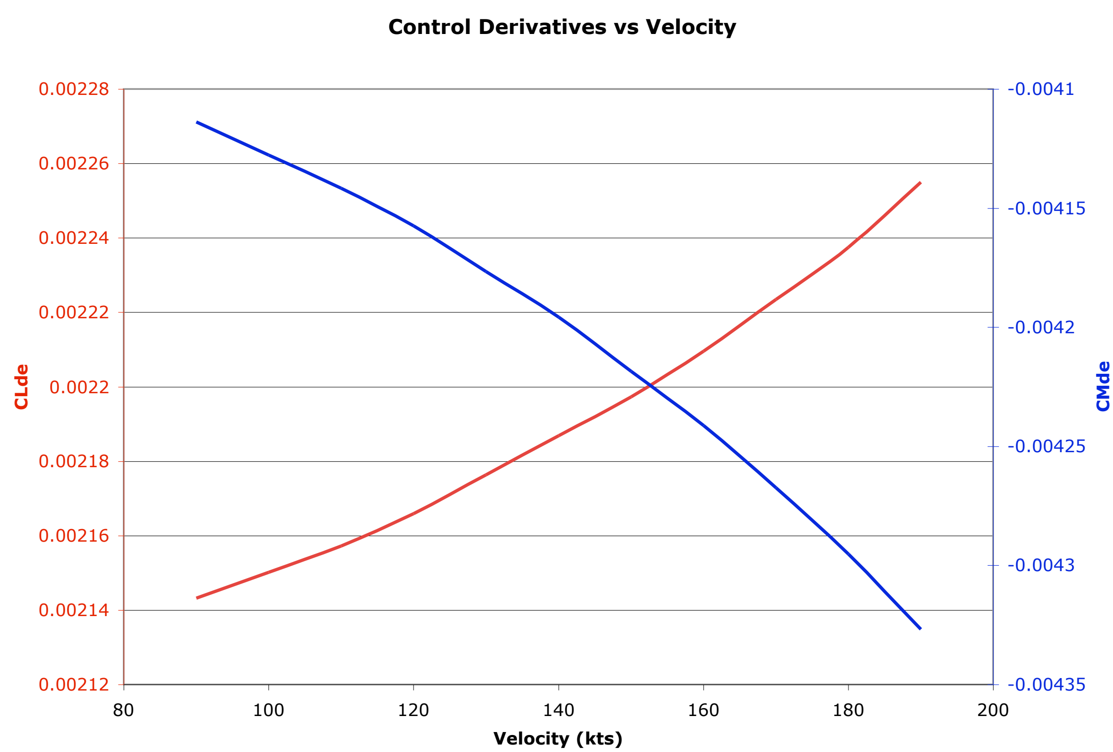

Figure 4.15. *Control Derivatives as a Function of Velocity*

Table 4.5 provides the resulting elevon deflection (δ) to trim (deflection sign convention defined in Figure 4.16) for a specific angle of attack and the $C_{L,max}$ of the aircraft including the control devices. This was calculated for each of the configurations as described in Chapter 3. The ΔC_L term in Table 4.5 is defined as the difference between the $C_{L,max}$ of the aircraft with control devices and the required C_L as determined in Chapter 3. This is then defined as the amount of additional lift needed and can be used in the following chapter to help size the high lift devices.

Figure 4.16. *Elevon Deflection Angle Sign Convention*

Table 4.5. Control Deflection To Trim and Maximum C_L

Landing With Spoilers					α =	0	9		
Weght (lbs)	Field Length (ft)	CL	V_a (kts)	Cmde	Clde	δ (deg)	δ (deg)	CLmax (clean)	ΔCL
697820	6000	1.15	139	-0.00419	0.00218	3.67	-11.35	0.78	0.37
1012700	6000	1.7	139	-0.00419	0.00218	3.67	-11.35	0.78	0.92
697820	7000	0.9	156	-0.00423	0.00220	3.64	-11.25	0.78	0.12
1012700	7000	1.35	155	-0.00423	0.00220	3.64	-11.25	0.78	0.57
697820	8000	0.75	171	-0.00427	0.00222	3.61	-11.14	0.78	-0.03
1012700	8000	1.1	171	-0.00427	0.00222	3.61	-11.15	0.78	0.32
Landing Without Spoilers									
Weight (lbs)	Field Length (ft)	CL	V_a (kts)	Cmde	Clde	δ (deg)	δ (deg)	CLmax (clean)	ΔCL
697820	6000	3.15	85	-0.00411	0.00214	3.75	-11.58	0.78	2.37
1012700	6000	4	89	-0.00411	0.00214	3.74	-11.57	0.78	3.22
697820	7000	2.7	91	-0.00412	0.00214	3.74	-11.56	0.78	1.92
1012700	7000	3.5	97	-0.00412	0.00215	3.74	-11.55	0.78	2.72
697820	8000	2.35	97	-0.00412	0.00215	3.73	-11.54	0.78	1.57
1012700	8000	3.1	103	-0.00413	0.00215	3.73	-11.52	0.78	2.32
Takeoff									
Max Thrust (lbs)	Field Length (ft)	CL	V2 (kts)	Cmde	Clde	δ (deg)	δ (deg)	CLmax (clean)	ΔCL
Trent 1000 75000	9000	1	167	-0.00426	0.00222	3.61	-11.17	0.78	0.22
	10000	0.9	176	-0.00428	0.00223	3.59	-11.11	0.78	0.12
	11000	0.85	181	-0.00430	0.00224	3.58	-11.07	0.78	0.07
PW4168 68600	9000	1.05	163	-0.00425	0.00221	3.62	-11.20	0.78	0.27
	10000	0.95	171	-0.00427	0.00222	3.60	-11.14	0.8	0.15
	11000	0.85	181	-0.00430	0.00224	3.58	-11.07	0.8	0.05
CF6-80E1 66870	9000	1.05	163	-0.00425	0.00221	3.62	-11.20	0.78	0.27
	10000	0.95	171	-0.00427	0.00222	3.60	-11.14	0.78	0.17
	11000	0.875	178	-0.00429	0.00223	3.59	-11.09	0.78	0.09
PW4060 60000	9000	1.25	149	-0.00422	0.00220	3.65	-11.29	0.78	0.47
	10000	1.1	159	-0.00424	0.00221	3.63	-11.23	0.78	0.32
	11000	1	167	-0.00426	0.00222	3.61	-11.17	0.78	0.22
Trent 500 56000	9000	1.425	140	-0.00420	0.00219	3.67	-11.34	0.78	0.64
	10000	1.275	148	-0.00421	0.00219	3.65	-11.30	0.78	0.49
	11000	1.15	156	-0.00423	0.00220	3.64	-11.25	0.78	0.37
TOGW (lbs) =	1012700								

From Table 4.5, the maximum elevon deflection angle is approximately -11.5 degrees, which is a reasonable deflection and within acceptable limits. This also allows for additional deflection that will be necessary to counteract the pitch due to the high lift devices (discussed in Chapter 5), though as stated earlier the efficiency of the control device will decrease with further deflection.

5. High Lift Devices

5.1 High Lift Types and Commercial Aircraft Comparison

Once the wing geometry and control devices have been determined the high lift devices can be applied and studied. The first step in sizing the high lift devices is to look at the different types and configurations used by similar aircraft, similar to what was done in Section 3.1.

Figure 5.1 illustrates the evolution of trailing edge device design for both Boeing and Airbus. This figure shows the tendency of Boeing shift from triple slotted flaps in

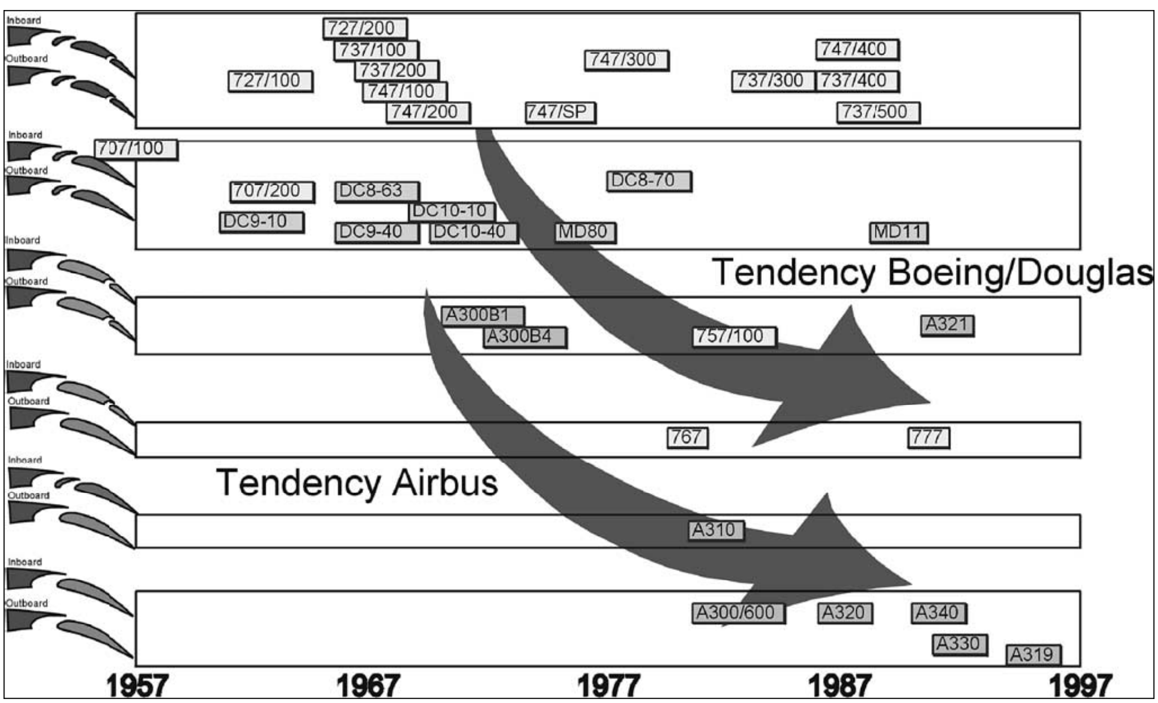

Figure 5.1. *Design Evolution of Trailing Edge Devices [27]*

the 50's and 60's to double slotted flaps in the late 90's as well as the tendency of Airbus shift from double slotted flaps to single slotted flaps during the same time period.

Table 5.1 provides data for the high lift devices of some large commercial transports, taken from K. C. Rudolph's report on high lift devices for commercial subsonic aircraft [28]. Rudolph also provides a summary for each common type of high lift device including typical sizing and deflection angles, given in Table 5.2. The data in Figure 5.1 and Tables 5.1 & 5.2 provide a nice starting point and guideline for the design of the high lift devices for this project which will be further developed in the following sections. In reference to the objectives for this project (see Section 1.2) only trailing edge devices, only leading edge devices, and a combination of the two will be applied and studied in terms of maintaining longitudinal stability and creating additional lift.

Table 5.1. Commercial Aircraft High Lift Devices

Airplane	LE Device	LE Angle (°)	Flap Chord % (c_f/c)	TE Device	TE Max Angle (°)	TE Takeoff Angle (°)
Boeing 747	Krueger	84	-	Triple-Slotted	23 (vane) 32 (main) 52 (aft)	-
Boeing 757	Slats	28 – 32	10 - 26	Double-Slotted	34 (main) 60 (aft)	-
Boeing 767	Slats	30 – 38	6.7 - 29	Double-Slotted	36 (main) 60.5 (aft)	15
Boeing 777	Slat	31.6 - 35	9 - 33	Double-Slotted	43 (main) 67 (aft)	5 to 15
DC-10 MD-11	Slats	-	16 - 19	Double-Slotted	-	-
Airbus A330/340	Slats	20.6 - 24	12 - 23.5	Single-Slotted	32	-

Table 5.2. Typical Commercial High Lift

Type	Parameter	Value	Units
Slats:	Takeoff Angle:	15-20	degrees
	Landing Angle:	21-38	degrees
Krueger Flaps:	Angle of Flap Rotation: (Angle from Horizontal):	60-80 (20-30)	degrees
Flaps:	Chord:	20-35	% (c_f/c)
	Takeoff Angle:	10-20	degrees
	Vane/Main Double-Slotted:	45-55	degrees
	Main/Aft Double-Slotted:	30-35 main	degrees
		28-30 aft	degrees
		60-65 total	degrees

5.2 Trailing Edge Devices

The first configuration applies only trailing edge devices to the blended wing body aircraft. Figure 5.2 [29] shows the general effect of trailing edge devices on the lift curve for two different deflection angles (δ_f). This figure shows that for a given angle of

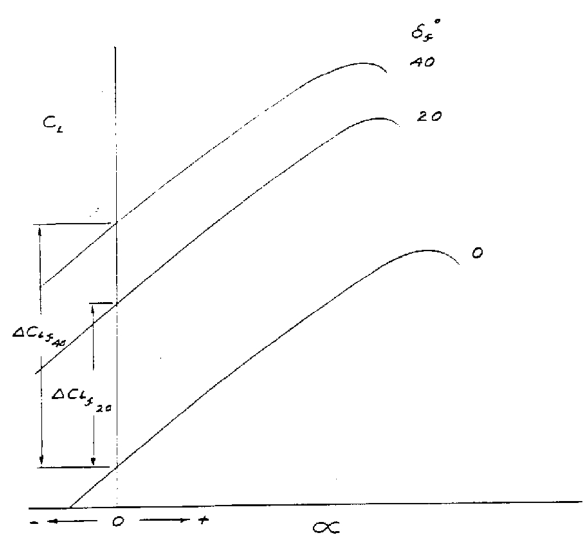

Figure 5.2. *General Effect of Trailing Edge Devices on Lift Curve Slope [29]*

attack the high lift device adds an increment in lift coefficient to the plain wing. At the same time however, it also decreases the stall angle of the wing. In general trailing edge devices are more desired than leading edge devices due to the additional lift for a given angle of attack. This differs from leading edge devices which increase the maximum lift by effectively increasing the maximum (stall) angle of attack (see Section 5.3). Also, in general trailing edge devices can produce more lift than leading edge devices of similar size. However, for tailless aircraft, the significant nose down (-) pitching moment presents a stability problem.

The wing geometry for this project provides an easy starting point for sizing the trailing edge devices. Since the goal is to minimize the pitching moment created, the trailing edge devices should be as close to the center of gravity as possible, this means the furthest forward position on the trailing edge of the wing – which corresponds to the "kink" point in the wing. Also, the trailing edge devices will be limited to the outboard portion of the wing due to the large thickness of the wing on the inboard portion as well as the fact that the inboard portion consists mostly of the reflexed airfoil shape. Because the reflexed airfoil has a negative camber at the trailing edge it could be difficult to successfully apply typical high lift devices while maintaining the beneficial pitching moment of the airfoil shape. Figure 5.3 is a simple illustration of this for a plain flap (25% chord) deflected 30 degrees. A quick approximation using JavaFoil shows the local airfoil moment coefficient changes from 0.028 to approximately -0.3.

This then places both the longitudinal control devices (elevons) and trailing edge devices on the outboard portion of the wing, with the elevons located toward the wing tip

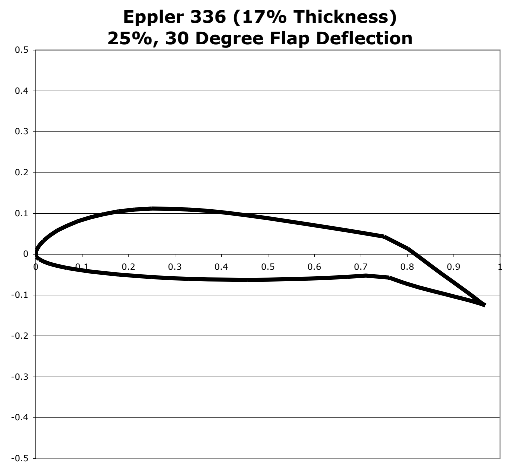

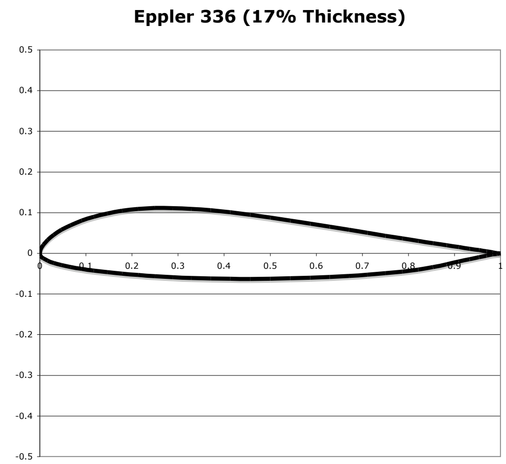

Figure 5.3. *Effect on Camber of Reflexed Airfoil With Trailing Edge Flap*

and the trailing edge devices located toward the wing root. In order to maximize the amount of lift generated by the trailing edge devices, while maintaining stability, as much of the trailing edge should be used for either elevons or high lift devices. These design constraints create a tradeoff – as the span of the trailing edge device increases the amount of lift increases, but the span of the control device is reduced and thus the ability to stabilize the aircraft is diminished. The opposite is also true – if the span of the control device is increased this increases the ability of the aircraft to remain stable, but decreases the span of the high lift devices and creates less lift. By analyzing this tradeoff, the spanwise location of the trailing edge devices and control devices could be defined such that the maximum amount of lift would be created while maintaining the stability of the aircraft in pitch. This was carried out for two different trailing edge, high lift configurations.

Configuration #1:

The first configuration was based on the typical commercial high lift data provided in Section 5.1. The elevon chord ratio was slightly increased to increase their effectiveness. A summary of the first configuration is presented in Table 5.3.

Table 5.3. Trailing Edge Devices – Configuration #1

Parameter	Value	Units
Trailing Edge Device	Main/Aft Double Slotted Flaps	-
Deflection Angle (δ_f) Landing (Max)	30 Main 30 Aft 60 Total	Degrees
Deflection Angle (δ_f) Takeoff	10 Main 10 Aft 20 Total	Degrees
Flap Chord Ratio	25	% (c_f/c)
Elevon Chord Ratio	30	% (c_e/c)

Using AAA and Part VI of Roskam's Airplane Design Series the additional lift and moment coefficients could be determined. Modifying Equations 4.26 and 4.27 to include the additional term due to the trailing edge devices the total aircraft moment and lift can be determined.:

$$C_{Mcg,TOTAL} = C_{Mcg,o} + C_{Mcg,\alpha}\alpha + C_{M\delta e}\delta_e + \Delta C_{M,f} \qquad \text{(Eqn 5.1)}$$

$$C_L = C_{Lo} + C_{L\alpha}\alpha + C_{L\delta e}\delta_e + \left(\frac{T}{qS}\right)\sin(\alpha) + \Delta C_{L,f} \qquad \text{(Eqn 5.2)}$$

It is important here to define the maximum allowable deflection of the control devices. Obviously the greater the deflection the larger the resulting moment. However, as the angle increases the effectiveness of the control device decreases and at very high angles the flow will not remain attached, the drag will increase, and the results will not be realistic. Therefore, for this project the angle of deflection will be limited to 60° (which corresponds also to the limit in AAA). Table 5.4 gives the results of the tradeoff for Configuration #1 including the point where the control devices are large enough to achieve longitudinal stability (highlighted). Once this point is determined, the takeoff configuration must also be calculated separately because the flap deflection in takeoff is less to reduce the amount of drag the flaps create. The terms η_{of} and η_{ie} correspond to the percent spanwise location of the end of the high lift devices and the beginning of the control devices, respectively. Table 5.4 shows a maximum additional lift coefficient of

Table 5.4. Trailing Edge Device Data - Configuration #1

High Lift Device			Elevon (δ_e=60°)			Total Additional C_L	Total Aircraft C_M
η_{of} %	ΔC_{Lf}	ΔC_{Mf}	η_{ie} %	$C_{M\delta e}\delta_e$	$C_{L\delta e}\delta_e$		
50	0.253	-0.117	51	0.205	-0.116	0.137	0.040
53	**0.295**	**-0.136**	**54**	**0.190**	**-0.106**	**0.189**	**0.007**
55	0.323	-0.148	56	0.179	-0.099	0.224	-0.017
Takeoff (20° Flap Deflection)							
53	0.158	-0.067	54	0.115	-0.064	0.094	0.001
			-22° Elevon Deflection				

approximately 0.19 for takeoff and 0.1 for landing. These values are fairly low but should be expected due to the large amount of negative lift created by the control devices to stabilize the aircraft and the small size of the trailing edge flaps. The flaps can only span from the "kink" (at 34.5% span) to 53% span in order to leave room for the control devices. Though this additional lift is small, it is still enough to give the aircraft sufficient lift for some of the landing and takeoff configurations discussed in Chapter 3. Table 5.5 repeats these configurations and shows whether or not the lift requirement is met with this configuration of trailing edge devices.

Table 5.5. Lift Coefficient Requirement Satisfied – TE Configuration #1

Landing With Spoilers: $C_{L,MAX}$ = 0.99			
Weight (lbs)	Field Length (ft)	C_L Required	Requirement Satisfied?
697820	6000	1.15	No
1012700	6000	1.7	No
697820	7000	0.9	Yes
1012700	7000	1.35	No
697820	8000	0.75	Yes
1012700	8000	1.1	No
Landing Without Spoilers: $C_{L,MAX}$ = 0.99			
Weight (lbs)	Field Length (ft)	C_L Required	Requirement Satisfied?
697820	6000	3.15	No
1012700	6000	4	No
697820	7000	2.7	No
1012700	7000	3.5	No
697820	8000	2.35	No
1012700	8000	3.1	No
Takeoff: $C_{L,MAX}$ = 0.89			
Max Thrust (lbs)	Field Length (ft)	C_L Required	Requirement Satisfied?
Trent 1000 75000	9000	1.0	No
	10000	0.9	No
	11000	0.85	Yes
PW4168 68600	9000	1.05	No
	10000	0.95	No
	11000	0.85	Yes
CF6-80E1 66870	9000	1.05	No
	10000	0.95	No
	11000	0.875	Yes
PW4060 60000	9000	1.25	No
	10000	1.1	No
	11000	1	No
Trent 500 56000	9000	1.425	No
	10000	1.275	No
	11000	1.15	No
TOGW (lbs) =	1012700		

Configuration #2

The second configuration, which is only a slight improvement and slight difference from the first, comes from realizing that more of the takeoff configuration requirements could be satisfied without losing any of the landing requirements by decreasing the landing flap deflection angle. In essence, this will allow for an increase in span of the flaps which will increase the takeoff lift coefficient (for the same flap deflection). Of course the landing lift coefficient will decrease, but not enough to lose any of the requirements that were already satisfied with Configuration #1. Table 5.6 & 5.7 summarize the data for Configuration #2. This slight adjustment satisfies one additional takeoff configuration while still maintaining the same landing configurations. Table 5.8 provides a summary of the configurations that can be satisfied with only trailing edge devices. Figure 5.4 shows the resulting geometry of the wing with the trailing edge flaps and elevon control devices.

Table 5.6. Trailing Edge Devices – Configuration #2

Parameter	Value	Units
Trailing Edge Device	Main/Aft Double Slotted Flaps	-
Deflection Angle (δ_f) Landing (Max)	20 Main 20 Aft 40 Total	Degrees
Deflection Angle (δ_f) Takeoff	10 Main 10 Aft 20 Total	Degrees
Flap Chord Ratio	25	% (c_f/c)
Elevon Chord Ratio	30	% (c_e/c)

Table 5.7. Trailing Edge Device Data - Configuration #2

High Lift Device			Elevon (δ_e=60°)			Total Additional C_L	Total Aircraft C_M
η_{of} %	ΔC_{Lf}	ΔC_{Mf}	η_{ie} %	$C_{M\delta e}\delta_e$	$C_{L\delta e}\delta_e$		
55	0.242	-0.108	56	0.179	-0.099	0.143	0.024
57	**0.262**	**-0.117**	**58**	**0.169**	**-0.093**	**0.169**	**0.005**
58	0.271	-0.121	59	0.164	-0.089	0.182	-0.005
60	0.290	-0.130	61	0.154	-0.083	0.207	-0.024
Takeoff (20° Flap Deflection)							
57	0.187	-0.080	58	0.128	-0.070	0.117	0.001
			-39° Elevon Deflection				

Table 5.8. Lift Coefficient Requirement Satisfied – TE Configuration #2

Landing With Spoilers: $C_{L,MAX}$ = 0.97			
Weight (lbs)	Field Length (ft)	C_L Required	Requirement Satisfied?
697820 (MLW)	7000	0.9	Yes
697820 (MLW)	8000	0.75	Yes
Takeoff: $C_{L,MAX}$ = 0.92			
Max Thrust (lbs)	Field Length (ft)	C_L Required	Requirement Satisfied?
Trent 1000 75000	10000	0.9	Yes
	11000	0.85	Yes
PW4168 68600	11000	0.85	Yes
CF6-80E1 66870	11000	0.875	Yes
TOGW (lbs) =	1012700		

Figure 5.4. *Wing Planform with Trailing Edge Flaps*

5.3 Leading Edge Devices

Next, a configuration with only leading edge devices can be studied in a similar way as the trailing edge devices. Figure 5.5 shows Figure 5.2 with the addition of the effects of leading edge devices (dashed line). Essentially, as stated earlier, leading edge devices allow for an increase in the maximum angle of attack and thus an increase in the maximum lift coefficient of the wing.

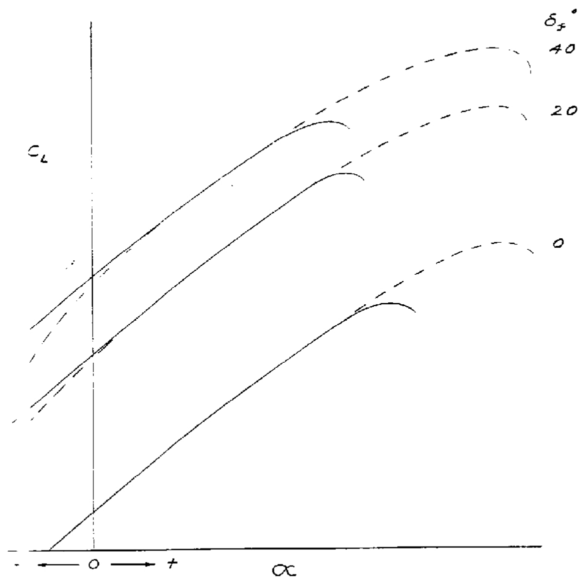

Figure 5.5. *Effect of Leading Edge Devices*

In addition to the data in Section 5.1 there are two important design considerations for the blended wing body aircraft of this project. First, because of the thickness of the inboard section, Krueger flaps must be used in this section as opposed to leading edge slats. Figure 5.6 illustrates why slats cannot be used in extremely thick/large sections. Second, because of the large chord lengths in the inboard section of the wing the chord ratio must be decreased when compared to the data of Section 5.1 and

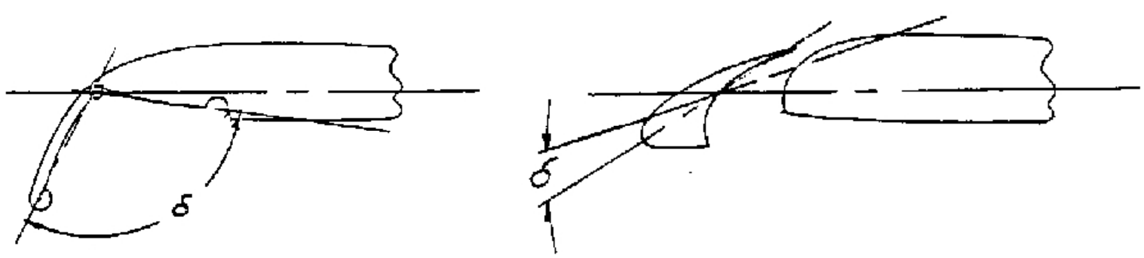

(a) *(b)*

Figure 5.6. *Geometry of (a) Krueger Flap and (b) Slat [29]*

the rest of the wing. With these considerations taken into account the leading edge flaps and slats can be applied to the entire leading edge of the wing. Table 5.9 and Figure 5.7 define the geometry of the leading edge devices. Table 5.10 gives the resulting aerodynamic data and elevon sizing determined using AAA and Part VI of Roskam's Airplane Design Series along with Equations 5.1 and 5.2.

Table 5.9. Leading Edge Devices

Parameter	Value	Units
Inboard Section: 7% - 34.5% Span		
Leading Edge Device	Krueger Flaps	-
Deflection Angle (δ_f) Landing (Max)	30 From Horizontal 60 Flap Rotation	Degrees
Deflection Angle (δ_f) Takeoff	20 From Horizontal 70 Flap Rotation	Degrees
Flap Chord Ratio	10 Inboard 20 Outboard	% (c_f/c)
Outboard Section: 34.5% - 99% Span		
Leading Edge Device	Slats	-
Deflection Angle (δ_f) Landing (Max)	35	Degrees
Deflection Angle (δ_f) Takeoff	20	Degrees
Flap Chord Ratio	20	% (c_f/c)

The additional lift coefficient on the trimmed aircraft is approximately 0.28 for landing and 0.24 for takeoff – shown in Table 5.10. Compared to the results for the wing with only trailing edge devices, these values are somewhat higher. As a result, a few more of the configurations are satisfied in terms of the required lift coefficient. A summary of all the takeoff and landing configurations, the maximum aircraft C_L, and whether or not the lift coefficient requirements were met is presented in Table 5.11.

Though Table 5.11 shows that many more configurations are satisfied compared to the case of trailing edge devices, it also shows a large number of configurations that do not have the lift coefficient requirement satisfied.

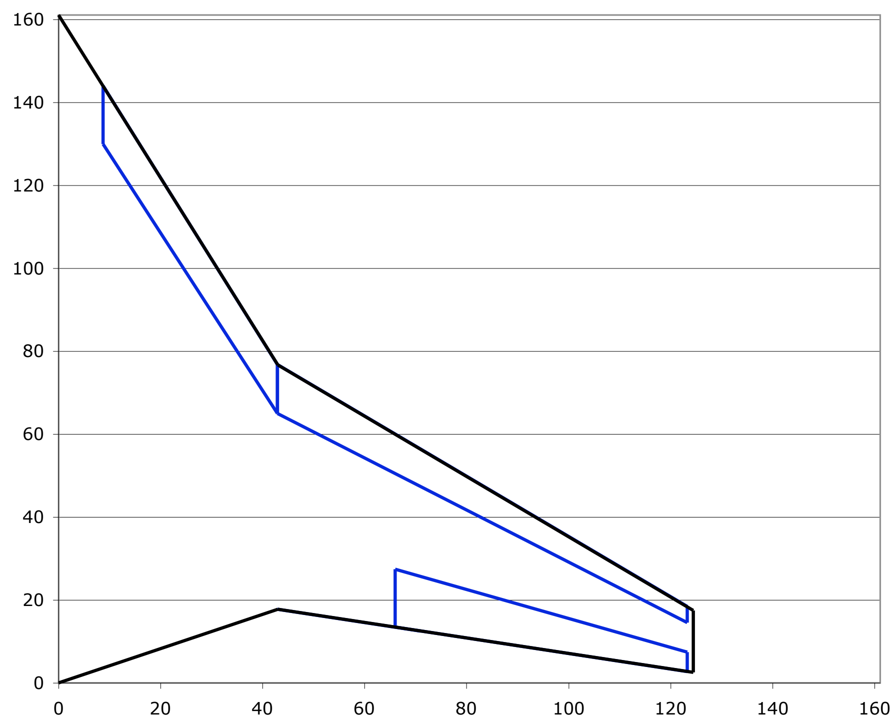

Figure 5.7. *Wing Planform With Leading Edge Devices*

Table 5.10. Leading Edge Device Data

High Lift Device		Elevon (δ_e=60°)			Total Additional C_L	Total Aircraft C_M
ΔC_{Lf}	ΔC_{Mf}	η_{ie} %	$C_{M\delta e}\delta_e$	$C_{L\delta e}\delta_e$		
0.2314	0.1320	52	-0.086	0.049	0.2804	-0.0016
0.2314	**0.1320**	**53**	**-0.084**	**0.047**	**0.2784**	**0.0004**
0.2314	0.1320	54	-0.082	0.046	0.2774	0.0024
Takeoff (20° Flap Deflection)						
0.1665	0.1820	53	-0.1342	0.075	0.2415	0.0002
		32° Elevon Deflection				

Table 5.11. Lift Coefficient Requirement Satisfied – Leading Edge Devices

Landing With Spoilers: $C_{L,MAX}$ = 1.08			
Weight (lbs)	Field Length (ft)	C_L Required	Requirement Satisfied?
697820	6000	1.15	No
1012700	6000	1.7	No
697820	7000	0.9	Yes
1012700	7000	1.35	No
697820	8000	0.75	Yes
1012700	8000	1.1	No
Landing Without Spoilers: $C_{L,MAX}$ = 1.08			
Weight (lbs)	Field Length (ft)	C_L Required	Requirement Satisfied?
697820	6000	3.15	No
1012700	6000	4	No
697820	7000	2.7	No
1012700	7000	3.5	No
697820	8000	2.35	No
1012700	8000	3.1	No
Takeoff: $C_{L,MAX}$ = 1.04			
Max Thrust (lbs)	Field Length (ft)	C_L Required	Requirement Satisfied?
Trent 1000 75000	9000	1.0	Yes
	10000	0.9	Yes
	11000	0.85	Yes
PW4168 68600	9000	1.05	No
	10000	0.95	Yes
	11000	0.85	Yes
CF6-80E1 66870	9000	1.05	No
	10000	0.95	Yes
	11000	0.875	Yes
PW4060 60000	9000	1.25	No
	10000	1.1	No
	11000	1	Yes
Trent 500 56000	9000	1.425	No
	10000	1.275	No
	11000	1.15	No
TOGW (lbs) =	1012700		

5.4 Leading Edge & Trailing Edge Devices

The third configuration of high lift devices includes a combination of both leading and trailing edge devices. The sizing of the leading edge devices will be the same as in the previous section, essentially the entire length of the leading edge. The trailing edge devices will be sized in the same way as in Section 5.2 – following Configuration #1 and obtaining the maximum size (spanwise) while maintaining large enough control devices to achieve longitudinal stability. Table 5.12 provides the spanwise sizing tradeoff for the trailing edge control and high lift devices, as well as the resulting additional lift. From

Table 5.12. Combined LE & TE Device Data

Leading Edge Devices		Trailing Edge Devices			Elevon (δ_e=60°)			Total Additional C_L	Total Aircraft C_M
ΔC_{Lf}	ΔC_{Mf}	η_{of} %	ΔC_{Lf}	ΔC_{Mf}	η_{ie} %	$C_{M\delta e}\delta_e$	$C_{L\delta e}\delta_e$		
0.2314	0.132	65	0.447	-0.202	66	0.127	-0.067	0.6114	0.0094
0.2314	**0.132**	**66**	**0.458**	**-0.207**	**67**	**0.122**	**-0.064**	**0.6254**	**-0.0006**
0.2314	0.132	67	0.469	-0.212	68	0.117	-0.061	0.639	-0.0107
Takeoff (20° Flap Deflection)									
0.1306	0.159	66	0.458	-0.207	67	0.095	-0.05	0.5386	-0.0006
					-41° Elevon Deflection				

Table 5.12 the maximum additional lift coefficient from the combined high lift devices sized to maintain longitudinal stability is approximately 0.63 for landing and 0.54 for takeoff. This is a significant improvement from the previous two cases and, as shown in Table 5.13, assuming the aircraft has spoilers, the lift coefficient requirements are mostly satisfied. The aircraft with this configuration of high lift devices, shown in Figure 5.8, meets the FAR requirements for landing at its maximum landing weight for a 6,000 ft

Table 5.13. Lift Coefficient Requirement Satisfied – Combined LE & TE Devices

Landing With Spoilers: $C_{L,MAX}$ = 1.43			
Weight (lbs)	Field Length (ft)	C_L Required	Requirement Satisfied?
697820	6000	1.15	Yes
1012700	6000	1.7	No
697820	7000	0.9	Yes
1012700	7000	1.35	Yes
697820	8000	0.75	Yes
1012700	8000	1.1	Yes
Landing Without Spoilers: $C_{L,MAX}$ = 1.43			
Weight (lbs)	Field Length (ft)	C_L Required	Requirement Satisfied?
697820	6000	3.15	No
1012700	6000	4	No
697820	7000	2.7	No
1012700	7000	3.5	No
697820	8000	2.35	No
1012700	8000	3.1	No
Takeoff: $C_{L,MAX}$ = 1.34			
Max Thrust (lbs)	Field Length (ft)	C_L Required	Requirement Satisfied?
Trent 1000 75000	9000	1.0	Yes
	10000	0.9	Yes
	11000	0.85	Yes
PW4168 68600	9000	1.05	Yes
	10000	0.95	Yes
	11000	0.85	Yes
CF6-80E1 66870	9000	1.05	Yes
	10000	0.95	Yes
	11000	0.875	Yes
PW4060 60000	9000	1.25	Yes
	10000	1.1	Yes
	11000	1	Yes
Trent 500 56000	9000	1.425	No
	10000	1.275	Yes
	11000	1.15	Yes
TOGW (lbs) =	1012700		

Figure 5.8. *Wing Planform With Combination LE & TE Devices*

landing distance. It also meets the requirements for takeoff for almost all of the different engines for a 9,000 ft distance. This is by far the best high lift configuration and shows a successful design in terms of being able to land and takeoff safely while maintaining stability in pitch.

6. Conclusion

6.1 Project Conclusions

In reference to the objectives of this project the goal was to look at the effects of applying high lift devices to a blended wing body aircraft, specifically the effects on the longitudinal stability. This gives an idea as to whether or not high lift devices are feasible for this type of aircraft and if the aircraft meets the requirements for safe takeoff and landing.

The results of this project show that the two configurations with only leading edge devices and only trailing edge devices both add a small amount of additional lift while maintaining stability. The leading edge devices would be recommended out of these two options because they allow for a slightly larger amount of additional lift and are easier to maintain stability in pitch (smaller control devices – more flexibility in sizing control devices). Both configurations allow for a 7,000 ft landing distance (with spoilers) with a maximum landing weight of 697,820 lbs (specified by NASA's BWB-450 project). This landing distance is comparable with the Boeing 747-400 which, from Table 3.1 is approximately 7,400 ft. For takeoff, the leading edge devices satisfy a few more configuration requirements including a 10,000 ft takeoff distance for a number of different engine types, as well as a 9,000 ft takeoff distance for the most powerful engine, the Trent 1000. The trailing edge devices only allow for a 10,000 ft takeoff distance using the Trent 1000, and for an 11,000 ft takeoff distance using a number of other engine types. This is comparable to the 747-400 which has a takeoff distance that ranges from 10,000 ft to 10,500 ft and the Airbus A380 which has a takeoff distance of about 9,800 ft.

By far the most optimum high lift configuration was the combination of leading and trailing edge devices. The maximum lift coefficient obtained was approximately 1.43 for landing and 1.34 for takeoff, a significant improvement over the previous two high lift configurations. With these lift coefficients the aircraft could now meet the requirements to safely land with a 7,000 ft distance at the maximum takeoff weight and with a 6,000 ft distance at the maximum landing weight – easily comparable to typical commercial transports (A380 – 6,200 ft landing distance). Also, for four of the five engines studied, all the takeoff requirements were met allowing for a takeoff distance of 9,000 ft which is again similar to, if not somewhat less than, other commercial aircraft (See Table 3.1 & 5.13 for data).

It is important to note that the landing distances here are only valid assuming the aircraft is using spoilers. Without spoilers there is a large increase in the maximum lift coefficient required (Table 5.13) which cannot be satisfied using any of the high lift configurations studied. Therefore, according to this project, spoilers are a requirement for the design of the wing.

Given the previous data, the obvious conclusion of this project is that it is possible to successfully apply high lift devices to this type of BWB aircraft under the previously stated requirements for longitudinal static stability and achieve enough lift to meet FAR requirements for takeoff and landing comparable to current large commercial aircraft.

There are a few observations that surface from this project as to why this is so - essentially to answer the question of how stability can be maintained without a horizontal tail while employing trailing edge devices. First, typical maximum lift coefficient values for conventional aircraft (given in Table 6.1) are significantly larger than those determined for the BWB aircraft of this project. This mainly has to do with the advantages of the large wing area this type of aircraft has, when compared to similar sized (wingspan, weight, etc.) aircraft, and the overall increase in the lift to drag ratio.

Table 6.1. Maximum Lift Coefficient For Some Conventional Airplanes [29]

Model	$C_{L\ max}$
B-47/B-52	1.8
367-80/KC-135	1.78
707-320/E-3A	2.2
727	2.79
DC-9	3
737-200	3.2
747/E-4A	2.45
767	2.45
777	2.5

Therefore, it can be seen that the resulting size of the high lift devices required for the BWB are much smaller than those for the conventional aircraft. The smaller size allows for a reduction in the additional pitching moment created and, as this project determined, achieved trim with the use of elevon control devices.

Also, the shape of the wing seems to have a significant impact on this project, especially the shape of the trailing edge. By using a cranked wing in which the inboard trailing edge sweep is negative (forward) and the outboard is positive (backward) it allows for an optimum location for the trailing edge devices that brings them closer to the center of gravity of the aircraft, thus reducing the pitching moment. This also creates an optimum location for the longitudinal control devices – towards the wing tip – which is furthest aft, creating a larger moment arm. Further refinement of the wing planform could take further advantage of this geometry. However, additional effects such as other control devices or static margin issues may need to be considered.

The third observation is that an unobstructed wing allows for greater efficiency in control devices and greater flexibility in their design. With the engines on the center portion of the aircraft, the wing is clear of nacelle obstructions allowing for continuous flaps and control devices. As stated in Reference 28, flaps that are not broken into segments by obstructions are more efficient (in terms of lift and drag) than those that are.

6.2 Future Considerations

Though this project has developed some significant results and conclusions, it is important to point out a few limitations. First, this project used preliminary design methods and the results should be regarded as preliminary results. The point of this project was to investigate the feasibility of high lift devices, not develop a full aircraft design including high lift devices. The results point to a feasibility for the reasons discussed previously but should be regarded as a stepping stone from which to build upon, not a final result. In order to complete this project a number of approximations were required and the only real way to further develop the data is through experimental testing or further, more in depth investigation, which is beyond the scope of this project.

The focus of the project was held specifically to the longitudinal stability and lift of the aircraft. Further development should include an in depth study of the stability in roll and yaw – static and dynamic – as well as aeroelastic effects and the effects of drag on the aircraft, to name a few. Each one of these, in and of itself, could be developed into its own full-length project and though not always directly, each has an impact on the issue. Therefore, the significance of this project is that it provides a method as well as numerical data from which to further develop the issue of high lift devices and the future design of the blended wing body aircraft.

References

1. Norris, G. & Wagner, M. (2005). *Airbus A380: Superjumbo of the 21st Century*. St. Paul, MN: Zenith Press.

2. Liebeck, R. H., Roman, D., and Allen, J. B., "Aerodynamic Design Challenges of The Blended-Wing-Body Subsonic Transport," AIAA-2000-4335, 2000.

3. Leifsson, L. T., and Mason, W. H., "The Blended Wing Body Aircraft," Virginia Polytechnic Institute and State University, Blacksburg, VA, USA.

4. Chambers, J. R., "Innovation in Flight: Research of the NASA Langley Research Center on Revolutionary Concepts for Aeronautics," NASA SP-2005-4539, 2005.

5. Liebeck, R. H., Page, M. A., and Rawdon, B. K., "Blended-Wing-Body Subsonic Commercial Transport," Future Aeronautical and Space Systems, Vol. 172, 1997 pp.156-165, AIAA, Inc.

6. McMasters, J. H., and Kroo, I., "Advanced Configurations for Very Large Subsonic Transport Airplanes," NASA CR-198351, Oct. 1996.

7. Liebeck, R. H., "Design of the Blended Wing Body Subsonic Transport," *Journal of Aircraft*, Vol. 41, No. 1, January-February 2004.

8. Hepperle, M., and Heinze, W., "Future Global Range Transport Aircraft," RTO Symposium on Novel Vehicle Concepts and Emerging Technologies, Bruxelles, April, 2003.

9. NASA, *The X-48B Blended Wing Body*. Retrieved November 8, 2006, from http://www.nasa.gov/vision/earth/improvingflight/x48b.html

10. Bradley, K. R., "A Sizing Methodology for the Conceptual Design of Blended-Wing-Body Transports," NASA/CR-2004-213016.

11. Raymer, D. P. (1999). *Aircraft Design: A Conceptual Approach*. 3rd Ed. Virginia: AIAA.

12. Boeing Company. *747 Airplane Characteristics for Airport Planning: 747-400/-400ER, 3.0 Airplane Performance (Document D6-58326-1)*. Retrieved November 22, 2006, from http://www.boeing.com/commercial/airports/acaps/7474sec3.pdf

13. *Jane's All The World Aircraft, 2003-2004*. Jackson, P. (Ed.). Coulsdon, Jane's, 2003, 94 ed.

14. Freighters Online. *Boeing - B747*. Retrieved November 22, 2006, from http://www.freightersonline.com/plane.aspx?a=13

15. Airbus Company. *A380 Airplane Characteristics for Airport Planning*. Retrieved April 30, 2007, from http://www.content.airbusworld.com/SITES/Technical_Data /docs/AC/DATA_CONSULT/AC_A380.pdf

16. McCormick, B. W. (1995). *Aerodynamics Aeronautics and Flight Mechanics*. Canada: John Wiley & Sons.

17. Oates, G. C. (1997). *Aerothermodynamics of Gas Turbine and Rocket Propulsion*. 3rd Ed. Reston, VA: AIAA.

18. Rolls Royce Company. *Trent 1000 Fact Sheet*. Retrieved December 8, 2006, from http://www.rolls-royce.com/civil_aerospace/downloads/airlines/trent_1000.pdf

19. Rolls Royce Company. *Trent 500 Fact Sheet*. Retrieved December 8, 2006, from http://www.rolls-royce.com/civil_aerospace/downloads/airlines/trent_500.pdf

20. Hoak, D. E., et al, "USAF Stability and Control Datcom," Flight Control Division, Air Force Flight Dynamics Laboratory, WPAFB, Ohio, 45433-0000, 1978, revised.

21. Selig, M. *UIUC Airfoil Coordinates Database*. Retrieved April 3, 2007, from http://www.ae.uiuc.edu/m-selig/ads/coord_database.html

22. Hepperle, M. *Javafoil* [Computer software]. Retrieved April 3, 2007, from http://www.mh-aerotools.de/airfoils/javafoil.htm

23. Anderson, J. D. (2001). *Fundamentals of Aerodynamics*. 3rd Ed. New York, NY: McGraw-Hill.

24. Roskam, J. (2006). Advanced Aircraft Analysis (Version 3.1) [Computer Software]. Lawrence, KS: DARcorporation.

25. Roskam, J. (1990. *Airplane Design: Part VI, Preliminary Calculation of Aerodynamic, Thrust and Power Characteristics*. Ottawa, KS: Roskam Aviation and Engineering Corporation.

26. Roskam, J. (1988). *Airplane Design: Part VII, Determination of Stability, Control and Performance Characteristics: FAR and Military Requirements*. Ottawa, KS: Roskam Aviation and Engineering Corporation.

27. Reckzeh, D., “Aerodynamic Design of the High-Lift-Wing for a Megaliner Aircraft,” Aerospace Science and Technology 7, pp. 107-119, 2003.

28. Rudolph, K. C., “High-Lift Systems on Commercial Subsonic Airliners,” NASA CR 4746, Sept. 1996.

29. Mason, W. H. *Configuration Aerodynamics, Chapter 8: High-Lift Aerodynamics*. Retrieved April 23, 2007 from http://www.aoe.vt.edu/~mason/Mason_f/ConfigAeroHiLift.pdf

Appendix

Matlab Takeoff Code

takeoff.m

```
clear
% Takeoff Velocity Calculator

% Units are ft-lb-s

% Symbols-----------------------------------------------------------------
% p       =  Air Density
% ku      =  Kinematic Viscosity
% u       =  Viscosity
% AR      =  Aspect Ratio
% b       =  Wing Span
% S       =  Wing Area
% V       =  Velocity
% n       =  Maximum Time Iterations
% L       =  Lift
% D       =  Drag
% CL      =  Lift Coefficient
% CDi     =  Induced Drag Coefficient
% T       =  Thrust
% TOGW    =  Take Off Gross Weight
% Re_w    =  Wing Reynold's Number
% MAC     =  Mean Aerodynamic Chord
% a       =  Speed of Sound
% M       =  Mach Number
% tc      =  Thickness to Chord Ratio
% xc      =  Maximum Thickness Location (% Chord)
% Alpha   =  Sweep Angle of Maximum Thickness Location
% Sw_w    =  Wing Wet Area
% Cf_w    =  Wing Skin Friction Coefficient
% FF_w    =  Wing Form Factor
% Cdo_w   =  Wing Parasite Drag Coefficient
% uf      =  Friction Coefficient
% ac      =  Acceleration
% Co      =  Root Chord
% TR      =  Taper Ratio
% tc      =  Thickness to Chord Ratio
% xc      =  Maximum Thickness Location (Rel to Chord)
% AlphaM  =  Sweep Angle of Max Thickness
% Alpha   =  LE Sweep Angle
% Re      =  Reynolds Number
% g       =  Acceleration Due To Gravity
% dt      =  Time Interval
% T_max   =  Maximum Thrust
% m_dot   =  Engine Mass Flow Rate (Maximum)
% V_e     =  Engine Exit Velocity
% V_s     =  Stall Velocity
% V_lof   =  Lift Off Velocity
```

```
% V_2      =  Velocity Over 35ft Obstacle
% CD       =  Total Drag Coefficient
% T        =  Thrust
% s_g      =  Local Ground Distance
% t        =  Time
% S_g      =  Total Ground Distance
% theta    =  Aircraft Angle
% s_a      =  Local Airborne Distance
% h        =  Local Height (Altitude)
% H        =  Final Height (Altitude)
% V_2_calc=  Calculated V_2
% CL_A     =  Airborne CL
% S_a      =  Final Airborne Distance
% THETA    =  Final Aircraft Angle
% S_total =  Total Takeoff Distance
% h_w      =  Wing Height Above Ground
% ---------------------------------------------------------------------

% Initial Parameters---------------------------------------------------
g=32.2;          %ft/s^2
uf=0.03;
% Sea Level Parameters
p=2.3769E-3;     %slugs/ft^3
ku=1.5723E-4;
a=1116.4;
u=p*ku;
% ---------------------------------------------------------------------

% Geometry/BWB Specs---------------------------------------------------

    % Wing Section I
    Co_1=161.12;
    TR_1=59/Co_1;
    MAC_1=(2/3)*Co_1*(1+TR_1+TR_1^2)/(1+TR_1);
    tc_1=.15;
    xc_1=.6;
    AlphaM_1=30*pi/180;
    S_1=Co_1*(1+TR_1)*43;

    % Wing Section II
    Co_2=59;
    TR_2=15/Co_2;
    MAC_2=(2/3)*Co_2*(1+TR_2+TR_2^2)/(1+TR_2);
    tc_2=.08;
    xc_2=.3;
    AlphaM_2=30*pi/180;
    S_2=Co_2*(1+TR_2)*81.5;

    % Airplane
    b=249;
    S=S_1+S_2;
    AR=b^2/S;
    h_w=10;
    TOGW=0.82*1235000;
```

```
% ----------------------------------------------------------------------

% Input-------------------------------------------------------------------
engine=input('Choose Engine:\n 1)Trent 500\n 2)Trent 1000\n 3)CF6-
80E1\n 4)PW4060\n 5)PW4168\n');
dt=input('Time Interval =');
% ----------------------------------------------------------------------

% Engine/Thrust Calculations--------------------------------------------
----
if engine==1
    % Trent 500
    T_max=56000;
    m_dot=1939;
elseif engine==2
    % Trent 1000
    T_max=75000;
    m_dot=2679;
elseif engine==3
    % CF6-80E1
    T_max=66870;
    m_dot=1926;
elseif engine==4
    % PW4060
    T_max=60000;
    m_dot=1800;
elseif engine==5
    % PW4168
    T_max=68600;
    m_dot=1990;
else
    fprintf('Error: Not a Valid Engine Input');
end
V_e=(T_max/m_dot)*32.17;
%-----------------------------------------------------------------------

% Starting Conditions---------------------------------------------------
V(1)=0;
Cdo_w(1)=0;
k=0;
t(1)=0;
s_g(1)=0;
n=10000;
%-----------------------------------------------------------------------
for j=0.6:.1:2.5

   k=k+1;
   CL(k)=j;

   % FAR Speed Calculations
   V_s(k)=sqrt(2*TOGW/(p*CL(k)*S));
   V_lof(k)=1.1*V_s(k);
   V_2(k)=1.2*V_s(k);
```

```
    % Ground Distance
    for i=1:n

        % Lift
        L(i)=.5*p*V(i)^2*S*CL(k);

        % Drag
        % 1. Induced Drag

CDi(i)=CL(k)^2/(pi*AR)*((33*((h_w)/b)^(1.5))/(1+33*((h_w)/b)^(1.5)));

        % 2. Parasite Drag

        if V(i)>0
        M(i)=V(i)/a;
        %    a. Wing Section I
                Re_w1(i)=p*V(i)*MAC_1/u;

Cf_w1(i)=0.455/(log10(Re_w1(i))^2.58*(1+0.144*M(i)^2)^0.65);

FF_w1(i)=(1+0.6*tc_1/xc_1+100*tc_1^4)*(1.34*M(i)^0.18*(cos(AlphaM_1))^0
.28);
Sw_w1=S_1*(1.977+0.52*tc_1);

        %    b. Wing Section II
                Re_w2(i)=p*V(i)*MAC_2/u;

Cf_w2(i)=0.455/(log10(Re_w2(i))^2.58*(1+0.144*M(i)^2)^0.65);

FF_w2(i)=(1+0.6*tc_2/xc_2+100*tc_2^4)*(1.34*M(i)^0.18*(cos(AlphaM_2))^0
.28);
                Sw_w2=S_2*(1.977+0.52*tc_2);

Cdo_w(i)=Cf_w1(i)*FF_w1(i)*Sw_w1/S_1+Cf_w2(i)*FF_w2(i)*Sw_w2/S_2;

        end;

        % Total Drag
        CD(i)=Cdo_w(i)+CDi(i);
        D(i)=.5*p*V(i)^2*S*CD(i);

        % Thrust (for 3 engines)
        T(i)=3*(m_dot/32.17)*(V_e-V(i));

        % Acceleration
        ac(i)=(g/TOGW)*(T(i)-D(i)-uf*(TOGW-L(i)));

        % Equations of Motion
        V(i+1)=V(i)+ac(i)*dt;
        s_g(i+1)=s_g(i)+V(i)*dt+ac(i)*dt^2/2;

        t(i+1)=t(i)+dt;
```

```
        if V(i+1)>=V_lof(k)
            S_g(k)=s_g(i+1); break, end
        if i==n
            fprintf('Error: Maximum Time Iterations Reached\n');
        end
    end

    % Airborne Distance
        % Initial Climb Angle
          theta(i+1)=0;
     s_a(i+1)=0;
    for y=1:5000
        clear h
        h(i+1)=0;
        for z=i+1:n
            % Linear variation of CL versus V
            slope=(CL(k)/1.21-CL(k)/1.44)/(V_lof(k)-V_2(k));
            CL_A(z)=slope*(V(z)-V_lof(k))+CL(k)/1.21;

            % Lift
            L(z)=.5*p*V(z)^2*S*CL_A(z);

            % Drag
            % 1. Induced Drag

CDi(z)=CL_A(z)^2/(pi*AR)*((33*((h(z)+h_w)/b)^(1.5))/(1+33*((h(z)+h_w)/b
)^(1.5)));

            % 2. Parasite Drag
            M(z)=V(z)/a;
            %    a. Wing Section I
                    Re_w1(z)=p*V(z)*MAC_1/u;

Cf_w1(z)=0.455/(log10(Re_w1(z))^2.58*(1+0.144*M(z)^2)^0.65);

FF_w1(z)=(1+0.6*tc_1/xc_1+100*tc_1^4)*(1.34*M(z)^0.18*(cos(AlphaM_1))^0
.28);
                    Sw_w1=S_1*(1.977+0.52*tc_1);

            %    b. Wing Section II
                    Re_w2(z)=p*V(z)*MAC_2/u;


Cf_w2(z)=0.455/(log10(Re_w2(z))^2.58*(1+0.144*M(z)^2)^0.65);

FF_w2(z)=(1+0.6*tc_2/xc_2+100*tc_2^4)*(1.34*M(z)^0.18*(cos(AlphaM_2))^0
.28);
                    Sw_w2=S_2*(1.977+0.52*tc_2);

Cdo_w(z)=Cf_w1(z)*FF_w1(z)*Sw_w1/S_1+Cf_w2(z)*FF_w2(z)*Sw_w2/S_2;

         % Total Drag
         CD(z)=Cdo_w(z)+CDi(z);
         D(z)=.5*p*V(z)^2*S*CD(z);
```

```
        % Climb Angle
        theta(z+1)=(L(z)-
        TOGW*cos(theta(z)))*(g*dt)/(TOGW*V(z))+theta(z);

        % Thrust (for 3 engines)
        T(z)=3*(m_dot/32.17)*(V_e-V(z));

        % Acceleration
        ac(z)=(g/TOGW)*(T(z)-D(z)-TOGW*sin(theta(z)));

        % Height
        h(z+1)=V(z)*dt*((T(z)-D(z))/TOGW-ac(z)/g)+h(z);

        % Equations of Motion
        V(z+1)=V(z)+ac(z)*dt;
        s_a(z+1)=s_a(z)+(V(z)*dt+ac(z)*dt^2/2)*cos(theta(z));

        t(z+1)=t(z)+dt;

        if V(z+1)>=V_2(k)
            if h(z+1)>=35
                  V_2_calc(k)=V(z+1);
                  H(k)=h(z+1);
                  S_a(k)=s_a(z+1);
                  THETA(k)=theta(i+1); break, end
               theta(i+1)=theta(i+1)+0.001*pi/180;
               fprintf('Increasing Theta\n'); break, end
           if z==n
               fprintf('Error: Maximum Time Iterations Reached\n');
           end
      end

      if V(z+1)>=V_2(k)
          if h(z+1)>=35 break, end
      end

      if y==5000
         fprintf('Error: Maximum Theta Iterations Reached\n');
      end
   end
   S_total(k)=S_g(k)+S_a(k);
end

fprintf('CL     Ground(ft)     Airborne(ft)    FL(ft)       V_2
V_2(Calc.)(ft/s)   H(Calc.)(ft)\n')
fprintf('-----------------------------------------------------------------
------\n')

for k=1:20
fprintf('%2.1f       %5.2f       %5.2f       %5.2f       %3.1f       %3.1f
%2.1f\n',CL(k),S_g(k),S_a(k),S_total(k),V_2(k),V_2_calc(k),H(k))
end
```

```
fprintf('\nTOGW= %7.0f lbs\n',TOGW)

if engine==1
    fprintf('Trent 500\n')
elseif engine==2
    fprintf('Trent 1000\n')
elseif engine==3
    fprintf('CF6-80E1\n')
elseif engine==4
    fprintf('PW4060\n')
elseif engine==5
    fprintf('PW4168\n')
end

fprintf('CL    FL(ft)\n')
fprintf('----------------------\n')

for k=1:20
fprintf('%2.1f    %5.2f\n',CL(k),S_total(k))
end

plot(S_total,CL)
```

Matlab Landing Code

landing.m

```
clear
% Landing Velocity Calculator
%
% This landing program assumes the use of spoilers
%
% Units are ft-lb-s

% Symbols----------------------------------------------------------------------
% TL       =  Field Length
% p        =  Air Density
% ku       =  Kinematic Viscosity
% u        =  Viscosity
% AR       =  Aspect Ratio
% b        =  Wing Span
% S        =  Wing Area
% V        =  Velocity
% n        =  Number of segments
% h        =  Segment Length
% x        =  Local Position on Field
% L        =  Lift
% CL       =  Lift Coefficient
% CDi      =  Induced Drag Coefficient
% T        =  Thrust
% MLW      =  Maximum Landing Weight
% Re_w     =  Wing Reynold's Number
% Re_n     =  Nacelle Reynold's Number
% MAC      =  Mean Aerodynamic Chord
% a        =  Speed of Sound
% M        =  Mach Number
% tc       =  Thickness to Chord Ratio
% xc       =  Maximum Thickness Location (% Chord)
% Sw_w     =  Wing Wet Area
% Cf_w     =  Wing Skin Friction Coefficient
% FF_w     =  Wing Form Factor
% Cdo_w    =  Wing Parasite Drag Coefficient
% Sw_n     =  Nacelle Wet Area
% Cf_n     =  Nacelle Skin Friction Coefficient
% FF_n     =  Nacelle Form Factor
% Cdo_n    =  Nacelle Parasite Drag Coefficient
% uf       =  Braking Friction Coefficient
% ac       =  Acceleration
% ln       =  Nacelle Length
% Co       =  Root Chord
% TR       =  Taper Ratio
% tc       =  Thickness to Chord Ratio
% xc       =  Maximum Thickness Location (Rel to Chord)
% AlphaM   =  Sweep Angle of Max Thickness
% Alpha    =  LE Sweep Angle
% Re       =  Reynolds Number
% ThetaD   =  Descent Angle
% ----------------------------------------------------------------------------
```

```
% Initial Parameters----------------------------------------------------
TL=input('Takeoff Field Length (ft):')/1.667;
g=32.2;         %ft/s^2
uf=0.4;
ThetaD=3*pi/180;

% Sea Level Parameters
p=2.3769E-3;    %slugs/ft^3
ku=1.5723E-4;
a=1116.4;
u=p*ku;
% ---------------------------------------------------------------------

% Geometry/BWB Specs----------------------------------------------------

    % Wing Section I
    Co_1=161.12;
    TR_1=59/Co_1;
    MAC_1=(2/3)*Co_1*(1+TR_1+TR_1^2)/(1+TR_1);
    tc_1=.15;
    xc_1=.6;
    AlphaM_1=30*pi/180;
    S_1=Co_1*(1+TR_1)*43;

    % Wing Section II
    Co_2=59;
    TR_2=15/Co_2;
    MAC_2=(2/3)*Co_2*(1+TR_2+TR_2^2)/(1+TR_2);
    tc_2=.08;
    xc_2=.3;
    AlphaM_2=30*pi/180;
    S_2=Co_2*(1+TR_2)*81.5;

    % Aircraft
    b=249;
    S=S_1+S_2;
    AR=b^2/S;
    MLW=input('Weight:')*0.82;
% ---------------------------------------------------------------------

% Input-----------------------------------------------------------------
n=input('Number of Segments =');
% ---------------------------------------------------------------------
h=TL/n;

% Starting Conditions---------------------------------------------------
V(1)=0;
Cdo_w(1)=0;
k=0;
x(1)=0;
```

```
for j=.1:.1:3
   k=k+1;
   CL(k)=j;
   V=0;
   ac=0;
   x=0;
   for i=1:n

        % Lift------------------------------------------------------------
        L(i)=.5*p*V(i)^2*S*CL(k);
        % --------------------------------------------------------------

        % Drag------------------------------------------------------------

        % 1. Parasite Drag

        if V(i)>0
        M(i)=V(i)/a;
        %    a. Wing Section I
                Re_w1(i)=p*V(i)*MAC_1/u;

Cf_w1(i)=0.455/(log10(Re_w1(i))^2.58*(1+0.144*M(i)^2)^0.65);

FF_w1(i)=(1+0.6*tc_1/xc_1+100*tc_1^4)*(1.34*M(i)^0.18*(cos(AlphaM_1))^0
.28);
                Sw_w1=S_1*(1.977+0.52*tc_1);

        %    b. Wing Section II
                Re_w2(i)=p*V(i)*MAC_2/u;

Cf_w2(i)=0.455/(log10(Re_w2(i))^2.58*(1+0.144*M(i)^2)^0.65);

FF_w2(i)=(1+0.6*tc_2/xc_2+100*tc_2^4)*(1.34*M(i)^0.18*(cos(AlphaM_2))^0
.28);
                Sw_w2=S_2*(1.977+0.52*tc_2);

Cdo_w(i)=Cf_w1(i)*FF_w1(i)*Sw_w1/S_1+Cf_w2(i)*FF_w2(i)*Sw_w2/S_2;

        end;

        % Total Drag
        CD(i)=Cdo_w(i);
        D(i)=.5*p*V(i)^2*S*CD(i);

        % Acceleration------------------------------------------------
        ac(i)=(g/MLW)*(D(i)+uf*(MLW));

        % Equation of Motion------------------------------------------
        V(i+1)=sqrt(2*ac(i)*h+V(i)^2);

        % Field Location
        x(i+1)=i*h;
```

```
        % Approach
        L(i+1)=.5*p*V(i+1)^2*S*CL(k);
        R=V(i+1)^2/(g*(L(i+1)/MLW-1));
        x_a=50/ThetaD+R*ThetaD/2;

        % Transition
        x_t=2*V(i+1);

        if abs(1.667*(TL-(x(i+1)+x_a+x_t)))<=1
            Vl(k)=V(i+1);
            Approach(k)=x_a;
            Transition(k)=x_t;
            Ground(k)=x(i+1);
            Total(k)=x_a+x_t+x(i+1);
            L_W(k)=L(i+1)/MLW;
            Radius(k)=R; break, end
    end
    % Plot One Takeoff Configuration at CL=1.5
    if j==4
       figure
       plot(x,V,'r')
    end;

end

figure
plot(Vl,CL)

fprintf('CL    Approach   Transition    Ground      Total          L/W
Radius      Approach Velocity\n')
fprintf('----------------------------------------------------------------
-----------------------------\n')

for k=1:30
fprintf('%2.1f    %5.0f        %5.0f        %5.0f         %5.0f
%5.3f        %5.0f
%5.2f\n',CL(k),Approach(k),Transition(k),Ground(k),Total(k),L_W(k),Radi
us(k),Vl(k))
end

fprintf('\nMLW= %7.0f lbs\n',MLW)
fprintf('TL= %5.0f ft\n',TL*1.667)
fprintf('h= %5.2f ft\n',h)
fprintf('CL    V_a (ft/s)\n')
fprintf('----------------------\n')

for k=1:30
fprintf('%2.1f    %5.2f\n',CL(k),Vl(k))
end
```

Matlab Stability Code

stability.m

```
clear

S=15496; %ft^2
b=249; %ft
AR=b^2/S;
c_bar=(118*9465+41*6031)/15496;

inboard=input('Inboard Airfoil: \n  (1)Eppler E336\n  (2)Eppler
E335\n');
outboard=input('Outboard Airfoil: \n  (1)SC(2)0710\n  (2)SC(2)0406\n');

if inboard == 1
    inCla=0.1193;
    inClo=0.0781;
    inCmac=0.028;
elseif inboard == 2
    inCla=0.1216;
    inClo=-0.0341;
    inCmac=0.047;
else
    fprintf('Error')
end

if outboard == 1
    outCla=0.1128;
    outClo=0.5322;
    outCmac=-0.118;
elseif outboard == 2
    outCla=0.1141;
    outClo=0.1667;
    outCmac=-0.04;
else
    fprintf('Error')
end

plots=input('Plots? (y,n)\n','s');
if plots=='y'
    a_plot=input('Angle of Attack for Plots (deg):');
else
    a_plot=0;
end

CLo_desired=input('CL Desired for Alpha(Effective)=0 (default is
0.1):');

if size(CLo_desired)==0
    CLo_desired=.1;
end

aerostart=input('Start of Aerodynamic Twist (Span, ft) (default is
43ft):');
```

```
aeroend=input('End of Aerodynamic Twist (Span, ft) (default is
65ft):');

if size(aerostart)==0
    aerostart=43;
end
if size(aeroend)==0
    aeroend=65;
end
if aerostart > 43
    y1final=43;
    y2final=aerostart;
    y3final=aeroend;
elseif aeroend < 43
    y1final=aerostart;
    y2final=aeroend;
    y3final=43;
else
    y1final=aerostart;
    y2final=43;
    y3final=aeroend;
end

y4final=124.5;

fid=fopen(strcat(num2str(aerostart),num2str(aeroend),num2str(100*CLo_de
sired),'.rtf'),'w');
fprintf(fid,'a_e     a_i       a_abs      CL       CMac\n');
fprintf(fid,'--------------------------------------------\n');

for i=1:2
    if i==1 | i==3
        y1=0:.5:y1final;
        y2=y1final:.5:y2final;
        y3=y2final:.5:y3final;
        y4=y3final:.5:y4final;
        start=a_plot;
        finish=a_plot;
    elseif i==2
        syms y1 y2 y3 y4
        start=-5;
        finish=12;
    end

    for a_e=start:finish

        % Chord Length
        c1=-(102.12/43)*y1+161.12;
        c1initial=161.12;
        c1final=-(102.12/43)*y1final+161.12;
        A_LE1=63;
        Cla_1=inCla;
        Clo_1=inClo;
        % Chord Length
        c4=-(44/81.5)*y4+59+43*(44/81.5);
```

```
        c4final=15;
        c4initial=-(44/81.5)*y3final+59+43*(44/81.5);
        A_LE4=36;
        Cla_4=outCla;
        Clo_4=outClo;

       % Chord Length
       if aerostart > 43
        c2=-(44/81.5)*y2+59+43*(44/81.5);
        c2initial=-(44/81.5)*y1final+59+43*(44/81.5);
        c2final=-(44/81.5)*y2final+59+43*(44/81.5);
        A_LE2=36;
        Cla_2=Cla_1;
        Clo_2=Clo_1;
        Cla_2final=Cla_1;
        Clo_2final=Clo_1;
       elseif aeroend < 43
        c2=-(102.12/43)*y2+161.12;
        c2initial=-(102.12/43)*y1final+161.12;
        c2final=-(102.12/43)*y2final+161.12;
        A_LE2=63;
        Cla_2=((Cla_4-Cla_1)/(y2final-y1final))*(y2-y1final)+Cla_1;
        Clo_2=((Clo_4-Clo_1)/(y2final-y1final))*(y2-y1final)+Clo_1;
        Cla_2final=Cla_4;
        Clo_2final=Clo_4;
       else
        c2=-(102.12/43)*y2+161.12;
        c2initial=-(102.12/43)*y1final+161.12;
        c2final=-(102.12/43)*y2final+161.12;
        A_LE2=63;
        Cla_2=((Cla_4-Cla_1)/(y3final-y1final))*(y2-y1final)+Cla_1;
        Clo_2=((Clo_4-Clo_1)/(y3final-y1final))*(y2-y1final)+Clo_1;
        Cla_2final=((Cla_4-Cla_1)/(y3final-y1final))*(y2final-
y1final)+Cla_1;
        Clo_2final=((Clo_4-Clo_1)/(y3final-y1final))*(y2final-
y1final)+Clo_1;
       end

      % Chord Length
       if aerostart > 43
        c3=-(44/81.5)*y3+59+43*(44/81.5);
        c3initial=-(44/81.5)*y2final+59+43*(44/81.5);
        c3final=-(44/81.5)*y3final+59+43*(44/81.5);
        A_LE3=36;
        Cla_3=((Cla_4-Cla_1)/(y3final-y2final))*(y3-y2final)+Cla_1;
        Clo_3=((Clo_4-Clo_1)/(y3final-y2final))*(y3-y2final)+Clo_1;
       elseif aeroend < 43
        c3=-(102.12/43)*y3+161.12;
        c3initial=-(102.12/43)*y2final+161.12;
        c3final=-(102.12/43)*y3final+161.12;
        A_LE3=63;
        Cla_3=Cla_4;
        Clo_3=Clo_4;
       else
        c3=-(44/81.5)*y3+59+43*(44/81.5);
```

```
        c3initial=-(44/81.5)*y2final+59+43*(44/81.5);
        c3final=-(44/81.5)*y3final+59+43*(44/81.5);
        A_LE3=36;
        Cla_3=((Cla_4-Cla_1)/(y3final-y1final))*(y3-y1final)+Cla_1;
        Clo_3=((Clo_4-Clo_1)/(y3final-y1final))*(y3-y1final)+Clo_1;
       end

        % Geometric Twist
        % Section 4: 65 < y < 124.5
        a4=(CLo_desired*4*S/(b*pi*Cla_4))*sqrt(1-(2*y4/b).^2)./c4-
Clo_4/Cla_4;
        a4initial=(CLo_desired*4*S/(b*pi*Cla_4))*sqrt(1-
(2*y3final/b).^2)/c4initial-Clo_4/Cla_4; %a4 at y3final
        % Section 3: 43 < y < 65
        a3=(CLo_desired*4*S./(b*pi.*Cla_3)).*sqrt(1.-
(2.*y3./b).^2)./c3-Clo_3./Cla_3;
        % Section 2: 10 < y < 43
        a2=(CLo_desired*4*S./(b*pi*Cla_2)).*sqrt(1-(2*y2/b).^2)./c2-
Clo_2./Cla_2;
        a2final=(CLo_desired*4*S/(b*pi*Cla_2final)).*sqrt(1-
(2*y2final/b)^2)/c2final-Clo_2final/Cla_2final; %a2 at y2final
        % Section 1: 0 < y < 10
        a1=(CLo_desired*4*S/(b*pi*Cla_1))*sqrt(1-(2*y1/b).^2)./c1-
Clo_1/Cla_1;
        a1final=(CLo_desired*4*S/(b*pi*Cla_1))*sqrt(1-
(2*y1final/b).^2)/c1final-Clo_1/Cla_1;
        if i==1
            twist=max([max(a1) max(a2) max(a3) max(a4)])-min([min(a1)
min(a2) min(a3) min(a4)]);
        end

    % Section 4: 65 < y < 124.5
        % Airfoil Data
        Cl_4=Cla_4*(a_e+a4)+Clo_4;
        Cl_4initial=Cla_4*(a_e+a4initial)+Clo_4; %Cl_4 at y3final
        Cm_4=outCmac;

    % Section 1: 0 < y < 10
        % Airfoil Data
        Cl_1=Cla_1*(a_e+a1)+Clo_1;
        Cl_1final=Cla_1*(a_e+a1final)+Clo_1;
        Cm_1=inCmac;

    % Section 2: 10 < y < 43
       if aerostart > 43
        Cl_2=Cla_1*(a_e+a2)+Clo_1;
        Cl_2final=Cla_1*(a_e+a2final)+Clo_1;
        Cm_2=Cm_1;
        Cl_3=((Cl_4initial-Cl_2final)/(y3final-y2final))*(y3-
y2final)+Cl_2final;
        Cm_3=((Cm_4-Cm_2)/(y3final-y2final))*(y3-y2final)+Cm_2;
       elseif aeroend < 43
        Cl_3=Cla_4*(a_e+a3)+Clo_4;
        Cl_3initial=Cla_4*(a_e+a2final)+Clo_4;
        Cm_3=Cm_4;
```

```
        Cl_2=((Cl_3initial-Cl_1final)/(y2final-y1final))*(y2-
y1final)+Cl_1final;
        Cl_2final=((Cl_3initial-Cl_1final)/(y2final-y1final))*(y2final-
y1final)+Cl_1final;
        Cm_2=((Cm_4-Cm_1)/(y2final-y1final))*(y2-y1final)+Cm_1;
       else
        Cl_2=((Cl_4initial-Cl_1final)/(y3final-y1final))*(y2-
y1final)+Cl_1final;
        Cl_2final=((Cl_4initial-Cl_1final)/(y3final-y1final))*(y2final-
y1final)+Cl_1final;
        Cm_2=((Cm_4-Cm_1)/(y3final-y1final))*(y2-y1final)+Cm_1;
        Cl_3=((Cl_4initial-Cl_1final)/(y3final-y1final)).*(y3-
y1final)+Cl_1final;
        Cm_3=((Cm_4-Cm_1)/(y3final-y1final))*(y3-y1final)+Cm_1;
       end

       % Section 1: 0 < y < 10
       ac1=.273;
       X1=ac1*c1final+y1final*tan(A_LE1*pi/180);
       A_AC1=atan((X1-ac1*c1initial)/y1final);
       ac4=.25;
       X4=ac4*c4final+(y4final-y3final)*tan(A_LE4*pi/180);
       A_AC4=atan((X4-ac4*c4initial)/(y4final-y3final));
       % Section 2: 10 < y < 43
      if aerostart > 43
       ac2=.273;
       X2=ac2*c2final+(y2final-y1final)*tan(A_LE2*pi/180);
       A_AC2=atan((X2-ac2*y1final)/(y2final-y1final));
      elseif aeroend < 43
       ac2=((.25-.273)/(y2final-y1final))*(y2-y1final)+0.273;
       X2=ac2*c2final+y2final*tan(A_LE2*pi/180);
       A_AC2=atan((X2-X1)/(y2final-y1final));
      else
       ac2=((.25-.273)/(y3final-y1final))*(y2-y1final)+0.273;
       X2=ac2*c2final+y2final*tan(A_LE2*pi/180);
       if y1final==y2final
           A_AC2=0;
       else
           A_AC2=atan((X2-X1)/(y2final-y1final));
       end
      end

       % Section 3
      if aerostart > 43
       ac3=((.25-.273)/(y3final-y2final))*(y3-y2final)+.273;
       ac3final=.25;
       ac3initial=.273;
       X3=(y3final-y2final)*tan(A_LE3*pi/180)+ac3final*c3final;
       A_AC3=atan((X3-ac3initial*c3initial)/(y3final-y2final));
      elseif aeroend < 43
       ac3=ac4;
       ac3final=ac4;
       ac3initial=ac4;
       X3=(y3final-y2final)*tan(A_LE3*pi/180)+ac3final*c3final;
       A_AC3=atan((X3-ac3initial*c3initial)/(y3final-y2final));
```

```
      else
       ac3=((.25-.273)/(y3final-y1final))*(y3-y1final)+.273;
       ac3final=.25;
       ac3initial=((.25-.273)/(y1final-y3final))*(y2final-
y1final)+.273;
       X3=(y3final-y2final)*tan(A_LE3*pi/180)+ac3final*c3final;
       if y3final==y2final
           A_AC3=0;
       else
           A_AC3=atan((X3-ac3initial*c3initial)/(y3final-y2final));
       end
      end

    if i==2

MAC_datcom=(2/S)*double(int(c1^2,y1,0,y1final)+int(c2^2,y2,y1final,y2fi
nal)+int(c3^2,y3,y2final,y3final)+int(c4^2,y4,y3final,y4final));

XA_top=int(c1*y1*tan(A_AC1)*Cla_1,y1,0,y1final)+int(c2*y2*tan(A_AC2)*Cl
a_2,y2,y1final,y2final)+int(c3*y3*tan(A_AC3)*Cla_3,y3,y2final,y3final)+
int(c4*y4*tan(A_AC4)*Cla_4,y4,y3final,y4final);

XA_bot=int(c1*Cla_1,y1,0,y1final)+int(c2*Cla_2,y2,y1final,y2final)+int(
c3*Cla_3,y3,y2final,y3final)+int(c4*Cla_4,y4,y3final,y4final);
        XA=double(XA_top/XA_bot);
        Xac=XA+ac1*c1initial;
        Xacpercent=(Xac/c1initial)*100;

CL=(2/S)*double(int(c1*Cl_1,y1,0,y1final)+int(c2*Cl_2,y2,y1final,y2fina
l)+int(c3*Cl_3,y3,y2final,y3final)+int(c4*Cl_4,y4,y3final,y4final));

CMac=(2/S)*(double(int(c1^2*Cm_1,y1,0,y1final)+int(c2^2*Cm_2,y2,y1final
,y2final)+int(c3^2*Cm_3,y3,y2final,y3final)+int(c4^2*Cm_4,y4,y3final,y4
final))-
double(int(c1*Cl_1*y1*tan(A_AC1),y1,0,y1final)+int(c2*Cl_2*y2*tan(A_AC2
),y2,y1final,y2final)+int(c3*Cl_3*y3*tan(A_AC3),y3,y2final,y3final)+int
(c4*Cl_4*y4*tan(A_AC4),y4,y3final,y4final)))+XA*CL;

CMac1=(2/S)*(double(int(c1^2*Cm_1,y1,0,y1final)+int(c2^2*Cm_2,y2,y1fina
l,y2final)+int(c3^2*Cm_3,y3,y2final,y3final)+int(c4^2*Cm_4,y4,y3final,y
4final)));
        CMac2=(2/S)*(-
double(int(c1*Cl_1*y1*tan(A_AC1),y1,0,y1final)+int(c2*Cl_2*y2*tan(A_AC2
),y2,y1final,y2final)+int(c3*Cl_3*y3*tan(A_AC3),y3,y2final,y3final)+int
(c4*Cl_4*y4*tan(A_AC4),y4,y3final,y4final)));
        CMac3=XA*CL;
        a_i=(CL/(pi*AR))*180/pi;
        a_abs=a_i+a_e;
        CMcg=CMac-8.056*CL/c_bar;

        fprintf(fid,'%2.0f   %8.4f  %8.4f  %8.4f  %8.4f
%8.4f\n',a_e,a_i,a_abs,CL,CMac,CMcg);
        if a_e==-5
            CL_1=CL;
            a_abs_1=a_abs;
```

```
        elseif a_e==10
            CL_2=CL;
            a_abs_2=a_abs;
            m=(CL_2-CL_1)/(a_abs_2-a_abs_1);
            CLo=m*(-a_abs_1)+CL_1;
        end

    end

    end

    if (i==1) & (plots=='y')
        figure
        subplot(3,1,2)
        plot(y1,Cl_1)
        hold on
        plot(y2,Cl_2)
        plot(y3,Cl_3)
        plot(y4,Cl_4)
        title('Lift Coefficient')
        ylabel('Cl')
        xlim([0 y4final])
        hold off

        subplot(3,1,1)
        plot(y1,a1)
        hold on
        plot(y2,a2)
        plot(y3,a3)
        plot(y4,a4)
        title('Geometric Twist')
        xlim([0 y4final])
        ylim([-10 10])
        ylabel('Alpha (deg)')
        hold off

        subplot(3,1,3)
        plot(y1,c1.*Cl_1)
        hold on
        plot(y2,c2.*Cl_2)
        plot(y3,c3.*Cl_3)
        plot(y4,c4.*Cl_4)
        title('Lift Distribution')
        xlim([0 y4final])
        ylabel('L/q')
        xlabel('Span (ft)')
        hold off

saveas(gcf,strcat(num2str(aerostart),num2str(aeroend),num2str(100*CLo_d
esired),'distribution'),'tiffn')

saveas(gcf,strcat(num2str(aerostart),num2str(aeroend),num2str(100*CLo_d
esired),'distribution'),'pdf')

        figure
```

```
        plot(y1,Cm_1)
        hold on
        plot(y2,Cm_2)
        plot(y3,Cm_3)
        plot(y4,Cm_4)
        title('Cm')
        xlim([0 y4final])
        hold off

        figure
        plot(y1,Cla_1)
        hold on
        plot(y2,Cla_2)
        plot(y3,Cla_3)
        plot(y4,Cla_4)
        title('Cla')
        xlim([0 y4final])
        hold off


        figure
        plot(y1,c1initial-y1*tan(A_LE1*pi/180))
        hold on
        plot(y2,c1initial-y1final*tan(A_LE1*pi/180)-(y2-
y1final)*tan(A_LE2*pi/180))
        plot(y3,c1initial-y1final*tan(A_LE1*pi/180)-(y2final-
y1final)*tan(A_LE2*pi/180)-(y3-y2final)*tan(A_LE3*pi/180))
        plot(y4,c1initial-y1final*tan(A_LE1*pi/180)-(y2final-
y1final)*tan(A_LE2*pi/180)-(y3final-y2final)*tan(A_LE3*pi/180)-(y4-
y3final)*tan(A_LE4*pi/180))
        plot(y1,c1initial-y1*tan(A_LE1*pi/180)-c1)
        plot(y2,c1initial-y1final*tan(A_LE1*pi/180)-(y2-
y1final)*tan(A_LE2*pi/180)-c2)
        plot(y3,c1initial-y1final*tan(A_LE1*pi/180)-(y2final-
y1final)*tan(A_LE2*pi/180)-(y3-y2final)*tan(A_LE3*pi/180)-c3)
        plot(y4,c1initial-y1final*tan(A_LE1*pi/180)-(y2final-
y1final)*tan(A_LE2*pi/180)-(y3final-y2final)*tan(A_LE3*pi/180)-(y4-
y3final)*tan(A_LE4*pi/180)-c4)
        plot(y1,c1initial-y1*tan(A_LE1*pi/180)-ac1.*c1,'r')
        plot(y2,c1initial-y1final*tan(A_LE1*pi/180)-(y2-
y1final)*tan(A_LE2*pi/180)-ac2.*c2,'r')
        plot(y3,c1initial-y1final*tan(A_LE1*pi/180)-(y2final-
y1final)*tan(A_LE2*pi/180)-(y3-y2final)*tan(A_LE3*pi/180)-ac3.*c3,'r')
        plot(y4,c1initial-y1final*tan(A_LE1*pi/180)-(y2final-
y1final)*tan(A_LE2*pi/180)-(y3final-y2final)*tan(A_LE3*pi/180)-(y4-
y3final)*tan(A_LE4*pi/180)-ac4.*c4,'r')
        plot([y4final y4final],[(c1initial-y1final*tan(A_LE1*pi/180)-
(y2final-y1final)*tan(A_LE2*pi/180)-(y3final-
y2final)*tan(A_LE3*pi/180)-(y4final-y3final)*tan(A_LE4*pi/180))
(c1initial-y1final*tan(A_LE1*pi/180)-(y2final-
y1final)*tan(A_LE2*pi/180)-(y3final-y2final)*tan(A_LE3*pi/180)-
(y4final-y3final)*tan(A_LE4*pi/180)-c4final)])
        plot([y1final y1final],[(c1initial-y1final*tan(A_LE1*pi/180))
(c1initial-y1final*tan(A_LE1*pi/180)-c1final)])
       if aerostart > 43
```

```
        text(aerostart,2+c1initial-y1final*tan(A_LE1*pi/180)-(y2final-
y1final)*tan(A_LE2*pi/180),'Start of Aero Twist','Rotation',30)
        text(aerostart,-5+c1initial-y1final*tan(A_LE1*pi/180)-(y2final-
y1final)*tan(A_LE2*pi/180)-
c2final,strcat('y=',num2str(aerostart)),'HorizontalAlignment','center')
       else
        text(aerostart,-5+c1initial-y1final*tan(A_LE1*pi/180)-
c1final,strcat('y=',num2str(aerostart)),'HorizontalAlignment','center')
        text(aerostart,2+c1initial-y1final*tan(A_LE1*pi/180),'Start of
Aero Twist','Rotation',30)
       end
       if aeroend < 43
        text(aeroend,2+c1initial-y1final*tan(A_LE1*pi/180)-(y2final-
y1final)*tan(A_LE2*pi/180),'End of Aero Twist','Rotation',30)
        text(aeroend,-5+c1initial-y1final*tan(A_LE1*pi/180)-(y2final-
y1final)*tan(A_LE2*pi/180)-
c2final,strcat('y=',num2str(aeroend)),'HorizontalAlignment','center')
       else
        text(aeroend,2+c1initial-y1final*tan(A_LE1*pi/180)-(y2final-
y1final)*tan(A_LE2*pi/180)-(y3final-y2final)*tan(A_LE3*pi/180),'End of
Aero Twist','Rotation',30)
        text(aeroend,-5+c1initial-y1final*tan(A_LE1*pi/180)-(y2final-
y1final)*tan(A_LE2*pi/180)-(y3final-y2final)*tan(A_LE3*pi/180)-
c3final,strcat('y=',num2str(aeroend)),'HorizontalAlignment','center')
       end
        plot([y2final y2final],[(c1initial-y1final*tan(A_LE1*pi/180)-
(y2final-y1final)*tan(A_LE2*pi/180)) (c1initial-
y1final*tan(A_LE1*pi/180)-(y2final-y1final)*tan(A_LE2*pi/180)-
c2final)])
        plot([y3final y3final],[(c1initial-y1final*tan(A_LE1*pi/180)-
(y2final-y1final)*tan(A_LE2*pi/180)-(y3final-
y2final)*tan(A_LE3*pi/180)) (c1initial-y1final*tan(A_LE1*pi/180)-
(y2final-y1final)*tan(A_LE2*pi/180)-(y3final-
y2final)*tan(A_LE3*pi/180)-c3final)])
        title('Planform')
        xlim([0 150])
        ylim([0 c1initial])

saveas(gcf,strcat(num2str(aerostart),num2str(aeroend),num2str(100*CLo_d
esired)),'tiffn')

saveas(gcf,strcat(num2str(aerostart),num2str(aeroend),num2str(100*CLo_d
esired)),'pdf')

    end
    if i==3
        Cle_1=(4*S*CL/(b*pi))*((sqrt(1-(2*y1/b).^2))./c1);
        Cle_2=(4*S*CL/(b*pi))*((sqrt(1-(2*y2/b).^2))./c2);
        Cle_3=(4*S*CL/(b*pi))*((sqrt(1-(2*y3/b).^2))./c3);
        Cle_4=(4*S*CL/(b*pi))*((sqrt(1-(2*y4/b).^2))./c4);
        ae_1=(4*S*CL./(Cla_1*b*pi)).*((sqrt(1-(2*y1/b).^2))./c1)-
Clo_1/Cla_1;
        ae_2=(4*S*CL./(Cla_2*b*pi)).*((sqrt(1-(2*y2/b).^2))./c2)-
Clo_2/Cla_2;
```

```
        ae_3=(4*S*CL./(Cla_3*b*pi)).*((sqrt(1-(2*y3/b).^2))./c3)-
Clo_3/Cla_3;
        ae_4=(4*S*CL./(Cla_4*b*pi)).*((sqrt(1-(2*y4/b).^2))./c4)-
Clo_4/Cla_4;

        Lprime1=Cle_1.*c1;
        Lprime2=Cle_2.*c2;
        Lprime3=Cle_3.*c3;
        Lprime4=Cle_4.*c4;

        figure
        subplot(3,1,1)
        plot(y1,Cle_1)
        hold on
        plot(y2,Cle_2)
        plot(y3,Cle_3)
        plot(y4,Cle_4)
        title('Cle')
        xlim([0 y4final])
        hold off

        subplot(3,1,2)
        plot(y1,ae_1)
        hold on
        plot(y2,ae_2)
        plot(y3,ae_3)
        plot(y4,ae_4)
        title('ae')
        xlim([0 y4final])
        hold off

        subplot(3,1,3)
        plot(y1,Lprime1)
        hold on
        plot(y2,Lprime2)
        plot(y3,Lprime3)
        plot(y4,Lprime4)
        title('Lprime')
        xlim([0 y4final])
        hold off
    end
end

fprintf(fid,'\n\nX(AC)= %5.2f ft = %5.2f %% Chord\n',Xac,Xacpercent);
fprintf(fid,'\nTwist = %5.2f deg\n',twist);
fclose(fid);
```
